



Université Louis Pasteur – Strasbourg I

Thèse

Pour obtenir le grade de

Docteur de l'Université Louis Pasteur de Strasbourg

Dicipline : Sciences de la vie

Présentée par :

Sudheendra UDUPI SEETHARAMACHARYA

FRE 2446

Laboratoire de RMN de la matière condensée

**Etudes structurales par Résonance Magnétique Nucléaire du solide de
polypeptides membranaires dans des bicouches lipidiques.
Applications aux peptides et aux proteins formants des canaux ioniques**

Soutenance prévue le 31-01-2005 devant la commission d'examen :

Prof. Jeremy LAKEY: Rapporteur externe

Prof. Alain MILON: Rapporteur externe

Prof. Thomas W. EBBESEN: Rapporteur interne

Prof. Burkhard BECHINGER: Directeur de these

Prof. Peter VÖHRINGER

Contents

Acknowledgements	ii
Abbreviations	iv
Lipids	vi
1 Introduction to biomembranes & methodologies	1
1.1 Biomembranes	1
1.1.1 Introduction	1
1.2 Lipid bilayers	2
1.2.1 Ion channels	3
1.3 Structure determination of biomembranes	4
1.4 Nuclear Magnetic Resonance	6
1.4.1 The Zeeman Interaction	8
1.4.2 The Chemical Shift Hamiltonian	9
1.4.3 The CSA Powder Spectrum	10
1.4.4 Magic-Angle Spinning	11
1.5 Cross polarization	12
1.5.1 The Hartmann-Hahn condition	12
1.5.2 Mismatch-Optimized IS transfer (MOIST)	13
1.6 Oriented solid-state NMR spectroscopy	13
1.7 Aim of the current research work	14
2 ^{15}N solid-state NMR spectroscopy investigations of the topological equilibria of a synthetic ion-channel peptide in oriented lipid bilayers	16
2.1 Introduction	16

2.2	Materials and methods	18
2.3	Results	20
2.4	Discussion	22
3	Solid-state NMR studies of phosphorylated model helical peptides	27
3.1	Introduction	27
3.2	Materials and methods	29
3.3	Results and discussion	29
4	Membrane associated α-helical segments of Bcl-X_L and Bax-C terminus investigations by solid-state NMR spectroscopy	33
4.1	Introduction	33
4.2	Materials and methods	35
4.3	Results	38
4.4	Discussion	39
5	¹⁵N and ³¹P solid-state NMR studies of antimicrobial peptides NK-2 and Citropin 1.1. in lipid bilayers	43
5.1	Introduction	43
5.2	Materials and methods	46
5.3	Results	47
5.4	Discussion	48
6	Conclusions	53
	Publications	77
	Bibliography	77

Acknowledgements

I would like to express gratitude to my supervisor Prof. Burkhard Bechinger for introducing me to the field of biomembranes and solid-state NMR and for his encouraging guidance. His enormous enthusiasm for research and his deep understanding of NMR and membrane proteins are the driving forces behind this thesis. I am deeply indebted to him for his support, warmth and for providing me the freedom to work.

I also sincerely thank Prof. Jeremy Lakey, Prof. Alain Milon, and Prof. Thomas W. Ebbesen, Prof. Peter Vohringer for agreeing to be the examiners and reviewing my thesis report.

I am grateful to Dr. Jerome Hirschinger, Dr. Jesus Raya, Dr. Karim el bayed, and Dr. Jean Pierre Kintzinger for valuable technical discussions I had with them. I would like to specially thank Dr. Philippe Bertani for the discussions, help with the spectrometer and for his guidance through problems during my stay in Strasbourg.

I also thank Dr. Elisabeth Trifilieff, Dr. Youn Trottier and Dr. Fabrice Klein for their help and collaborations.

I am grateful to all my present and past laboratory members for making my stay joyful and comfortable. Their help throughout my stay and with my work is unforgettable. My special thanks to Thierry, Josephine, Chris, Lydia, Christophe, Svetlana, Satish, Monica, Pol, Christina, Gerd, Cleria, Axel, Masae, Gerad, Nadia, Gilbert, Irma, Evegeiny, Doris, Cedric, Nicolas, Martina, James, Nani, Sudhip, Mahesh, Rangeet, Ragu, Arun, Guru, Vinay, Lawrence, Srini, Ramesh, Anil, Prakash, Ullas, Chary, Shankar, Senthil, Ravi, Arup, Kaushik, Sri, Kummi, Harish, Marie, Maggy, Nathalie and Julia.

I am indebted to Max-Planck Society, Germany and Region Alsace, France for their financial help and my thanks to the Max-Planck Institute of Biochemistry, Martinsried and Louis Pasteur University, Strasbourg for allowing me to carry out

research work in their laboratories.

Last but not the least I would like to thank my family. Special thanks to my parents, doddamma, Anna, Vrunda, Krupa, Chitra and Samantha for their enduring love and support.

Abbreviations

Peptide sequences

a) Chapter 2

LS14: (LSSL L SL)₂-CONH₂

LS21: (LSSL L SL)₃-CONH₂

AcLS21: Ac(LSSL L SL)₃-CONH₂

b) Chapter 3

(Pser-6)LS14: LSSL L SLLSSL L SL-CONH₂

(Pser-9)LS14: LSSL L SLLSSL L SL-CONH₂

c) Chapter 4

HLH/ helix5-loop-helix6 / α 5-loop- α 6 :

Ac(RDGVNWGRIVAFFSFGGALCVESVDKEMQVLVSRIAAMAT)YLND HLE

Bcl-X(C): Ac(ERFNR WFLTG MTVAG VVLLG SL)FSR K

Bax-C: GTPTW QTVTI FVAGV LTASL TIWKK MG

d) Chapter 5

NK-2Val: KILRG VCKKI MRTFL RRISK DILTG KK

NK-2Ile: KILRG VCKKI MRTFL RRISK DILTG KK

Citropin1.1: GLFDV IKKVA SVIGG L-NH₂

Lipids

POPC: 1-palmitoyl-2-oleoyl-*sn*-glycero-3-phosphocholine

POPG: 1-palmitoyl-2-oleoyl-*sn*-glycero-3-[phospho-*rac*-(1-glycerol)]

POPE: 1-palmitoyl-2-oleoyl-*sn*-glycero-3-phosphoethanolamine

DPhPC: 1,2-diphytanoyl-*sn*-glycero-3-phosphocholine

DOPC: 1,2-dioleoyl-*sn*-glycero-3-phosphocholine

DOTAP: 1,2-dioleoyl-3-trimethylammonium-propane

POPS: 1-palmitoyl-2-oleoyl-*sn*-glycero-3-phospho-L-serine

DOPE: 1,2-dioleoyl-*sn*-glycero-3-phosphoethanolamine

DOPG: phospholipid 1,2-dioleoyl-*sn*-glycero-3-[phospho-*rac*-(1-glycerol)]

Other

SS-NMR: solid-state nuclear magnetic resonance

MAS: magic angle spinning

OS NMR: oriented sample solid-state NMR

CD: circular dichroism

TM: transmembrane

IP: in-plane

FWHM: full width at half maximum

Fmoc: 9-Fluorenylmethoxycarbonyl

MOM: mitochondrial outer membrane

MMP: mitochondrial membrane permeation

ER: endoplasmic reticulum

NE: nuclear envelope

AMP: Antimicrobial peptide(s)

NK-lysin: Natural Killer-Lysin

nNOS: neuronal isoform of nitric oxide synthase

HPLC: high performance liquid chromatography

Lipids

Some of useful lipid structures*.

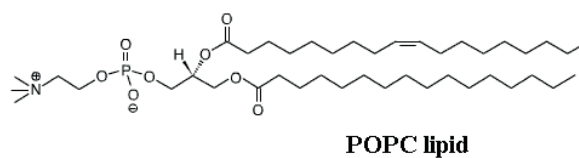


Figure 1: Chemical structure of POPC

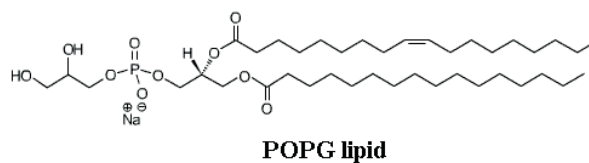


Figure 2: Chemical structure of POPG

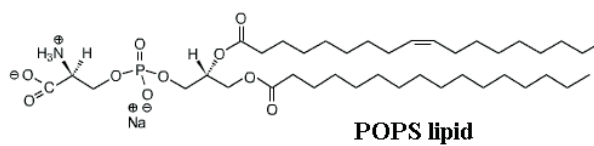


Figure 3: Chemical structure of POPS

*<http://www.avantilipids.com/index.htm>

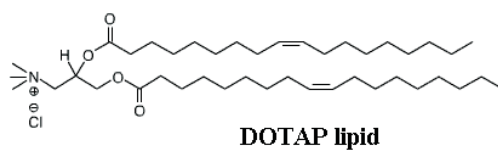


Figure 4: Chemical structure of DOTAP

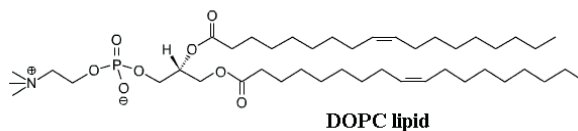


Figure 5: Chemical structure of DOPC

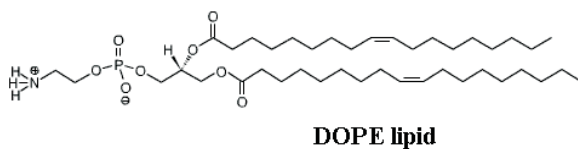


Figure 6: Chemical structure of DOPE

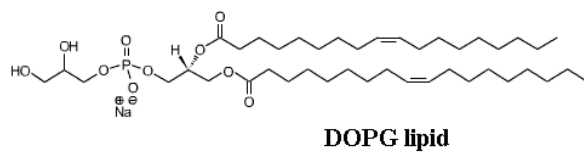


Figure 7: Chemical structure of DOPG

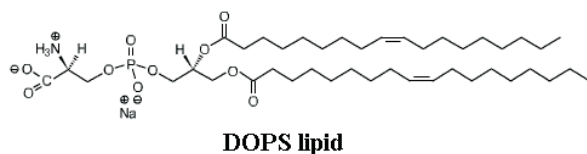


Figure 8: Chemical structure of DOPS

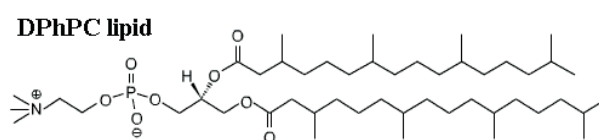


Figure 9: Chemical structure of DPhPC

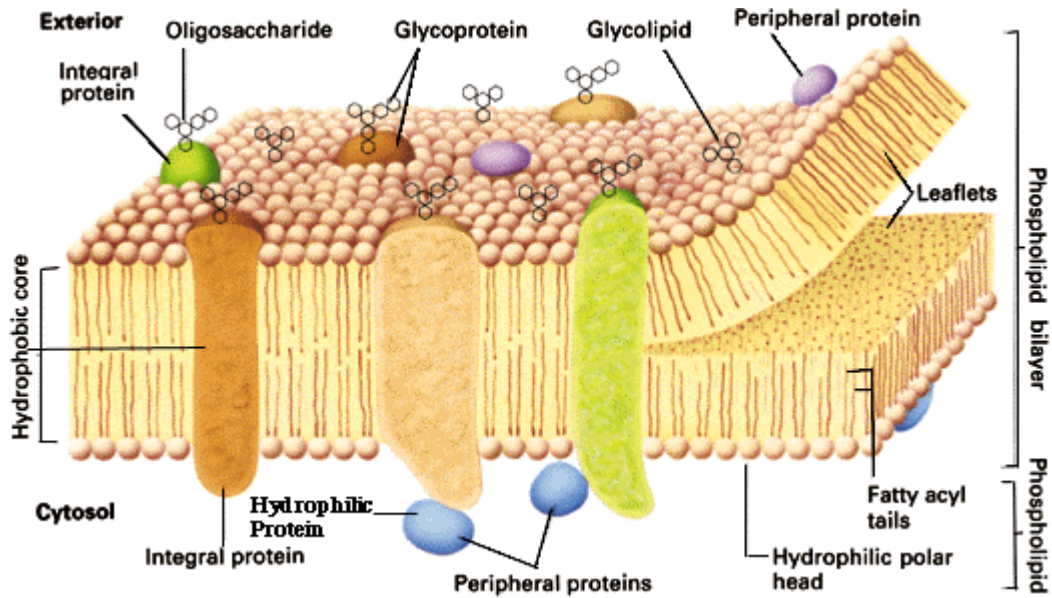


Fig. 1.1: Schematic view of a membrane (Adopted from <http://ntri.tamuk.edu/cell/membranes.html>)



Fig. 1.2: Schematic view of micelles, bicelles and a lipid bilayer containing proteins.

Chapter 1

Introduction to biomembranes & methodologies

1.1 Biomembranes

1.1.1 Introduction

Membranes are organized assemblies composed mainly of lipids, proteins and which are often covered by sugars. They are highly selective barriers, which contain pumps and gates. A membrane bilayer with an embedded protein is shown schematically in Fig 1.1. The bilayer structure has a thickness of about 5nm, and consists of different lipids and proteins. The lipids and proteins are held together by co-operative non-covalent forces.

In aqueous solution, the polar head groups of lipids like to be exposed to water, while the hydrophobic hydrocarbon tails tend to avoid it. There are different arrangements of lipids. The most relevant to NMR investigations are micelles and lipid bilayers/ bicelles. Models of a lipid bilayer, micelles and bicelles are shown in the figure 1.2. The usual structure in biological systems is a bilayer membrane¹.

In water, phospholipids assemble and in many cases spontaneously form bilayer phases. The driving forces are the hydrophobic and van der Waals interactions between the fatty acyl chains. Biomembranes are usually not simple lipid bilayers. They contain proteins, phospholipids, and glycolipids. Generally, the biomembranes assume a mosaic structure where the membrane components are asymmetrically

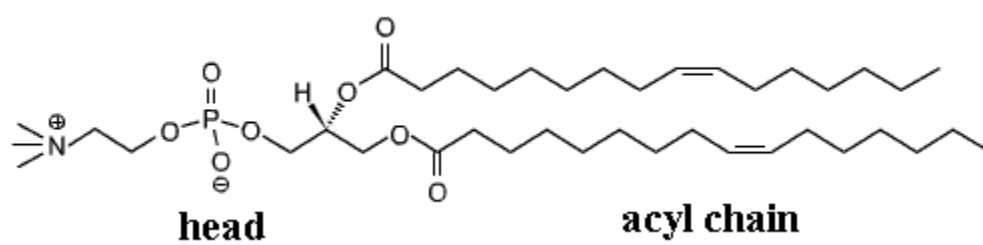


Fig: 1.3 Structure of lipid molecule

distributed between the two sides and laterally. The cell membranes inner and outer monolayers differ in composition and structure. Because of protein asymmetry, the functional characteristics of the inner and outer surfaces vary. Moreover, in membranes all copies of a protein are incorporated in the same orientation².

The biological membrane is a dynamic structure with a complex chemical composition whose physical properties can have important consequences for cell physiology. The phase behaviour of biological membranes is complex and often difficult to describe in detail.

1.2 Lipid bilayers

Lipids are amphipathic biomolecules, i.e. they contain both hydrophilic and hydrophobic moieties and they are highly soluble in organic solvents. The polar head group can be either charged or neutral (zwitterion). The nonpolar tail usually consists of two hydrocarbon chains (figure 1.3). In general, the fatty acyl chains contain an even number of carbon atoms, most frequently 16 or 18. The carbon-carbon bonds may be saturated or unsaturated. The chain length and their degree of unsaturation has a strong effect on membrane fluidity. Lipid molecules of the type found in the cell membranes readily form monolayers when spread on the water surface. In aqueous solutions, two such monolayers align back-to-back resulting in a bilayer. Such structures are spontaneously formed when phospholipids are dispersed in aqueous buffer. At physiological temperatures, biological lipid bilayer membranes are liquid crystalline systems and below transition temperatures, they become gel-like systems. The bilayers are often specified as planar to show that they are flat and to distinguish them from curved membrane systems such as liposomes. Pure lipid bilayers show inert behavior and a high electrical resistance i.e. they exhibit a large resistance for ions. This situation changes, if channel proteins are incorporated into them, a process called 'reconstitution'. Electrophysiological measurements on planar lipid bilayers where single channel currents can be readily measured have played an important role in the development of channel concepts of model membrane bilayer³. Molecular structure of some of the commonly used lipids are shown in pages v-vii.

1.2.1 Ion channels

Ion channels are formed by membrane-inserted proteins or peptides. Their function is to facilitate the penetration of ions across biological membranes. Membranes, or phospholipid bilayers, build a hydrophobic, low dielectric barrier to hydrophilic and charged molecules. Ion channels provide a high conducting, hydrophilic pathway across the hydrophobic interior of the membrane.

Ion channels can be classified according to the chemical or physical modulator controlling their gating activity¹, as summarized below:

- ligand-gated channels
- voltage-gated channels
- second messenger-gated channels
- mechanosensitive channels

Channels are also ion selective. They can discriminate between size and charge of the permeant molecule. Currently the 3-D structures of most ion channels remains up to date unknown, with two notable exceptions, porins and a K-channel, both of bacterial origin *. The *bacterial porins* is first among the solved ion channel structure at atomic resolution less than 0.3nm. The *bacterial porins* is a family of homo-trimeric channel proteins, in which each subunit contains 16 to 18 transmembrane, anti-parallel β -strands forming a β -barrel structure⁴. Whereas the crystal structure of a non-voltage gated, two-transmembrane spanning K-channel from the bacteria *Streptomyces lividans* (KcsA K⁺ channel) has been solved to 3.2 angstrom resolution (without amino acids 126-158 at the carboxy terminal end)⁵. The inner helices of KcsA K⁺ channel were tilted with respect to the membrane normal by about 25°. Helices were found to be slightly kinked with the wider part facing the outside of the cell allowing the structure to form the pore region near the extracellular surface of the membrane. However, biological ion channels can respond with structural and conformational changes to various stimuli (e.g. membrane electric field, ligand binding, and covalent modifications¹). The transmembrane conductivity is a function of the open/closed channel conformation.

*<http://www.mpibp-frankfurt.mpg.de/michel/public/memprotstruct.html>

1.3 Structure determination of biomembranes

Membrane proteins are abundant in nature. They are estimated to constitute a third of the proteome. A common property of membrane proteins is the embedding of a part of their structure in the lipid-bilayers. Therefore, transmembrane proteins mediate communication between both sides of the membrane. In their lipid-embedded domain, two types of secondary structure have predominantly been observed, i.e. β -strands and α -helices. β -strands are found in the outer membrane of Gram-negative bacteria, mitochondria and chloroplasts, forming pores known as β -barrels. Single and bundled transmembrane (TM) α -helices have a broader range of functionalities and complexities. Membrane proteins are involved in almost every process of the cell, so they carry scientific importance. It is established that they account for the activity of nearly 60-70% of all prescription drugs⁶. Despite of their significance, only few structures of membrane proteins are known[†]. The reasons for this are the experimental difficulties that have been encountered using classical techniques, such as X-ray diffraction, or solution NMR for studying the lipid-embedded protein domains.

The biochemical expression and the growth of well-ordered three-dimensional crystals of required size has been the major obstruction in attaining high-resolution structures of membrane proteins. The number of variables involved in crystallization of membrane proteins (e.g. pH, temperature, protein concentration) is greater than for soluble proteins, because of the need for detergents to solubilize the hydrophobic part of these proteins. Therefore obtaining a crystal that diffracts below 3\AA remains a difficult task despite innovative crystallizing strategies improving the production of crystals⁷.

Electron crystallography takes advantage of the fact that membrane proteins arrange themselves more readily into 2D planar ordered structures a less stringent condition than the formation of 3D crystals. 3D information is gained by combining projections of 2D crystals that have been recorded at different tilt angles. The purple membrane of *Halobacterium halobium* contains sheets of bacteriorhodopsin, a protein of 248 amino acid residues which binds retinal in our eyes. During 1975, 7\AA model of bacteriorhodopsin was first obtained by using electron microscopy using two-dimensional crystals⁸. Later this technique was extended to high resolution (3\AA) where the details about the complete assembly of seven helices was obtained⁹. The

[†]<http://www.mpibp-frankfurt.mpg.de/michel/public/memprotstruct.html>

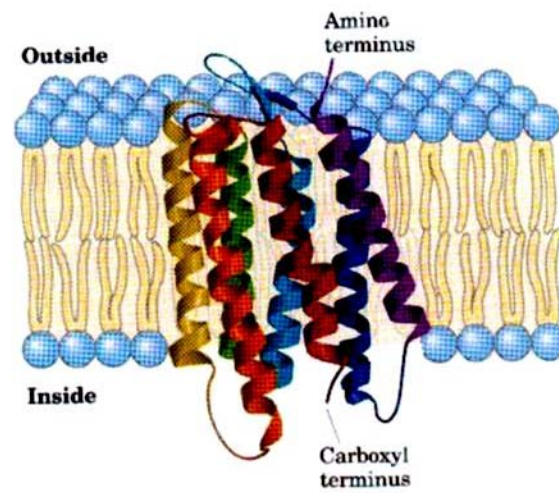


Figure. 1.4: Schematic view of bacteriorhodopsin, a membrane protein containing seven helices from electron microscopy (Source: David L, Nelson and Michael M, Cox. Principles of Biochemistry).

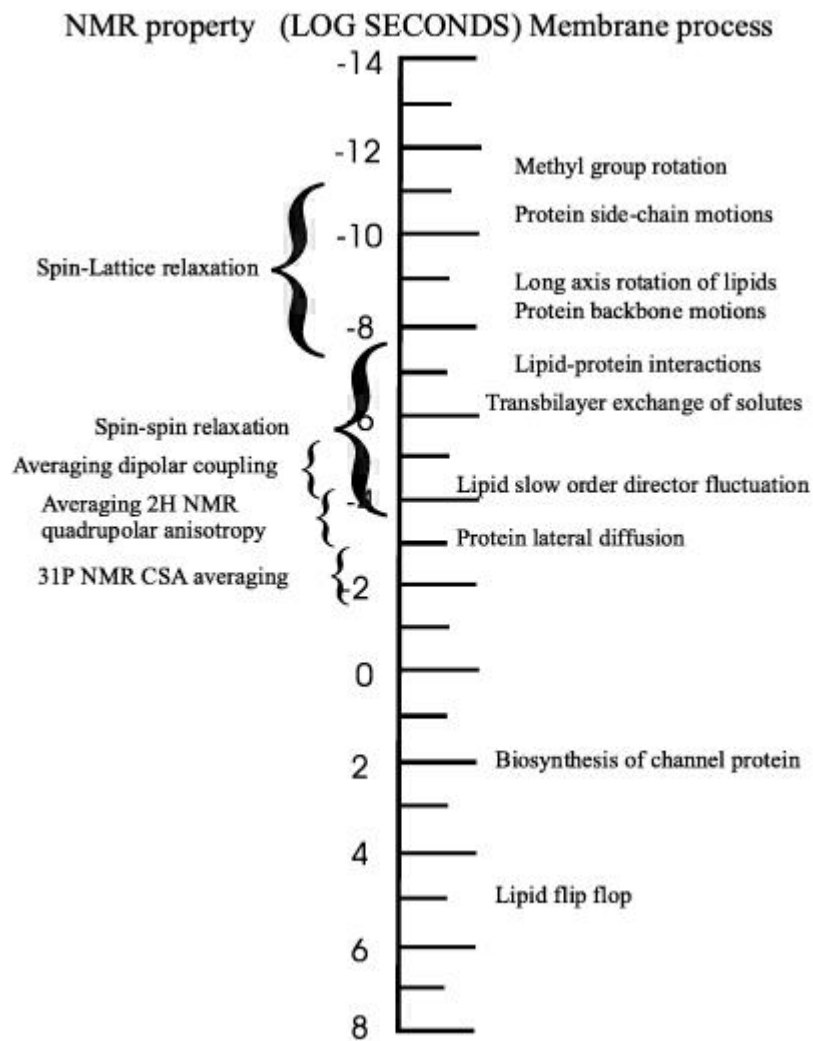


Fig. 1.5: NMR timescale and proteins dynamics (Watts A, BBA. Reviews on Biomembranes 1998)

helices were found to be tilted by about 20° with respect to the plane of membrane (Figure 1.4). Near-atomic resolution of aquaporin-1 was recently obtained with cryo-EM method¹⁰.

Difficulty for studying the membrane proteins by solution NMR is that they are embedded in extended lipid bilayers. Therefore, membrane mimicking environments that can solubilize membrane proteins and produce fast tumbling molecules have been sought in the form of organic solvents or detergents.

In solution NMR the spectral resolution depends strongly on how fast the molecules tumble. Large molecules or complexes tumble slowly, i.e, they have long rotational correlation times (a quantitative measure of rate of molecular rotation) which results in line broadening and loss of signal intensity. Membrane proteins impose the limitations for studying proteins using solution NMR techniques. In case of organic solvents and detergents, tertiary structures can be totally or partially lost. Also, the resulting size of mixed protein-detergent micelles eventually becomes a limiting factor mainly for alpha helical proteins, which show a strong signal overlap in solution state NMR spectra¹¹. Loss of signal intensities and line broadening of the NMR signals are often due to the transverse relaxation. At higher magnetic field strengths, chemical shift anisotropy (CSA) of ^1H , ^{15}N and ^{13}C nuclei can lead to significant transverse relaxation. The rate of transverse nuclear spin relaxation increases with molecular size and has greater effect on the solution NMR structural studies of biological macromolecules. However, by using Transverse Relaxation-Optimized Spectroscopy (TROSY), transverse relaxation can be largely suppressed, which results in improved spectral resolution and improved sensitivity for large proteins (e.g 110-kDa protein 7,8-dihydroneopterin aldolase (DHNA) and outer membrane protein A)^{12,13}. TROSY utilizes the constructive interference between dipole-dipole coupling and chemical shift anisotropy¹⁴.

Solid-state NMR can be used when crystallization is difficult or when the volume of mixed protein-detergent micelles exceeds the level that can be tackled with solution NMR. In solid-state NMR, protein samples are used, where the reorientation of a molecule is very slow on the NMR time scale or nonexistent, as in the case of membrane proteins reconstituted in lipid bilayers (Figure 1.5)

The problem of slow tumbling (which is associated with lipid bilayers or large molecules) can be solved in solid-state NMR either by using uniaxially oriented samples (OS NMR)¹⁵, or by magic-angle spinning (MAS NMR)¹⁶. Complementary information such as orientational constraints relative to the membrane plane (in ori-

ented sample solid-state NMR) and distances or torsional constraints (in MAS NMR) can be obtained using these approaches. A unique set-up of experiments combining oriented sample solid-state NMR and MAS NMR was also used for studying the membrane embedded protein samples¹⁷. Higher rotation speeds were also attained by placing the sample on a flexible substrate that can be rolled inside the rotor¹⁸. Uniaxially oriented samples are generally prepared magnetically (e.g. bicelles) or mechanically by exposing to a magnetic field. as shown in Figure 1.6.

The PISEMA (Polarization Induced Spin Exchange at the Magic Angle) experiment enables the determination of peptide orientations of alpha helical peptides¹⁹. When the resonance patterns are plotted for all the residues in a uniformly ¹⁵N-labelled peptide, they form characteristic wheel-like representations referred to as Polarity Index Slant Angle (PISA) wheels, which will allow the determination of the average α -helix tilt angle^{20,21}. In magic angle spinning NMR line narrowing and increased resolution are obtained by averaging the anisotropic couplings in a sample that contains randomly oriented samples. This is achieved by spinning the sample around an axis, tilted at 54.7° relative to the externally applied field. Using this method, orientational information is lost, but dipolar interactions can be reintroduced. At the same time, homonuclear or heteronuclear couplings can be reintroduced which is used for precise distance measurements. Compared with solution NMR, it is possible to obtain measurements with a greater accuracy and precision (0.1-0.2Å). The specific incorporation of isotopes into the larger proteins can be utilized by a combination of synthetic step with expressed protein ligation strategies, which uses both native protein ligation and protein expression. This method allows the folded recombinant proteins to be joined together.^{22,23}.

1.4 Nuclear Magnetic Resonance

‡

Solution NMR spectra consist of a series of sharp resonances, due to averaging of anisotropic NMR interactions by rapid random tumbling (when samples are spun). In contrast, solid-state NMR spectra are very broad, as the full effects of anisotropic, i.e. orientation-dependent interactions are observed. The presence of broad NMR lineshapes once thought to be a hindrance, actually contains much information on

‡ 24,25,26,27

the structure and dynamics of molecules in the solid state²⁴.

In the solid-state, there are many ways for a nuclear spin to communicate with its surroundings. The various Hamiltonians are described as follows^{24,25}:

- Zeeman Hamiltonian \mathcal{H}_Z : This pertains to the strong Zeeman interaction due to the external magnetic field B_0 . This interaction is time independent. Its strength far exceeds most of the other interactions in NMR spectroscopy.

- RF Hamiltonian \mathcal{H}_{RF} : This arises due the presence of the RF irradiation field B_{RF} and is time dependent.

The internal spin interactions Hamiltonian \mathcal{H}_{int} are characterized by a spatial part and a spin part. They are in general time dependent and the time dependence arising due to a manipulation of either the spatial part or the spin part or both:

- Dipole-dipole Hamiltonian \mathcal{H}_{DD} : This is due to direct magnetic interaction between nuclear spins. If the spins involved are the same kind of spins like \mathcal{H}_{II} and \mathcal{H}_{SS} , it is called homonuclear dipolar interaction (\mathcal{H}_{DD}^{homo}). If the spins are of different kind, e.g. \mathcal{H}_{IS} , it is called heteronuclear dipolar interaction ($\mathcal{H}_{DD}^{hetero}$)

- \mathcal{H}_Q : Interaction of quadrupolar nuclei with surrounding electric field gradients.

- \mathcal{H}_{CS} : Indirect magnetic interaction between the nuclear spins and B_0 mediated via the electron cloud.

\mathcal{H}_{int} can be further cast into isotropic and anisotropic forms. The isotropic part has no orientation dependence (with respect to B_0). However, in general, each nuclear spin has a well defined orientation with respect to B_0 . Therefore, the total spectral response of the whole powdered sample (where all the orientation present) in the solid-state is a cumulative response of the ensemble of nuclear spins.

Due to these interactions, spin state energies are shifted resulting in their direct manifestation in the NMR spectra. In most cases, we can assume the high-field approximation; that is, the Zeeman interaction and other external magnetic fields are much greater than internal NMR interactions. Correspondingly, these internal interactions can be treated as perturbations of the Zeeman Hamiltonian.

A priori, all NMR interactions are anisotropic - their three dimensional nature can be described by second-rank Cartesian tensors, which are 3×3 matrices.

$$\mathcal{H} = I \cdot \vec{\sigma} \cdot S = \begin{pmatrix} I_x & I_y & I_z \end{pmatrix} \begin{pmatrix} \sigma_{xx} & \sigma_{xy} & \sigma_{xz} \\ \sigma_{yx} & \sigma_{yy} & \sigma_{yz} \\ \sigma_{zx} & \sigma_{zy} & \sigma_{zz} \end{pmatrix} \begin{pmatrix} S_x \\ S_y \\ S_z \end{pmatrix} \quad (1.1)$$

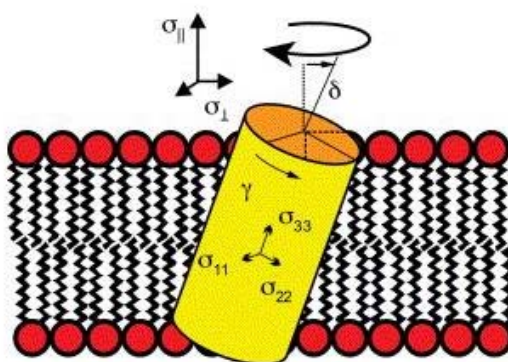


Figure 1.6: Oriented bilayers and projection of chemical shift tensors (B.Bechinger BBA. Biomembranes, 2004)

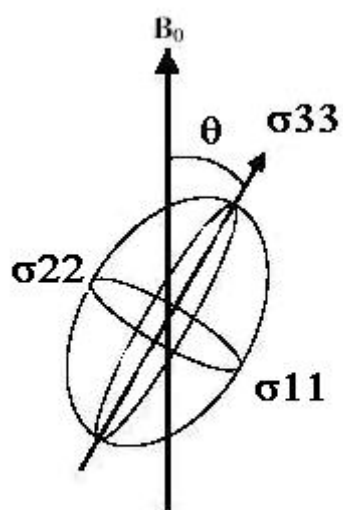


Figure 1.7: Ellipsoid representation of the CSA tensor

The tensor takes into account the orientation dependence of an NMR interaction with respect to the cartesian axis system of the molecule. These tensors can be diagonalized to yield three principal components which describe the interaction in their own principal axis system (PAS), all off-diagonal elements being zero:

$$\mathcal{H}_{PAS} = \begin{pmatrix} \sigma_{xx} & 0 & 0 \\ 0 & \sigma_{yy} & 0 \\ 0 & 0 & \sigma_{zz} \end{pmatrix} \quad (1.2)$$

Such interaction tensors are commonly pictured as ellipsoids (figure 1.7) or ovaloids, with the σ_{zz} component assigned to the largest principal component.

1.4.1 The Zeeman Interaction

The Zeeman Hamiltonian is the strongest interaction, although the fine structure of the spectrum is often dictated by various internal spin interactions. The Hamiltonian for a nuclear spin system in a static field is given by:

$$\mathcal{H}_Z = -\boldsymbol{\mu} \cdot \mathbf{B}_0 \quad (1.3)$$

where $\boldsymbol{\mu}$ is the nuclear magnetic moment operator and B_0 is the static magnetic field. Considering that

$$\boldsymbol{\mu} = \gamma \hbar \mathbf{I} \quad (1.4)$$

where \mathbf{I} is the nuclear spin operator, γ is the gyromagnetic ratio of the nucleus and B_0 is aligned along the z-axis, we obtain

$$\mathcal{H}_Z = -\gamma \hbar I_z B_0 \quad (1.5)$$

We are interested in the possible states that the spin system may take in a magnetic field. These are given by the eigenfunctions of \mathcal{H}_Z , which are just the eigenfunctions of I_z . They are $|I, m\rangle$. I is the total spin quantum number and m takes $2I + 1$ values, from $-I \dots \dots + I$. The eigenvalue equation is given by

$$\mathcal{H}_Z |I, m\rangle = E_{I,m} |I, m\rangle \quad (1.6)$$

where $E_{I,m}$ is the energy of the eigenstate $|I, m\rangle$. We can now write:

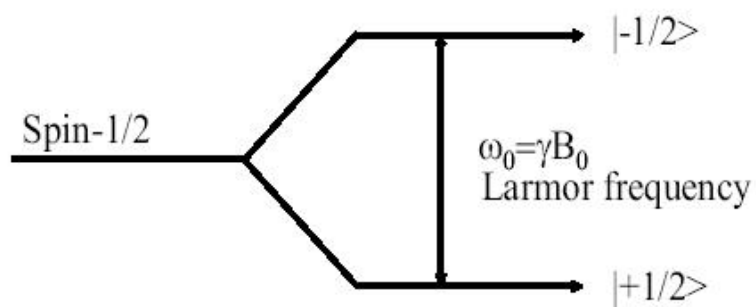


Figure 1.8: The figure shows the energy levels for a spin 1/2 system in the presence of an external static magnetic field B_0 .

$$\mathcal{H}_Z|I, m\rangle = -(\gamma\hbar B_0)I_Z|I, m\rangle = -(\gamma\hbar B_0)m|I, m\rangle \quad (1.7)$$

Comparing the above equations we get

$$E_{I,m} = -(\gamma\hbar B_0)m \quad (1.8)$$

For spin 1/2, there are two possible eigenstates with energies $E_{1/2,\pm 1/2} = \mp 1/2\gamma\hbar B_0$. These states are the Zeeman states. The transition energy between these spin states, $\Delta E = \gamma\hbar B_0 = h\nu$. In frequency units this corresponds to $\omega_0 = \gamma B_0$, the Larmor frequency of precession.

Figure 1.8 shows the energy levels for a spin 1/2 system in the presence of an external static magnetic field, B_0 . The levels are labeled according to their magnetic quantum number 'm'.

All the other spin interactions perturb the Zeeman states. Transitions between them results in the observation of NMR spectra.

1.4.2 The Chemical Shift Hamiltonian

The chemical shift (CS) Hamiltonian may be written as

$$\mathcal{H}_{CS} = \hbar\gamma\vec{I} \cdot \hat{\sigma} \cdot \vec{B}_0 \quad (1.9)$$

where γ is the gyromagnetic ratio. The CS tensor in the lab frame may be written as

$$\sigma = [\sigma_{0=isotropic} + \sigma_{1=anisotropic} + \sigma_{2=symmetric}] \quad (1.10)$$

We transform the chemical shift anisotropy (CSA) tensor into the diagonalized PAS representation. Figure 1.7 shows the ellipsoid representation of the CSA tensor with the ellipse fixed on to the molecule. The long axis of the ellipsoid (the principal axis of the ellipsoid) corresponds to the σ_{33} of the PAS axis.

The CS tensor σ in the PAS, with the symmetric part being zero may be written as

$$\sigma^{PAS} = \begin{pmatrix} \sigma_{xx}^{PAS} & 0 & 0 \\ 0 & \sigma_{yy}^{PAS} & 0 \\ 0 & 0 & \sigma_{zz}^{PAS} \end{pmatrix} = \sigma_{iso} \begin{pmatrix} 1 & 0 & 0 \\ 0 & 1 & 0 \\ 0 & 0 & 1 \end{pmatrix} + \begin{pmatrix} \delta_{xx} & 0 & 0 \\ 0 & \delta_{yy} & 0 \\ 0 & 0 & \delta_{zz} \end{pmatrix} \quad (1.11)$$

Using following definitions,

$$\sigma_{iso} = 1/3(\sigma_{xx}^{PAS} + \sigma_{yy}^{PAS} + \sigma_{zz}^{PAS}) \quad (1.12)$$

$$\Delta\sigma = \sigma_{zz}^{PAS} - \sigma_{xx}^{PAS}$$

$$\delta = \sigma_{zz}^{PAS} - \sigma_{iso}$$

$$\eta = \frac{\sigma_{xx}^{PAS} - \sigma_{yy}^{PAS}}{\delta} \quad (1.13)$$

where σ_{iso} is the isotropic chemical shift, $\Delta\sigma$ is the chemical shift anisotropy parameter, δ , a CSA value and η , an asymmetry parameter of CSA. We can rewrite the CSA tensor as:

$$\sigma^{PAS} = \sigma_{iso} \begin{pmatrix} 1 & 0 & 0 \\ 0 & 1 & 0 \\ 0 & 0 & 1 \end{pmatrix} + \Delta\sigma \begin{pmatrix} -1/2(1-\eta) & 0 & 0 \\ 0 & -1/2(1+\eta) & 0 \\ 0 & 0 & 1 \end{pmatrix} \quad (1.14)$$

A tensor of axial symmetry satisfies $\sigma_{xx}^{PAS} = \sigma_{yy}^{PAS}$. η governs the shape of the tensor and is such that $0 \leq \eta \leq 1$.

1.4.3 The CSA Powder Spectrum

A typical powder spectrum of an isolated spin 1/2 system is shown in the figure 1.9. The spectrum is broadened by CSA. Note that the variation in the shape of the powder pattern depends on the η value. The discontinuities in the pattern correspond to the principal values of the CSA tensor. The spectra are plotted by adopting the convention, $|\sigma_{zz}^{PAS} - \sigma_{iso}| > |\sigma_{yy}^{PAS} - \sigma_{iso}| > |\sigma_{xx}^{PAS} - \sigma_{iso}|$.

The CSA powder patterns shown in the figure 1.9 are composed of a large number of sharp lines derived from spins at all orientations. Such a spectrum is called an inhomogeneously broadened spectrum. The CS Hamiltonian, with the assumption that the magnetic field is along the zaxis can be written as:

$$\mathcal{H}_{CS} = -\gamma I_z \sigma_{zz}^{lab} B_0 \quad (1.15)$$

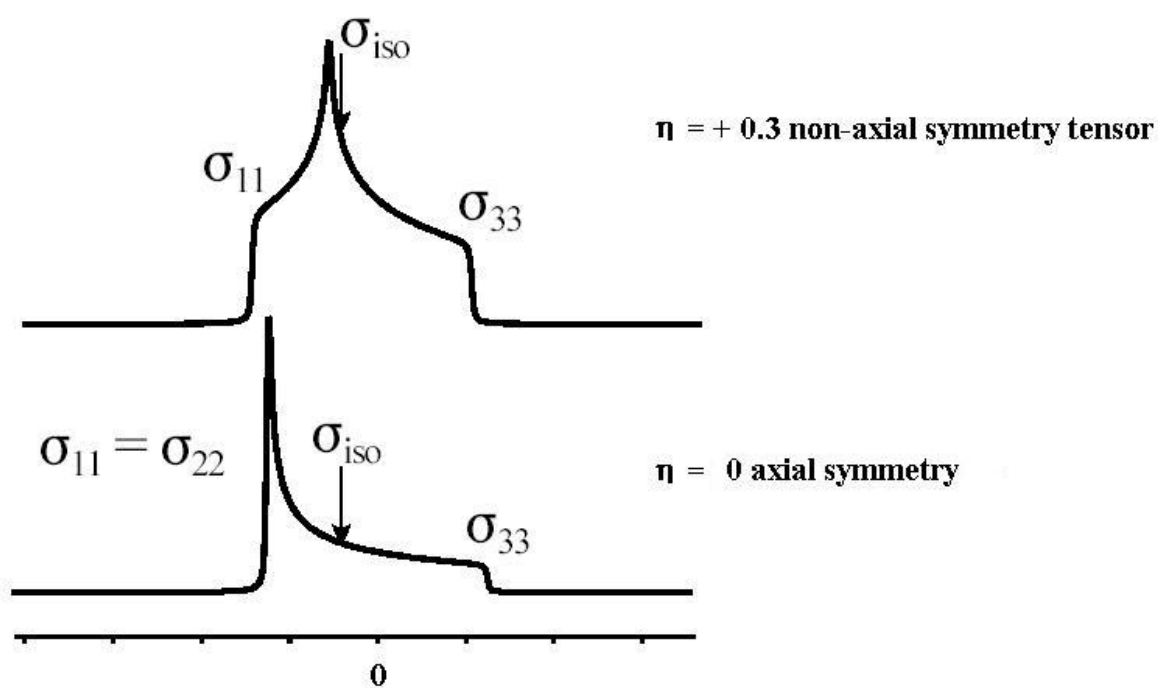


Figure 1.9: Asymmetry parameter influence on the spectrum

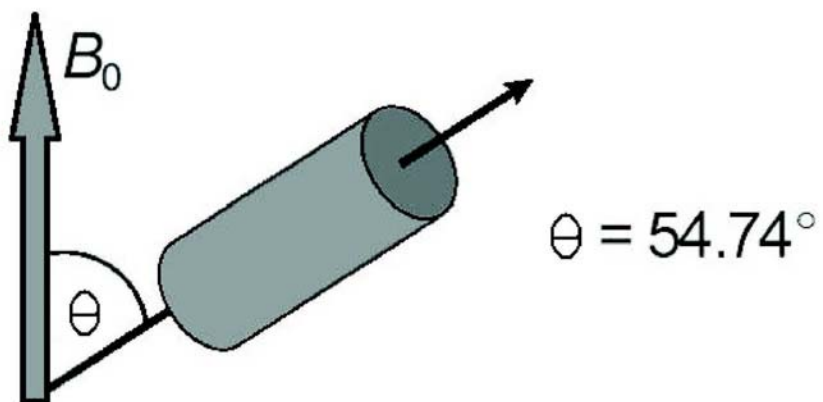


Figure 1.10: Magic angle spinning

The NMR spectral frequency corresponds to the transition energy between the $|+1/2\rangle$ and $|-1/2\rangle$ levels. The contribution to this from the chemical shielding ω_{CS} , is obtained as

$$\omega_{CS} = -\omega_0 \sigma_{zz}^{lab} \quad (1.16)$$

To proceed further, we need to express σ_{zz}^{lab} in terms of the principal values of the shielding tensor and the orientation of its PAS with respect to laboratory frame. We can write

$$\sigma_{zz}^{lab} = \begin{pmatrix} 0 & 0 & 1 \end{pmatrix} \sigma^{lab} \begin{pmatrix} 0 \\ 0 \\ 1 \end{pmatrix} \quad (1.17)$$

This projects out the zz component of σ_{lab} .

Using Euler angles, we can write,

$$\omega_{CS}(\theta, \phi) = (\sigma_{xx}^{PAS} \sin^2 \theta \cos^2 \phi + \sigma_{yy}^{PAS} \sin^2 \theta \sin^2 \phi + \sigma_{zz}^{PAS} \cos^2 \theta) \quad (1.18)$$

Using definitions of η and δ

$$\omega_{CS}(\theta, \phi) = -\omega_0 \sigma_{iso} - 1/2 \omega_0 \delta (3 \cos^2 \theta - 1 + \eta \sin^2 \theta \cos 2\phi) \quad (1.19)$$

For an axially symmetric CSA tensor we get a simpler expression for the chemical shift frequency:

$$\omega_{CS}(\theta, \phi) = -\omega_0 \sigma_{iso} - 1/2 \omega_0 \Delta\sigma (3 \cos^2 \theta - 1) \quad (1.20)$$

The figure (1.9) shows effect of the asymmetry parameter on the chemical shift frequencies.

1.4.4 Magic-Angle Spinning

In solution, rapid isotropic tumbling averages the spatial component to zero. Magic-angle spinning (see figure 1.10) introduces artificial motion by placing the axis of the sample rotor at the magic angle (54.74°) with respect to B_0 . The term $3\cos^2\theta - 1 = 0$ when $\theta = 54.74^\circ$ as the dipolar and chemical shielding interactions containing $(3\cos^2\theta - 1)$ terms get averaged. The spinning rate of MAS must be greater than or equal to the magnitude of the anisotropic interaction to average it to zero. If the sample is spun at a rate less than the magnitude of the anisotropic interaction, a

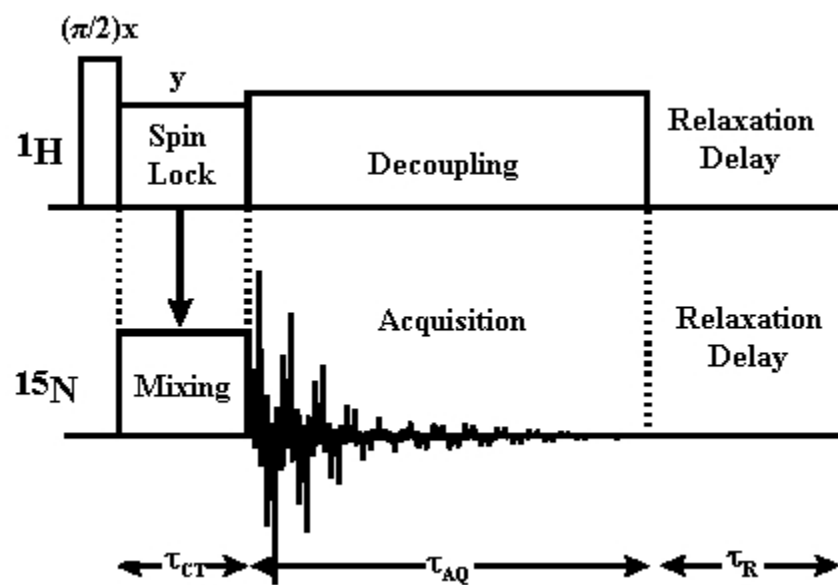


Figure 1.11: The cross polarization pulse sequence

manifold of spinning sidebands becomes visible, which are separated by the spinning frequency (in Hz). Even with MAS slower than the breadth of the anisotropic interaction, the signal becomes concentrated in the spinning sidebands, rather than spread over the entire breadth as in the case of the static NMR spectrum.

1.5 Cross polarization

Cross polarization is one of the most basic techniques in solid state NMR. In this technique, polarization from abundant spins such as ^1H or ^{19}F is transferred to dilute spins such as ^{13}C or ^{15}N . It transfers the magnetization to the rare spin reservoir under Hartmann-Hahn conditions.

Cross polarization is useful for solids where heteronuclear couplings exists. The overall effect is to enhance the signal-to-noise ratio:

Cross polarization enhances the signal from dilute spins potentially by a factor of (γ_I/γ_S) where I is the abundant spin and S is the dilute spin²⁸ and due to spin-lattice relaxation effect.

Cross polarization requires that nuclei be dipolar coupled to one another. The key to obtaining efficient cross polarization is setting the **Hartmann-Hahn condition** properly. In this case, the B_1 field of the dilute spin (e.g., $\omega_{1\text{N}-15}$) is set equal to that of the abundant spin (e.g., $\omega_{1\text{H}-1}$) by adjusting the power on each of the channels (Figure 1.11). If these are set properly, the proton and nitrogen magnetization precess in the rotating frame at the same rate, allowing transfer of the abundant spin polarization to nitrogen.

1.5.1 The Hartmann-Hahn condition

Cross-polarization is achieved in a double resonance experiment. Transverse magnetization of the I spins is generated by a 90° pulse at frequency ν_{0I} . However, the transmitter is not turned off afterwards, only the radio-frequency phase is shifted by 90° . Thus the B_{1I} field is now applied parallel to the I magnetization. In the frame rotating with frequency ν_{0I} around the Z axis, the B_{1I} field is the dominant magnetic field.

A similar protocol is followed for the S spins. A second radio frequency field B_{1S} is applied at frequency ν_{0S} , coincident with the lock field for the I spins. If the

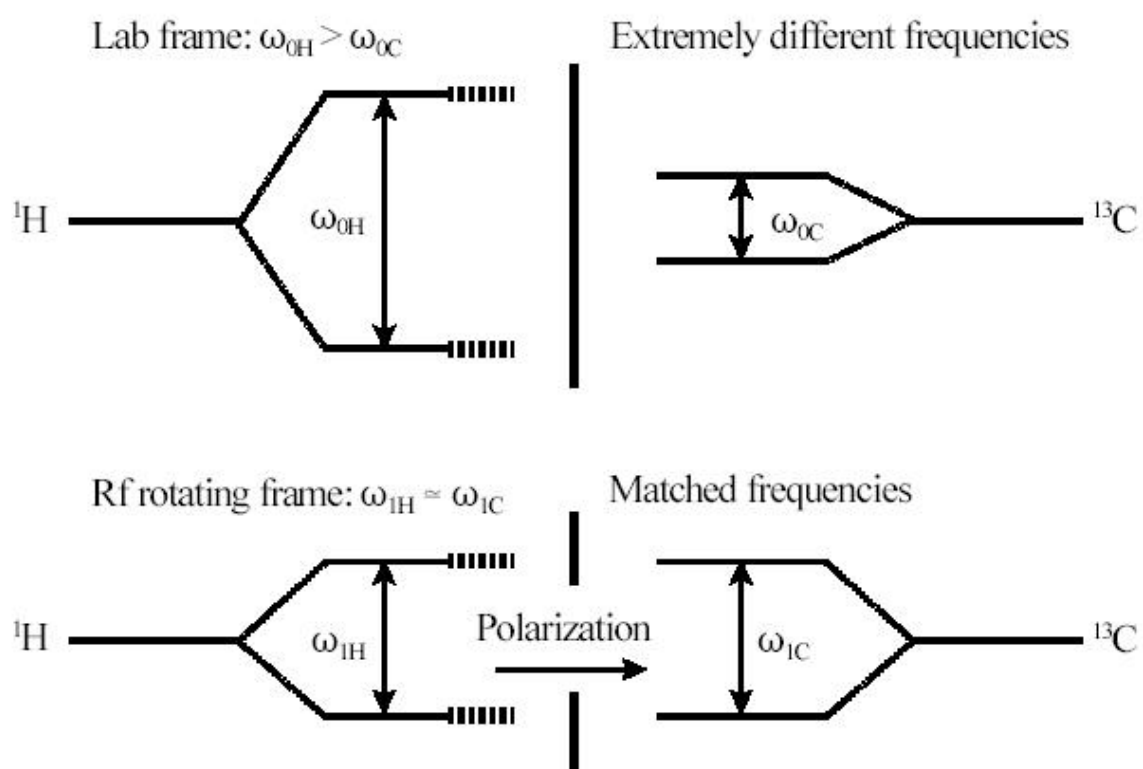


Figure 1.12: Matching frequencies in Hartmann-Hahn condition

magnitudes B_{1S} and B_{1I} of the both radio frequency fields are matched to satisfy $\gamma_S B_{1S} = \gamma_I B_{1I}$ the *Hartmann-Hahn condition* is satisfied²⁹ (Figure 1.12).

Each spin species precesses with the same frequency $\nu_1 = \nu B_1/2\pi$ around the axis of its radio frequency field in its own rotating frame. Because both rotating frames share the same Z axis, there will be an oscillation of local I and S magnetization components along the Z axis with the same frequency ν_1 . By this, frequency match magnetization can be exchanged between both spin species.

1.5.2 Mismatch-Optimized IS transfer (MOIST)

Instead of keeping the spin-locking fields at a constant phase, simultaneous π phase shifts are introduced on both channels, separated by intervals long enough to allow the system to attain equilibrium before the next phase shift.

This resembles normal Hartmann-Hahn cross polarization except for the synchronous phase reversals of the two spin-locking radio frequency fields. This has a strong beneficial effect on the efficiency of cross polarization away from the perfect match. Thus, the sequence involving repeated simultaneous π phase shifts of the two channels allows efficient cross polarization even under Hartmann-Hahn mismatch conditions as they occur under real experimental conditions²⁸.

1.6 Oriented solid-state NMR spectroscopy

In oriented solid-state NMR, there will be net degree of molecular alignment by sandwiching the samples between glass plates and then stacking them. This forces the bilayer normals to be aligned perpendicular to the plates. Earlier solid-state NMR studies, utilised these uniaxially oriented membranes for analysing structure and motion³⁰. In our study of membrane associated peptides, we have also used this technique extensively.

Solid-state NMR studies on membrane-associated peptides, which are selectively labelled by ^{15}N isotope at single sites, are of great interest to structural biologists. Proton-decoupled ^{15}N solid-state NMR spectra of ^{15}N labelled peptides reconstituted into lipid bilayers allow a sensitive measurement of the precise alignment of helical polypeptides with respect to membrane normal³¹. Earlier studies indicate that ^{15}N chemical shift ≤ 100 ppm correlate with helical orientations approximately

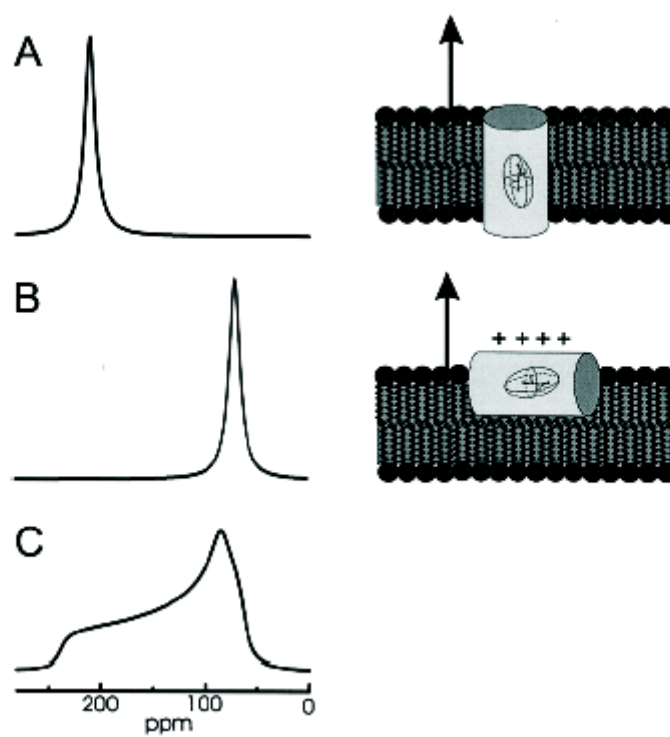


Figure 1.13: Simulated spectra of ^{15}N amide chemical shift resonances from α -helical peptides. Figure A) transmembrane orientation, B) in-plane orientation and C) a powder pattern where all the orientations are present randomly (B. Bechinger / *Biochimica et Biophysica Acta* 1999).

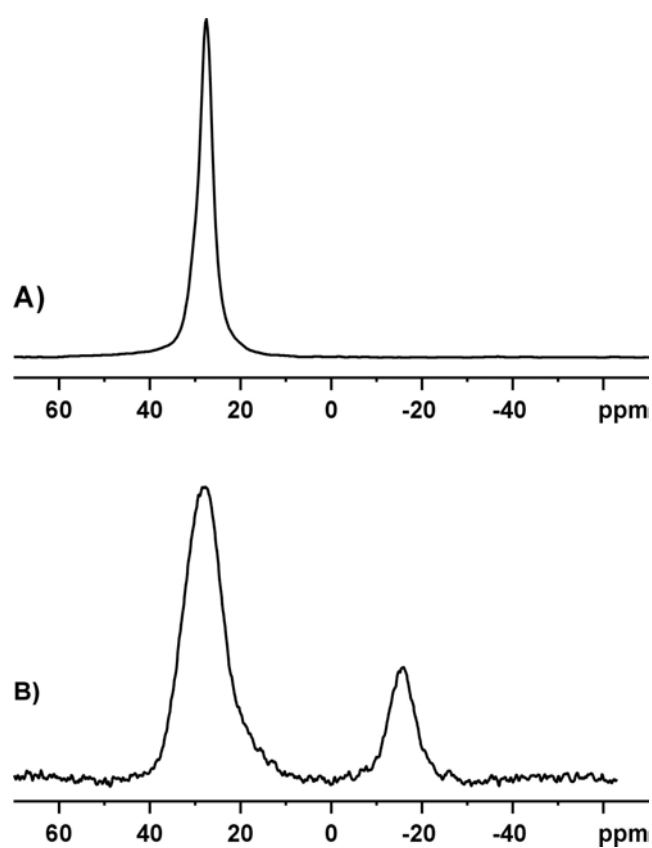


Figure 1.14: Proton-decoupled ^{31}P solid-state NMR spectra of oriented phospholipid bilayer. Figure A) a perfect oriented phospholipid bilayer, B) partial misalignment of the lipid bilayer due to the peptide.

parallel to the membrane surface, whereas chemical shift values greater than 190 ppm are indicative of transmembrane alpha-helices (Figure 1.13).

Proton-decoupled ^{15}N solid-state NMR has proven to be an important tool for measuring the interactions of polypeptide α -helices with oriented and non-oriented lipid bilayers¹⁶. In the past, oriented solid-state NMR spectroscopy has been applied for studying membrane-inserted lytic peptides³², peptide channel antibiotics^{33,34,35,36} and membrane associated proteins³⁷.

Proton decoupled ^{31}P solid-state NMR has also been used for studying the oriented phospholipid bilayers. When all the lipid molecules are perfectly oriented, one dominant ^{31}P peak at about 30 ppm will be observed (figure 1.14A). However, some minor contributions to the total intensity of ^{31}P peak can be observed as being due to the effect of peptide induced conformational changes or small misalignment of the membranes in the lipid headgroup region (figure 1.14B).

1.7 Aim of the current research work

The main aim of this research work is the application of oriented solid-state NMR spectroscopy to study channel forming peptides in membrane bilayers. The investigations were performed on various channel forming peptides such as synthetic model ion channel peptides, helical fragments of anti-apoptotic Bcl- X_L and pro-apoptotic Bax-C terminus peptides. Studies were also done on peptide antibiotics NK2, and citropin 1.1. The information obtained by studying these peptides using proton-decoupled ^{31}P and ^{15}N solid-state NMR contributed to our understanding their membrane association and modes of functioning of these peptides.

In chapter 2, experiments related to the alignment of synthetic LS peptides comprising leucines and serines in lipid bilayers of variable composition using proton-decoupled ^{15}N solid-state NMR are reported. These peptides are known for their ion channel conducting properties, resembling to those of the nicotinic acetylcholine receptor. In spite of electrophysiology and computer simulation studies on these peptides, we lack structural details of LS peptides. Therefore our studies help further understanding of these peptide in membrane bilayer.

Chapter 3 includes initial efforts on investigating the phosphorylated model peptides reconstituted in lipid bilayer, by using proton-decoupled ^{31}P and ^{15}N solid-state NMR spectroscopy. The goal is to extend the solid-state NMR technique that

make accessible the structure, topology and dynamics of the polypeptide phosphorylation sites.

Chapter 4 describes the proton-decoupled ^{15}N and ^{31}P solid-state NMR investigations of membrane associated α -helical domains of Bcl-X_L and Bax. These proteins are important effectors in apoptosis. The study provides essential details on the arrangements of helical fragments in membrane bilayers.

Finally in chapter 5, the antibiotic peptides NK2 and citropin 1.1 are studied by proton-decoupled ^{15}N and ^{31}P solid-state NMR spectroscopy. The experimental results will be used to establish structure-activity relationships.

The experimental results generated from this research have been summarized with a general conclusion at the end of the chapter 6.

Chapter 2

^{15}N solid-state NMR spectroscopy investigations of the topological equilibria of a synthetic ion-channel peptide in oriented lipid bilayers

2.1 Introduction

Membrane channel proteins fulfill important functions during cellular signal transduction, neuronal excitability, muscle function and many other important physiological processes. Defects associated with these proteins can have severe pathological consequences, a prime example being the putative chloride channel involved in cystic fibrosis. Unfortunately, membrane proteins are difficult to purify in quantitative amounts sufficient for structural studies and are difficult to investigate by structural techniques. Therefore, very little high-resolution structural information is available for channel proteins^{5,38,39,40,41,42}. In order to better understand the structural requirements of pore-formation peptides that are known to increase the conductivity across phospholipids bilayers, peptides such as alamethicin or melittin^{43,44,45,46,47},

have been extensively studied in the past. Furthermore protein domains that are thought to line the pore of large channel proteins have been prepared and studied by structural methods (reviewed in^{48,49,50,51,52,53,54,55} etc). Although small, these peptides exhibit a dynamic and complex behavior within the 'soft' membrane environment. In order to simplify matters further, synthetic organic model compounds or minimalist peptide sequences have been designed, prepared and studied by biophysical methods^{56,57,58,59,60,61,62}.

Among those, the (LSSLLSL)₃ peptide first presented by de Grado and co-workers has been investigated in considerable detail⁵⁹. This peptide has been designed with the potential to form an amphipathic α -helix in membrane environments. Designing these helices without including charged amino acid side chains increased the possibility that they assemble into ion-conducting transmembrane helical bundles. In this configuration the serines line a water filled channel and help in the solvation of passing ions⁶³. At the same time the leucines remain in contact with the hydrophobic membrane interior.

In planar lipid bilayer experiments, the presence of transmembrane potentials causes the (LSSLLSL)₃ peptide to form discrete openings which exhibit conductivities of predominantly 70 pS (0.5 M KCl, -100 mV;⁶⁴). More channels are formed at *cis*-negative voltages, a finding that is suggestive that the peptide first inserts into the membrane with its C-terminus⁶⁴. The electrophysiological properties together with molecular modeling calculations suggest that the predominant channel structure is a transmembrane helical bundle of six parallel α -helices enclosing a channel diameter of about 8 Å^{59,64}. The channels are moderately cation-selective, an observation attributed to the alignment of serine side chains along the pore lumen⁶⁴. The rectifying properties of this and related channels correlate with the configuration of the α -helix macrodipole⁶⁵. Furthermore, the ion conductivities through such a hexameric channel have been modeled using computational methods^{66,67}.

However, when tryptophan-derivatives of the peptides were investigated by fluorescence spectroscopy, the peptide has been found to insert into the membrane with a predominant orientation parallel to the membrane surface⁶³. In contrast, no direct structural evidence has, to our knowledge, so far been published for the postulated transmembrane orientations of these peptides. Notably, increases in membrane conductance have previously been observed also for charged peptides that probably do not adopt stable transmembrane alignments at the peptide concentrations used during channel measurements (reviewed in^{68,69}). It is, therefore, desirable to have

further experimental evidence for the proposed model.

Proton-decoupled ^{15}N solid-state NMR experiment has proven to be a convenient method to investigate the interactions of polypeptide α -helices with oriented or non-oriented phospholipid bilayers (recently reviewed in¹⁶). While ^{15}N chemical shifts < 100 ppm are indicative of helix alignments approximately parallel to the membrane surface, values > 180 ppm are associated with transmembrane orientations. By introducing a non-perturbing ^{15}N label into the peptide backbone, the method can thus be used to investigate the membrane alignments of these sequences. When the ^{15}N chemical shift measurement of the oriented bilayers is combined with solid-state NMR measurables obtained from other nuclei, a very detailed analysis of the structure and topology of membrane associated peptides can be obtained (e.g.^{34,70}). The oriented solid-state NMR technique works with extended lipid membranes and has been applied to study membrane-inserted peptide channels and antibiotics^{33,34,35,36}, lytic peptides³², model sequences⁶⁹, as well as membrane-associated proteins³⁷.

When we used this technique to investigate LS sequences in DOTAP* bilayers, a lipid also used for DNA and polypeptide transport into the cell⁷¹, a tendency of the LS21 peptide to adopt TM alignments has been observed. We therefore decided to investigate the lipid-peptide interactions of these peptides in a more systematic manner. In this chapter LS14, AcLS21 and LS21 have been prepared, reconstituted in DOTAP, DPhPC or DOPC membranes and their alignment investigated under a variety of different conditions in order to understand the effect of lipid composition on the orientation of LS21 peptides. The implications of our results for the proposed model of channel formation will be discussed.

2.2 Materials and methods

Phospholipids were purchased from Avanti Polar Lipids (Birmingham, AL). The peptides LS14 (LSLLSSL)₂ and LS21 (LSLLSSL)₃ were prepared by solid-phase peptide synthesis on a Millipore 9050 automatic peptide synthesizer using Fmoc (9-fluorenylmethyloxycarbonyl) chemistry^{72,73} and a TentaGel SRAM-Leu-Fmoc resin (RAPP Polymer, Tubingen, Germany). The resin assures that C-terminal amides are obtained after the cleavage reaction. Despite the apparent simplicity in composition of the heptad repeat (Figure 2.1) the chemical preparation of quantitative

*<http://www.avantilipids.com/LipidsForLiposomeFormation.html>

amounts of the LS21 sequence has proven difficult to achieve in the past (e.g.⁶³).

By using the standard synthetic protocols of the peptide synthesizer, double couplings of residues 3, 6, 10 and 13 each involving serines and in particular, by applying the novel 'pseudo proline' technology⁷⁴ at the serine-serine positions (Fmoc-ser(tbu)-ser(Ψ -Me Pro)-OH from Nova Biochem), the yield during the LS21 synthesis could be much improved when compared to the individual addition of serines. At position 7 of LS14 and at position 11 of LS21, respectively, the ¹⁵N labeled derivative of leucine was inserted (Cambridge Isotopes Inc., USA). The synthetic products were purified using reversed phase high performance liquid chromatography using an acetonitrile / water gradient and a ProntoSIL 300-5-C4 5.0 μ m column (Bischoff Chromatography, Leonberg, Germany). The identity and purity of the synthesized peptides were analyzed by matrix-assisted laser desorption ionization mass spectrometry (MALDI-MS) and analytical reverse phase HPLC. The cationic lipid 1,2-dioleoyl-3-trimethylammonium-propane (DOTAP) as well as the zwitterionic phospholipids 1,2-dioleoyl-*sn*-glycero-3-phosphocholine (DOPC) and 1,2-diphytanoyl-*sn*-glycero-3-phosphocholine (DPhPC) were purchased from Avanti Polar Lipids (Birmingham, AL).

In order to reconstitute the peptides into oriented lipid bilayers, typically 7-16 mg peptide was dissolved in trifluoroethanol/water (4 ml / 0.3 ml) and mixed with 200 mg lipid in dichloromethane. Unless indicated otherwise the peptide-to-lipid molar ratio was 2 mol%. During the sample preparation, the pH of the sample was set to the indicated pH values by using about 65 μ l of 0.1mM Tris buffer and 40 μ l of 1N NaOH. The lipid-peptide mixture was applied onto 30 ultra-thin cover glasses (9 \times 22 mm; Paul Marienfeld GmbH & Co. KG, Lauda-Konigshofen, Germany), first dried in air and thereafter in high vacuum (1.8×10^{-2} mbar) over night.

Later the samples were equilibrated in a closed chamber where a defined relative humidity was obtained due to contact with saturated salt solutions of KNO₃ (93 % r.h.), NH₄NO₃ (84 % r.h.), NH₄Cl (75% r.h.), respectively⁷⁵. After 3-5 days the glass plates were stacked on top of each other and the stacks were stabilized and sealed with teflon tape and plastic wrappings.

For solid-state NMR spectroscopy the samples were introduced into the flattened coils⁷⁶ of a double-resonance probe and inserted into the magnetic field (9.4 Tesla) of a Bruker Avance 400MHz wide-bore solid-state NMR spectrometer. The sample was oriented with the membrane normal parallel to the B₀ field of the spectrometer. Proton-decoupled ¹⁵N solid-state NMR spectra were acquired using the MOIST

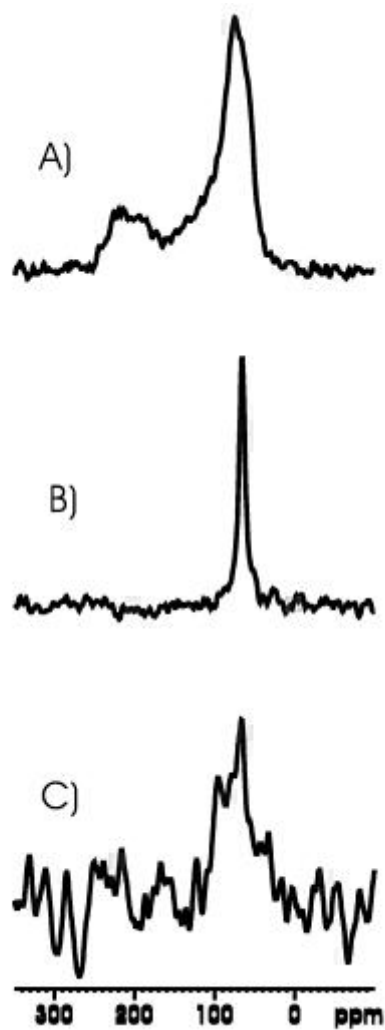


Figure 2.2: Proton decoupled ^{15}N solid-state NMR spectra of LS21 peptide at room temperature at 0° orientation. A) Dry powder, B) 2mol% LS21 reconstituted in DOTAP bilayer at pH 7.5 and r.h 93%, C) 2mol% LS21 reconstituted in DPhPC bilayer at pH 7.5 and r.h 93%

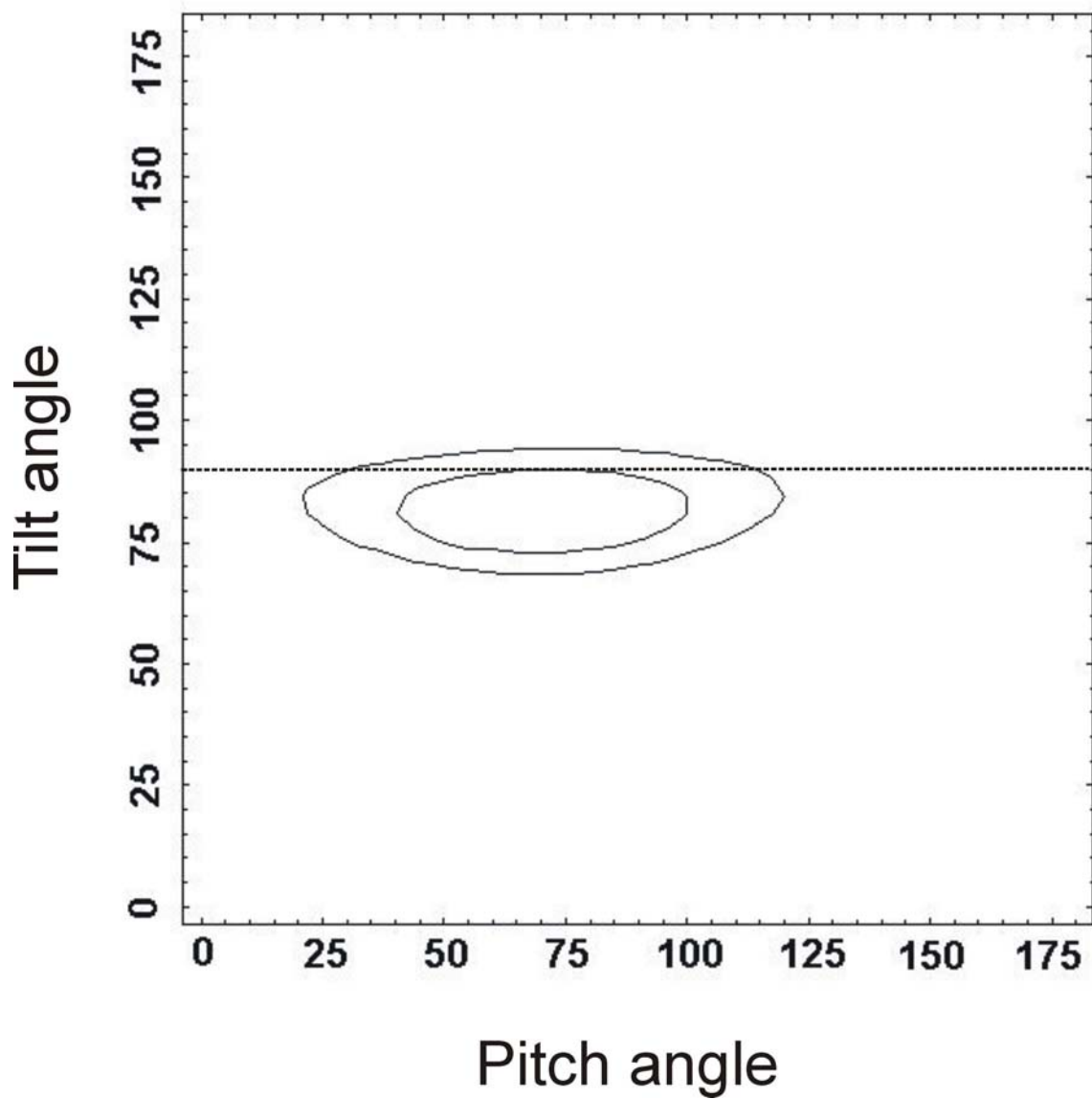


Figure 2.3: The possible spatial orientations of the LS21 peptide from ^{15}N analysis are represented by the helical tilt and the rotational pitch angles. The orientational contour is for the experimental chemical shift measurement and ± 5 ppm deviation are shown. The successive rotations of the helix are around the helix long axis (z-direction) and an axis perpendicular to that (y-direction).

cross-polarization pulse sequence²⁸. The static solid-state NMR spectra were acquired using the following parameters: ^1H B_1 field of approximately 45KHz, 1ms contact time, 3s recycle delay, spectral width: 37 kHz, 512 data points, number of acquisitions: 35000. During acquisition the sample was cooled with a stream of air at room temperature. An exponential apodisation corresponding to a line-broadening of 200 Hz was applied before Fourier transformation. NH_4Cl (41.5 ppm) was used as a reference corresponding to approximately 0 ppm for liquid NH_3 .

2.3 Results

The LS14 and the LS21 channel peptides were prepared by solid-phase peptide synthesis, labeled with ^{15}N at a single site within the central part of the polypeptide, reconstituted into uniaxially oriented lipid bilayers and investigated by proton-decoupled ^{15}N solid-state NMR spectroscopy. Using CD and tryptophan fluorescence spectroscopies it has been shown previously that these and other amphipathic peptides adopt α -helical conformations in membrane environments^{59,63,68}.

For comparison the proton-decoupled ^{15}N solid-state NMR of powder pattern of dry LS21 is shown in Figure 2.2A. In this sample all orientations are present at random and the spectrum therefore represents the full ^{15}N chemical shift anisotropy of the labeled amide bond covering approximately 175 ppm^{77,78,79,80,81}. The 'hole' observed in the central region of the spectrum is due to the reduction of ^1H - ^{15}N dipolar interactions close to the magic angle concomitant with decreased cross-polarization efficiency at these frequencies.

Figure 2.2B shows the proton-decoupled ^{15}N solid-state NMR spectra of 2 mole% LS21 when reconstituted in DOTAP lipid bilayers at pH 7.5 at 0° orientation.

The spectrum of the ^{15}N labeled leucine at position 14 of the LS21 peptide is characterized by a single peak at 65 ppm. This value is indicative of an orientation of the helix long axis parallel to the membrane surface¹⁶. The resonance is characterized by a narrow line shape with full width at half maximum (FWHM) of 8 ppm indicative of a well aligned and homogeneous sample.

The contour figure representation shown in figure 2.3 represents the spatial alignments of LS21 that agree with the measured ^{15}N chemical shift. In order to calculate this map, the peptide model of LS21 was placed in the reference coordinate system, where initially the z-axis was oriented parallel to the helix axis. The z-

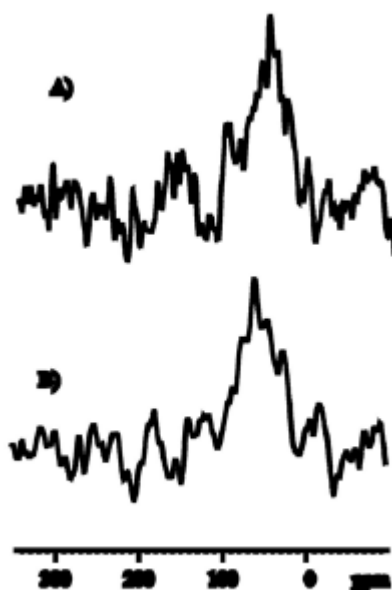


Figure 2.4: Proton decoupled ^{15}N solid-state NMR spectra of LS21 peptide at room temperature. A) 2mol% LS21 reconstituted in DOPC bilayer at pH 7.5 and r.h 93%, B) 5mol% LS21 reconstituted in DOTAP bilayer at pH 7.5 and r.h 93%.

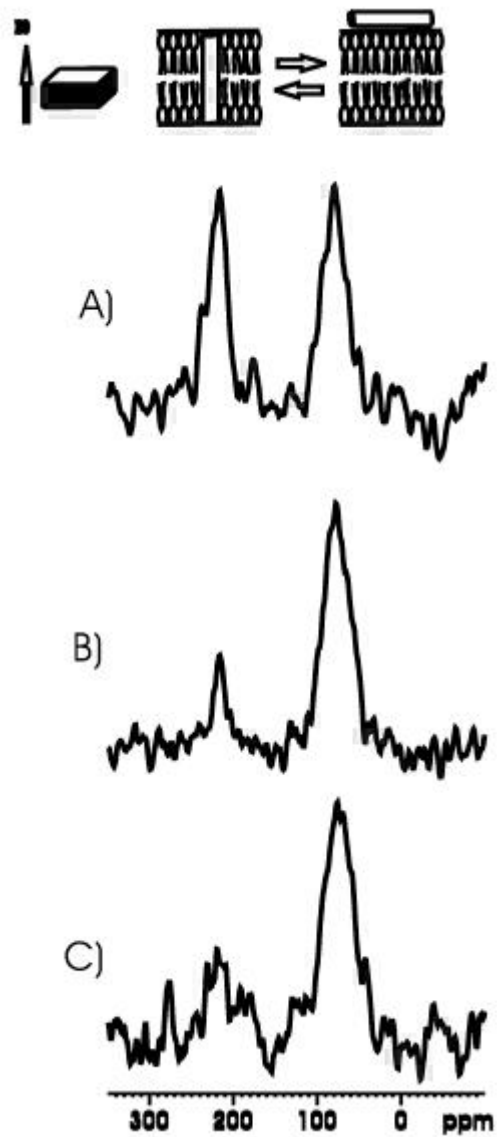


Figure 2.5: Proton decoupled ^{15}N solid-state NMR spectra of 2mol% LS21 reconstituted in DOTAP lipid bilayer at pH 8.5 at room temperature A) at r.h 93%, B) at r.h 84% and C) at r.h 75% .

y plane separates the hydrophobic from the hydrophilic part of the amphipathic polypeptide. The peptide was successively rotated around two angles perpendicular to each other. For each alignment the resulting values of ^{15}N chemical shift was calculated.

Furthermore, the LS21 peptide was reconstituted at pH 7.5 into DPhPC lipid bilayers, a lipid that forms electrically well-insulated membranes. This was therefore, also used during the electrophysiological investigations of LS21 and LS14⁵⁹. Although the ^{15}N chemical shift value of the peak maximum remains constant when the peptide is transferred from DOTAP to DPhPC membranes, the FWHM increases to 32 ppm (figure 2.2C). When the pH is increased to 8.5 the ^{15}N chemical shift value of 65 ppm remains unaffected (not shown).

In order to test if the altered composition of the fatty acyl chains or the modifications of head group region had an effect on the topology of LS21, the peptide was thereafter reconstituted into DOPC phospholipids bilayers. The proton-decoupled ^{15}N solid-state NMR spectra of LS21 reconstituted into oriented DOPC phospholipid bilayers show broadened ^{15}N resonances that extend into the 100 ppm region (Fig. 2.4A). When the peptide/DOTAP molar ratio is increased from 2 mol% to 5 mol% a considerable line broadening is observed indicative of decreased orientational order (Fig. 2.4B).

Notably, the proton-decoupled ^{31}P NMR spectra (not shown) of the DOPC samples exhibit an additional peak at -17 ppm indicative of pronounced distortions in DOPC phospholipids head group orientations due to the presence of LS21. This increased dispersion in ^{15}N chemical shift values is, therefore, indicative of macroscopic distortions of the membrane, peptide conformational changes, modifications in the distribution of alignments, exchange between isotropic and oriented peptide configurations and /or alterations in the exchange rates between peptide structures and topologies

In the next step we investigated the effect of pH and the degree of hydration on the topology of the LS21 peptide when reconstituted into oriented DOTAP lipid bilayers (Fig. 2.5). At pH 8.5 and 93% r.h. two signal intensities at 79 ppm and 217 ppm are visible at a ratio of approximately 1:1 (Figure 2.5A).

This result indicates the co-existence of in-plane and transmembrane peptide orientations. Notably, exchange between these configurations is slow on the time scale of the ^{15}N chemical shift anisotropy (10^{-4} s). When this sample is slowly dehydrated the equilibrium between in-plane and the transmembrane oriented peptide

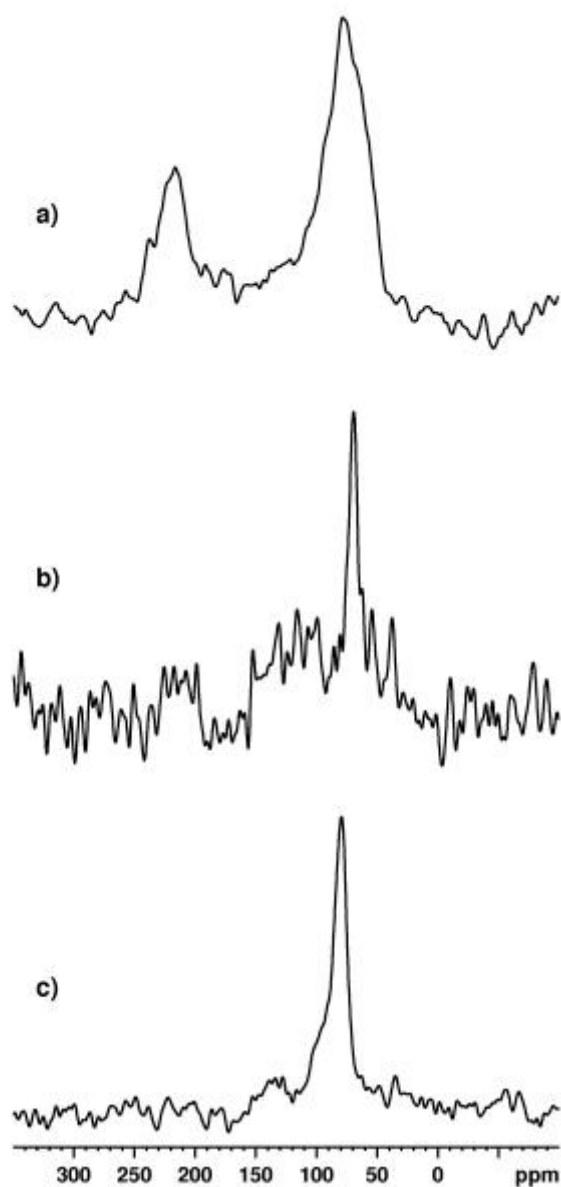


Figure 2.6: Proton decoupled ^{15}N solid-state NMR spectra of 2mol% a) AcLS21 at pH 8.5, b) AcLS21 at pH 6.5 and c) LS21 at pH 6.5 reconstituted in DOTAP lipid bilayer at r.h 93% and at room temperature.

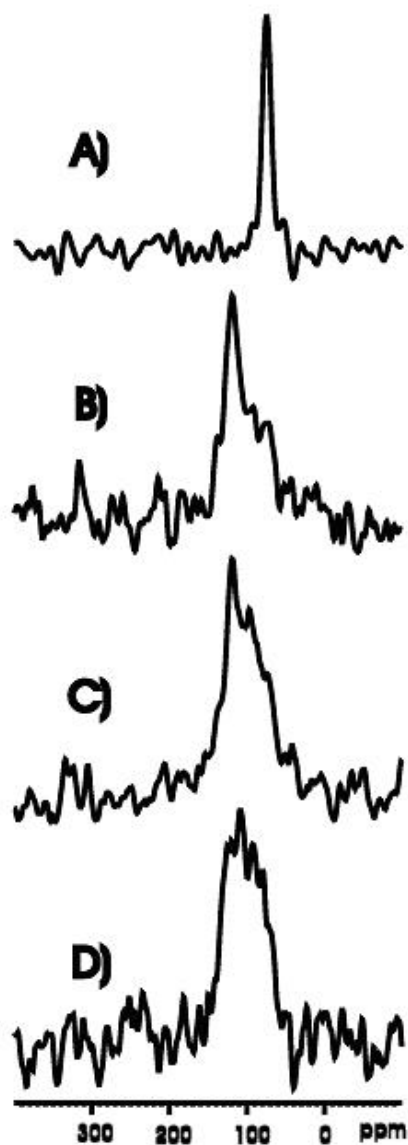


Figure 2.7: Proton decoupled ^{15}N solid-state NMR spectra of 2mol% LS14 reconstituted in DOTAP lipid bilayer at room temperature. A) pH 7.5 at r.h 93% B) pH 8.5 and r.h 93%, C) pH 8.5 and r.h 84% and D) pH 8.5 and r.h 75%.

shifts in favor of the former one (Figure 2.5). After the sample has been equilibrated at reduced hydration levels of 84% and 75% r.h, respectively, the ^{15}N NMR peak intensity at 79 ppm dominates, although significant intensities in the 217 ppm region are retained (Figure 2.5B and 2.5C). In order to understand the effect of the charge on the orientation of the LS21, we have investigated the acetylated LS21 peptide at its N-terminus at pH 8.5. Also in this preparation the co-existence of in-plane and transmembrane orientations of Ac-LS21 becomes apparent in proton-decoupled ^{15}N solid-state NMR spectroscopy (Figure 2.6a).

When the AcLS21 and LS21 peptides are reconstituted into oriented DOTAP lipid bilayers at acidic pH 6.5, ^{15}N NMR signal gives a relatively sharp peak at around 69 ppm and 80 ppm respectively (Figure 2.6b and 2.6c). This is again an indication that these peptides are inserted to the membrane bilayer in an in-plane orientation.

Finally we investigated the leucine-serine heptad repeat peptide encompassing a total length of only 14 residues. An alpha-helical peptide of this length is generally believed to be too short to span a biological membrane⁵⁹. Indeed when LS14 is reconstituted in DOTAP lipid bilayers at pH 7.5 and 93% r.h. the proton-decoupled ^{15}N solid-state NMR spectrum is characterized by a narrow signal at 75ppm with FWHM of 13 ppm / 0.5 kHz (Fig. 2.7A).

This result is indicative of a well defined alignment of this helix parallel to the membrane surface. When the pH of this sample is increased to 8.5, the main peak intensity is shifted to 119 ppm, which corresponds the isotropic value of leucine amides^{77,78,82,83}. At the same time significant signal intensities are also visible in the 70 ppm region. When the degree of hydration is reduced, the resonance intensities remain between 120 and 70 ppm, while the mean of the ^{15}N signal intensity shifts towards the low-field end of the NMR spectrum (Fig. 2.7B-C).

2.4 Discussion

The LS21 and LS14 peptides have been designed to form amphipathic helices in membrane environments⁵⁹. The LS21 peptide has been shown to exhibit channel properties in DPhPC membranes, thereby resembling the fungal peptide alamethicin or large channel proteins^{44,59}. This peptide has, therefore, been suggested as a model for proteins forming transmembrane helical bundles, in particular when

transmembrane electrical potentials are applied^{63,64}. The channel properties of its N-acetylated form exhibits ten times longer channel life times and has been investigated in even greater detail in electrophysiological experiments^{65,84}.

On the other hand LS14 is too short for such an arrangement and, therefore, only induces stochastic currents when added to planar lipid bilayers⁵⁹. Other amphipathic peptides which carry many lysines at their hydrophilic face had initially been thought of as forming TM channels. However, a considerable amount of experimental data shows that neither the channel properties nor the structural and topological characteristics agree with such a model (reviewed in⁸⁵). Furthermore theoretical estimates of the energies involved in associating a large number of charged residues in a small channel volume indicates a high energetic penalty when such a TM helical bundle is formed⁴⁶. Other models such as the carpet model or the detergent-like mode have therefore been suggested to be the underlying mechanism for these highly charged peptides^{68,86}. However, in the case of the LS21 peptide the hydrophilic side of the amphipathic helix is composed of polar but uncharged serines and the formation of transmembrane helical bundles by these peptides remains a reasonable model⁶⁴.

The ¹⁵N chemical shift < 100 ppm, which was observed for the LS peptides in all the samples that we tested (Figs. 2.2, 2.4), indicates that an alignment parallel to the membrane surface is the preferred configuration of this series of amphipathic peptides when interacting with the lipid bilayer. The data are in excellent agreement with static fluorescence quenching experiments which indicate an in-plane alignment of LS21 and a location of the helix axis a few Å below the polar head group / hydrocarbon boundary⁶³. The in-plane orientation ideally reflects the perfect amphipathic separation of polar and hydrophobic residues (Fig. 2.1) as it allows the serines to be exposed to the water phase when at the same time the leucines are immersed in the bilayer interior. In a similar manner, other amphipathic helices with charged side chains and/or with high hydrophobic moment have been found oriented parallel to the membrane surface^{87,88,89}. In contrast sequences composed of leucine and alanines or of leucines alone adopt stable transmembrane alignments. But to our knowledge, no channel formation has been demonstrated for these sequences^{90,91,92,93}. The observed differences in the peptide-lipid interactions and in orientational mosaic spread of LS21 (Figure 2.3) when the fatty acyl composition of phosphocholines is changed are probably related to the different packing constraints of the phospholipids when the tight packing of branched fatty acyl chains is compared to that of unsaturated

ones.

When LS21 was reconstituted into cationic DOTAP lipid membranes at pH 8.5 an additional signal intensity > 200 ppm is observed (Fig. 2.5). This is indicative of the co-existence of surface and transmembrane oriented peptides, which are in slow exchange on the 10^{-4} s NMR time scale.

In contrast the LS14 peptide is too short to span the lipid membrane and remains surface-associated at this and other conditions tested (Fig. 2.7). Considerable ^{15}N signal intensities reach into the 'isotropic' region (120 ppm) of the ^{15}N chemical shift dispersion, in particular when the degree of hydration is increased (Fig. 2.7). This data suggests that LS14 is associated with the lipid interface but in conformational and / or topological exchange in the membrane-associated layer.

The ensemble of data can thus be explained by a model where the peptide in the water phase is in dynamic equilibrium with the membrane-inserted configurations. In the membrane-associated state it can adopt in-plane (IP) or transmembrane (TM) alignments^{31,94}. Oriented ^{15}N solid-state NMR experiments or other biophysical experiments have previously been used to demonstrate the existence of IP \leftrightarrow TM equilibria of peptaibols^{89,95}, melittin^{32,96,97}, as well as pH-dependent peptide antibiotics and model sequences (reviewed in⁸⁹).

Furthermore, LS21 has been shown to exist as an equilibrium mixture of monomers and dimers in the absence of a voltage gradient across the bilayer⁵⁹. In a simplified manner these exchange processes can be represented by the following equation: soluble aggregates in the aqueous phase \leftrightarrow membrane surface associated IP \leftrightarrow TM. Within these phases sub-equilibria such as IP1 \leftrightarrow IP2 \leftrightarrow ...⁶³ or TM1 \leftrightarrow TM2 \leftrightarrow ... \leftrightarrow TM_{*n*} exist, where the indices indicate the number of associated monomers. A parallel bundle of six transmembrane helices (TM₆) has been modelled to be the predominant channel observed in electrophysiological experiments⁶⁴. Within this framework the exchange between tilted or weakly surface associated ('isotropic' on the NMR time scale) and IP-oriented LS14 (Figure 2.7), as well as between IP and TM aligned LS21 (Figure 2.5) can be explained.

From first approximation, the close to 1:1 distribution of ^{15}N signals < 100 ppm and > 200 ppm visible in Figure 2.5A indicates that the IP \leftrightarrow TM equilibrium is governed by a free enthalpy change close to zero under these conditions. We estimate that the signal-to-noise ratio of the ^{15}N solid-state NMR spectra allows us to detect a signal which encompasses at least 5% of the total intensity. Hence, the difference of the Gibbs free enthalpy describing this two-state equilibrium (ΔG_0) must not

exceed ± 7.5 kJ/mole. This value indicates that relatively small energetic changes can indeed modify the distribution of signal intensities such as observed in Figures 2.2 and 2.5 when the membrane hydration level or the sample pH are changed.

However, the question arises why the transmembrane configuration is only detectable in the presence of the cationic trimethylaminopropane lipid and at elevated pH? In order to explain this observation we reason in the following manner although other explanations cannot be excluded: It has been shown in this and in earlier work using fluorescence spectroscopy⁶³ that the LS amphipathic helix preferentially aligns parallel to the membrane surface. However, it has also been suggested that the formation of transmembrane helical bundles is responsible for the observed channel activity⁶⁴. Single-channel measurements indicate that such transmembrane helical aggregates of LS21 exhibit a 10 fold increase in life times when the N-terminal amino group of the peptide is uncharged, as this reduces the electrostatic repulsion by like-charges within the complex⁶⁴. However, ¹⁵N NMR spectroscopy of N-terminus acetylated LS21 indicates that residual charge has no significant effect on the peptide orientation when compared to the LS21 peptide (Figure 2.6). Notably, these investigations are only marginally sensitive to changes to the formation of TM oligomers.

Therefore, other contributions that might be specific to the DOTAP environment might help to stabilize a transmembrane configuration. These include van der Waals interactions, the lipid head group packing and the resulting steric constraints in both in-plane and TM configurations, the presence of counterions next to the positively charged surface, the lipids hydration environment⁹⁸, or specific lipid-lipid- and lipid-peptide interactions.

Nevertheless, the data suggest that $\Delta G_{IP \leftrightarrow TM}$ is small for LS21 in DOTAP lipid bilayers and can be overcome by changes in the chemical environment. For alamethicin, transmembrane electrical fields have been suggested to result in more peptide partitioning into the membrane⁹⁹, and to reorient the helix macroscopic dipole (reviewed in^{44,46}). A similar model has also been presented for LS21⁵⁹. Here we present, to our knowledge for the first time, direct experimental proof, that transmembrane orientations of this or other highly amphipathic peptides occur in lipid bilayers. Therefore, the data support the hypothesis that the transmembrane electric field induces the re-orientation of a fraction of LS21 peptides⁶³, which is sufficient to allow the observation of channels formed by transmembrane helical bundles in electrophysiological experiments. The gating charge for LS21 channel

formation has been measured to encompass 3.6 elementary charges⁶⁴. Therefore, for an hexameric channel structure to be adopted, the energy of moving 0.6 elementary charges (per monomer) in a transmembrane electric field of 100mV corresponds to about 5 kJ/mole. This energy is sufficient to significantly increase the number of transmembrane helical peptides and thereby sufficient to explain the observed voltage-induced increases in conductivity⁵⁹.

Chapter 3

Solid-state NMR studies of phosphorylated model helical peptides

3.1 Introduction

Phosphorylation is an important process in a living organism and used for regulating enzymatic reactions, protein trafficking and transmission of extracellular signals in cells^{100,101,102}. The phosphorylation of serines 52 and 56 of the channel forming membrane protein¹⁰³, viral protein U (Vpu) of HIV-1 is important for degradation of viral receptor CD4 in the endoplasmic reticulum. Therefore the phosphorylation sites are also of considerable interest in regulation of proteins activities and of enzymatic reactions. The incorporation of phosphate groups in the polypeptide chain may change its conformations and its mode of intermolecular interactions. As a consequence, detailed structural information on these phosphorylated peptide is strongly desired.

In view of the importance of phosphates in biological systems, we undertook an investigation of phosphorylated model peptide reconstituted in lipid bilayers with the goal of developing novel solid-state NMR techniques that make the structure, topology and dynamics of the peptide phosphorylation sites accessible. The membrane-associated model peptides carrying phosphoserines were studied using

proton-decoupled ^{31}P and ^{15}N solid-state NMR spectroscopy. ^{31}P solid-state NMR spectroscopy is an attractive technique, because of the high sensitivity of this nucleus (100% natural abundance and high γ) and its biological importance (e.g, phosphorylated peptides). In a first step, efforts were made for analyzing chemical shift tensors of related compounds, thereby making available the basis for a fair interpretation of the spectra. Notably the orientation of the ^{31}P tensors is sensitive to the state of esterification and/or protonation¹⁰⁴ of the PO_4 group. In anisotropic environments, the NMR resonance frequencies are orientation dependent. Consequently, the chemical shift frequencies and dipolar-coupling interactions are all dependent on the specific orientation of the interaction tensor with respect to the magnetic field. However to quantitatively interpret these frequencies for orientational constraints, we need two important pieces of information: (i) a precise knowledge of the static tensor elements, i.e. their magnitudes and orientation with respect to molecular frame. (ii) the refined model for molecular motions that result in averaging of the tensor.

Within liquid crystalline bilayers, motions are strongly anisotropic. Consequently the averaging of chemical shift and dipolar interactions is incomplete resulting in broad NMR lineshapes. For example, fast rotational motions around one axis reduce the chemical shift anisotropy represented by the spectrum. The amount by which it is reduced is related to the amplitude of the motion. In case of isotropic motion, the spectrum collapses to a single peak with a chemical shift identical to that, which would have been observed in a solution spectrum. Furthermore, the shape and the width of the spectrum critically depends on the orientation of the axis of motional averaging with respect to the principal components of the chemical shift tensor σ_{11} , σ_{22} and σ_{33} . Therefore the ^{31}P spectral lineshapes are sensitive to both type and rate of motions. By using low temperature experiments, molecular diffusion can be essentially eliminated. Once both the static and motionally averaged tensors are characterised, it is possible to measure orientational constraints in a quantitative manner¹⁰⁵. This chapter describes the initial efforts carried out to analyse the orientational behaviour of phosphoserines within model peptides, when reconstituted in membrane bilayer.

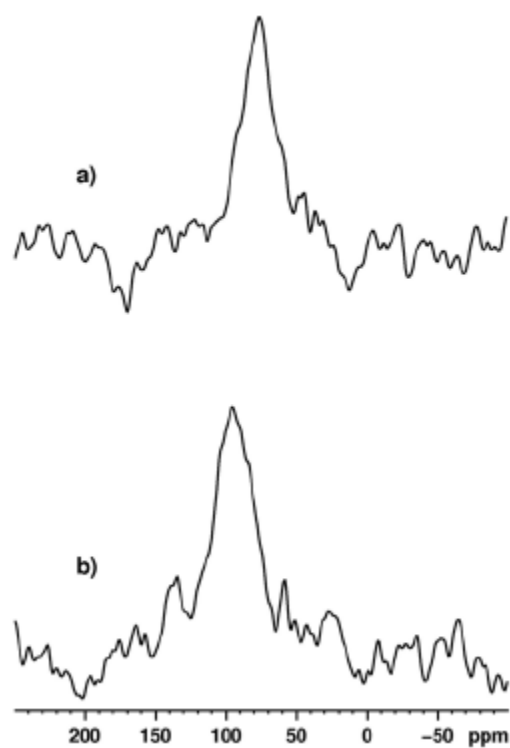


Fig.3.1. Proton decoupled ^{15}N solid-state NMR spectra of 2mol% a) (Pser-9)LS14 and b) (Pser-6)LS14 reconstituted in DOTAP lipid bilayer at pH 7.5, 93% r.h and at room temperature.

3.2 Materials and methods

For current solid-state NMR studies, we have chosen an amphipathic peptide sequence similar to the ones studied in the chapter 2, comprising leucine and serine residues. Apolar leucines and polar serines that interact favourably with lipid bilayer and in membrane environment have a strong propensity for alpha-helix formation. For solid-state NMR measurements, peptides sequences of 14 residues were synthesized with ^{15}N labeled leucine (at position 7) and phosphoserine (at position 6 or 9). For both the peptides, the ^{15}N labelled leucine is thus located in the centre of the alpha-helix. The details about the synthesis, purification and reconstitution in lipid bilayers are described in chapter 2.

(Pser-6)LS14: LSSLL^PS^{15N}LLSSLLSL

(Pser-9)LS14: LSSLLS^{15N}LL^PSSLLSL

Solid-state NMR spectra were acquired on a wide-bore Bruker AMX 400 MHz Avance spectrometer as described previously (chapter 2). A flat coil probe, specially developed for oriented membrane samples or a 4 mm MAS probe for unoriented samples were used. Proton-decoupled ^{31}P NMR spectra were recorded using Hahn-echo or cross-polarization pulse sequences. Proton-decoupled ^{15}N solid-state NMR spectra were acquired using a cross-polarization pulse sequence.

We used DMfit, a program developed by D.Massiot and C.Bessada¹⁰⁶ for the spectral analysis of the side band pattern of one-dimensional solid-state NMR spectra. We used the following convention for the calculating NMR parameters: $|\sigma_{33} - \sigma_{iso}| > |\sigma_{22} - \sigma_{iso}| > |\sigma_{11} - \sigma_{iso}|$. We used 64 number of steps and 8192 number of points for the computing the spectra.

3.3 Results and discussion

Our main goal in this research work was to probe ^{31}P characterization for phosphoserine in lipid bilayer using solid-state NMR spectroscopy. In order to test this, initially we proceed by investigating proton-decoupled ^{15}N oriented solid-state NMR. We used a cationic lipid DOTAP to avoid the background signal of phosphorus. Figure 3.1 show proton-decoupled ^{15}N solid-state NMR spectra, when (Pser-6)LS14 and (Pser-9)LS14 are reconstituted in DOTAP bilayer at room temperature, pH 7.5 and 93% relative humidity. Chemical shift value of about 75 ppm (Figure 3.1a) and 96 ppm (Figure 3.1b) are indicative of an in-plane orientation of both the peptides

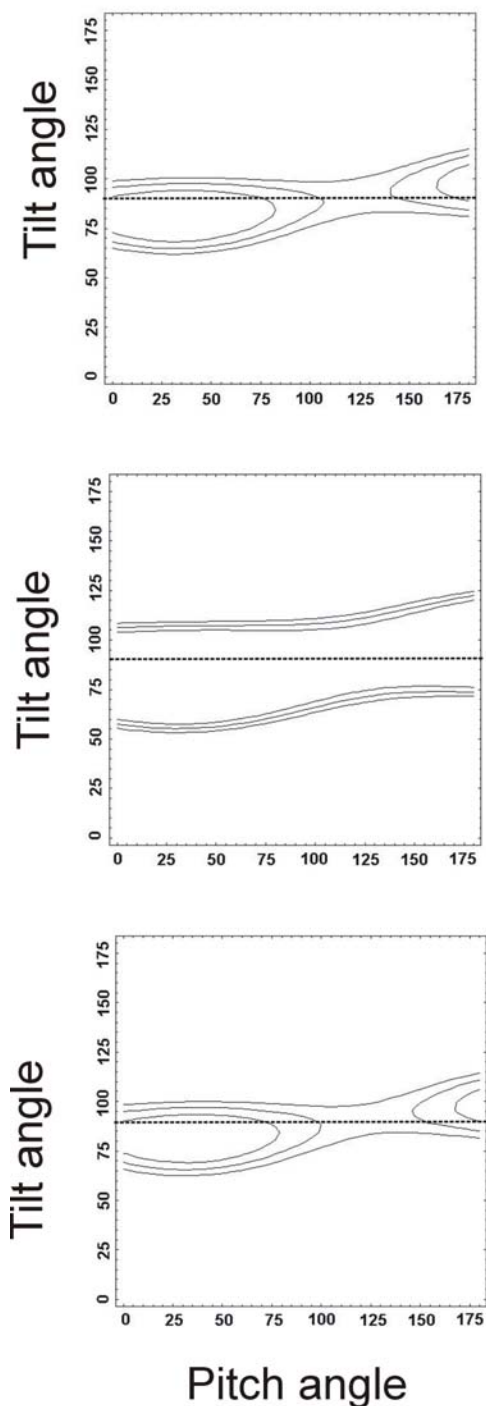


Figure 3.2: The possible spatial orientations of the LS14 peptide from ^{15}N analysis are represented by the helical tilt and the rotational pitch angles. The orientational contour is for the experimental chemical shift measurement and $\pm 5\text{ppm}$ deviation are shown. The successive rotations of the helix around the helix long axis (z-direction) and an axis perpendicular to that (y-direction) are illustrated. a) (Pser-9)LS14, b) (Pser-6)LS14 and c) LS14.

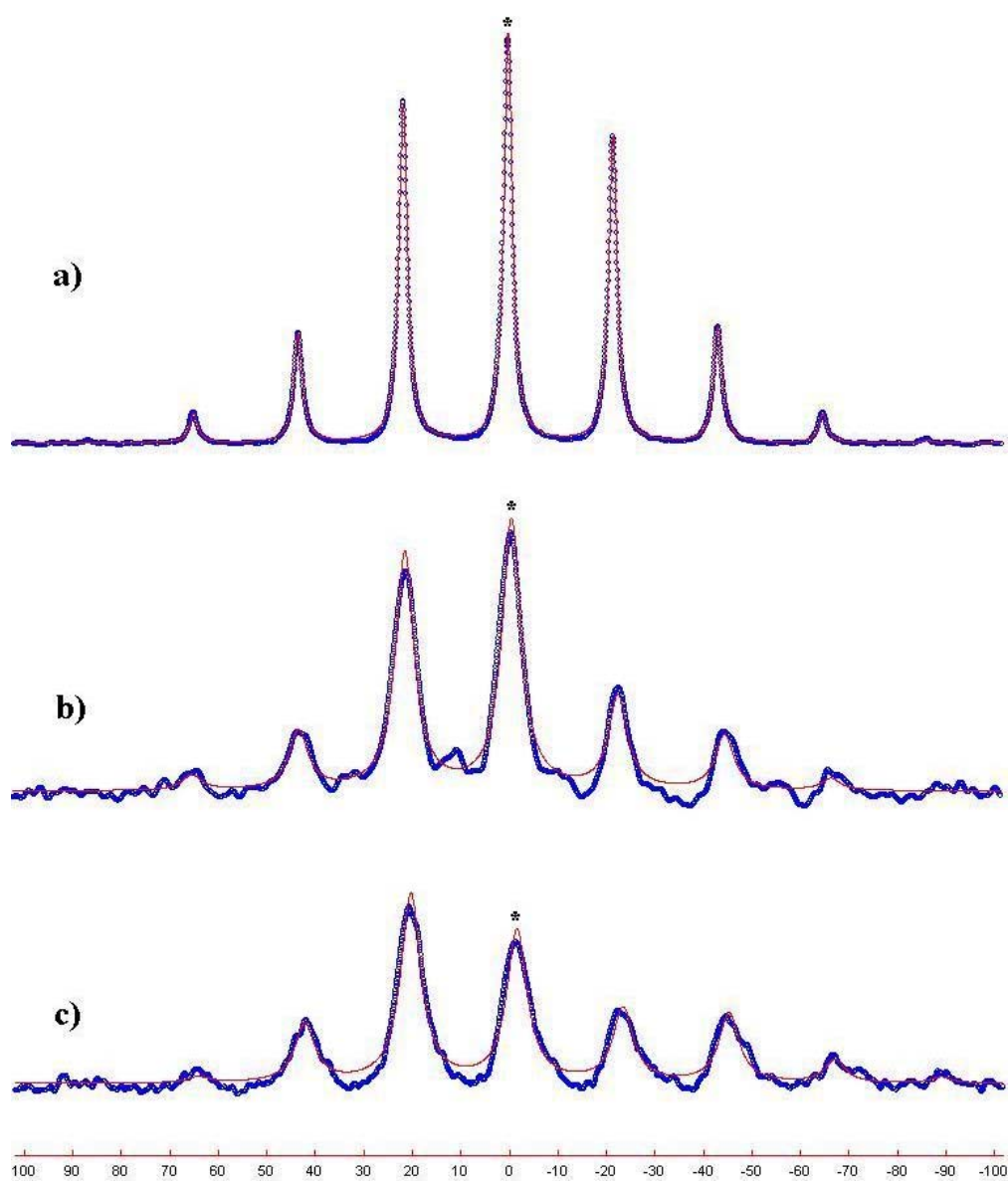


Figure 3.3: CP-MAS ^{31}P solid-state NMR spectra of phosphorylated peptide at room temperature. a) Phosphoserine powder, b) Lyophilized (Pser-9)LS14 and c) Lyophilized (Pser-6)LS14 at 3.6 KHz spinning frequency. Circled line is experimental spectra whereas smooth line is simulated spectra.

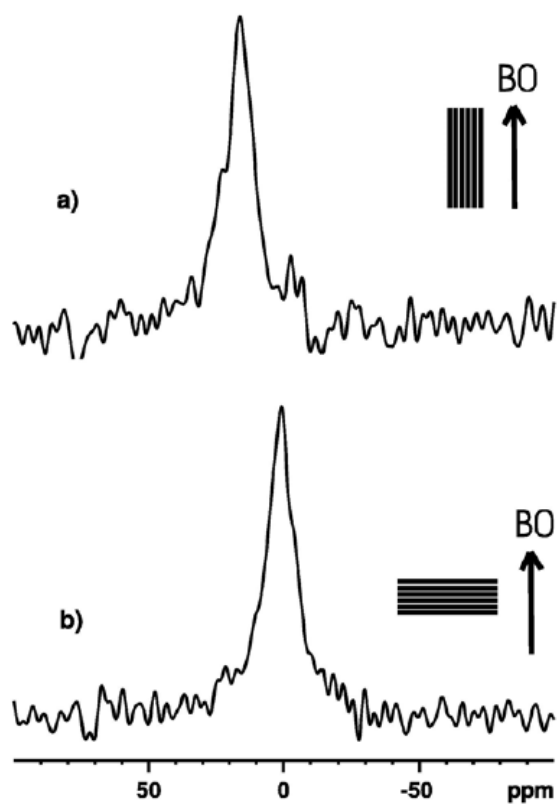


Figure 3.4: Proton-decoupled ^{31}P solid-state NMR spectra of 2mol% (Pser-6)LS14 peptide reconstituted in oriented DOTAP lipid bilayers at room temperature. The glass plates were aligned with normal a) perpendicular and b) parallel to the B_0 field.

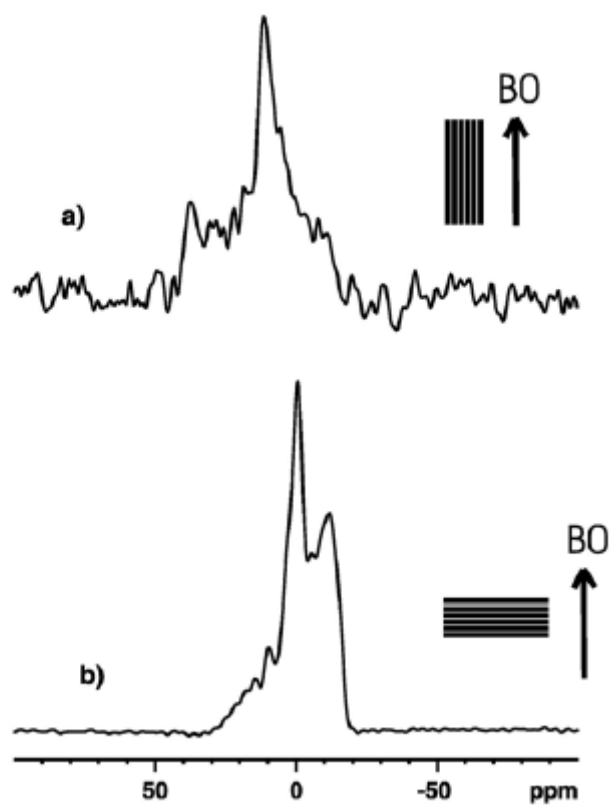


Figure 3.5: Proton-decoupled ^{31}P solid-state NMR spectra of 2mol% (Pser-9)LS14 peptide reconstituted in oriented DOTAP lipid bilayers at room temperature. The glass plates were aligned with the normal a) perpendicular and b) parallel to the B_0 field.

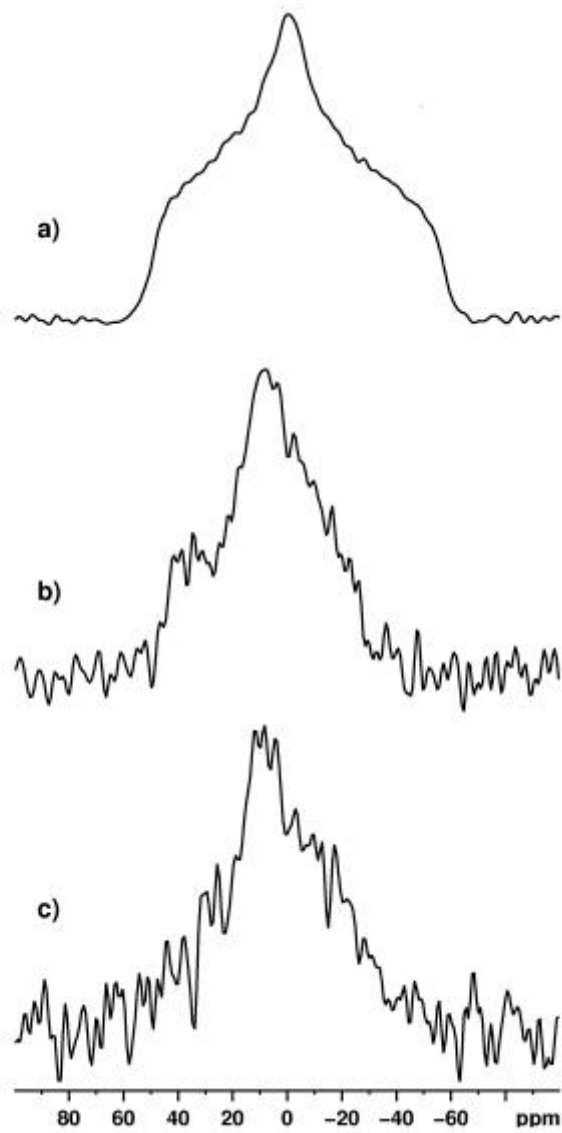


Figure 3.6: Proton-decoupled ^{31}P solid-state NMR spectra of a) phosphoserine powder sample at RT and b) (Pser-6)LS14 c) (Pser-9)LS14 reconstituted in DOTAP lipid bilayers at -25°C .

to the membrane surface, when reconstituted in a cationic DOTAP lipid bilayer. Interestingly the ^{15}N chemical shift value 75 ppm of (Pser-9)LS14 is same as LS14.

Contour figure (Figure 3.2) represents the spatial alignments of (Pser-6)LS14, (Pser-9)LS14 and LS14 that agree with the measured ^{15}N chemical shift. In order to calculate this, peptide model was been placed in the reference coordinate system, where initially the z-axis was oriented parallel to the helix axis. The z-y plane separates the hydrophobic from the hydrophilic part of the amphipathic polypeptide. The peptide was successively rotated around two angles perpendicular to each other. For each alignment the resulting values of ^{15}N chemical shift was calculated.

In a next step, the powdered sample of phosphoserine and dry peptides of LS14 labelled with phosphoserine were investigated by proton-decoupled ^{31}P solid-state NMR. The proton-decoupled ^{31}P solid-state NMR line shape of the phosphoserine powder (Figure 3.3a and 3.6a) exhibits the characteristic features of a nonaxial shielding tensor. The values of the principal elements of phosphoserine shielding tensors obtained by Kohler and co-workers are given in the following table:

Table 3.1: Values of the chemical shielding tensors of phosphoserine¹⁰⁷

	σ_{xx}	σ_{yy}	σ_{zz}
L-phosphoserine	-53	-4	59

Side band patterns of the powdered samples of dry (Pser-6)LS14 and (Pser-9)LS14 (figure 3.3c and 3.3b) are measured at spinning rate of 3.5 KHz at magic angle spinning solid-state NMR spectroscopy.

When (Pser-6)LS14 and (Pser-9)LS14 are reconstituted in non-oriented DOTAP lipids at pH 7.5 and 93% were investigated by ^{31}P MAS solid-state NMR, two isotropic peaks are observed for (Pser-9)LS14 around 1.3 ppm and 2.9 ppm (Figure 3.7a). On the other hand, the ^{31}P MAS spectrum of (Pser-6)LS14 exhibits a single peak at 2 ppm with much reduced side-bands intensities (Figure 3.7b).

Proton-decoupled ^{31}P static solid state NMR studies of (Pser-6)LS14 when reconstituted in oriented DOTAP lipids are characterized by ^{31}P chemical shift values of 3 ppm and 16 ppm, when the glass plates are oriented with the normal perpendicular and parallel to the B_0 field respectively. At alignments of the sample normal parallel to B_0 field, two contributions are observed for (Pser-9)LS14 with a dominant peak at 0 ppm and a broad line shape extending from a maximum 14 ppm into the + 30 ppm region (Figure 3.5b). When the sample is tilted by 90° ,

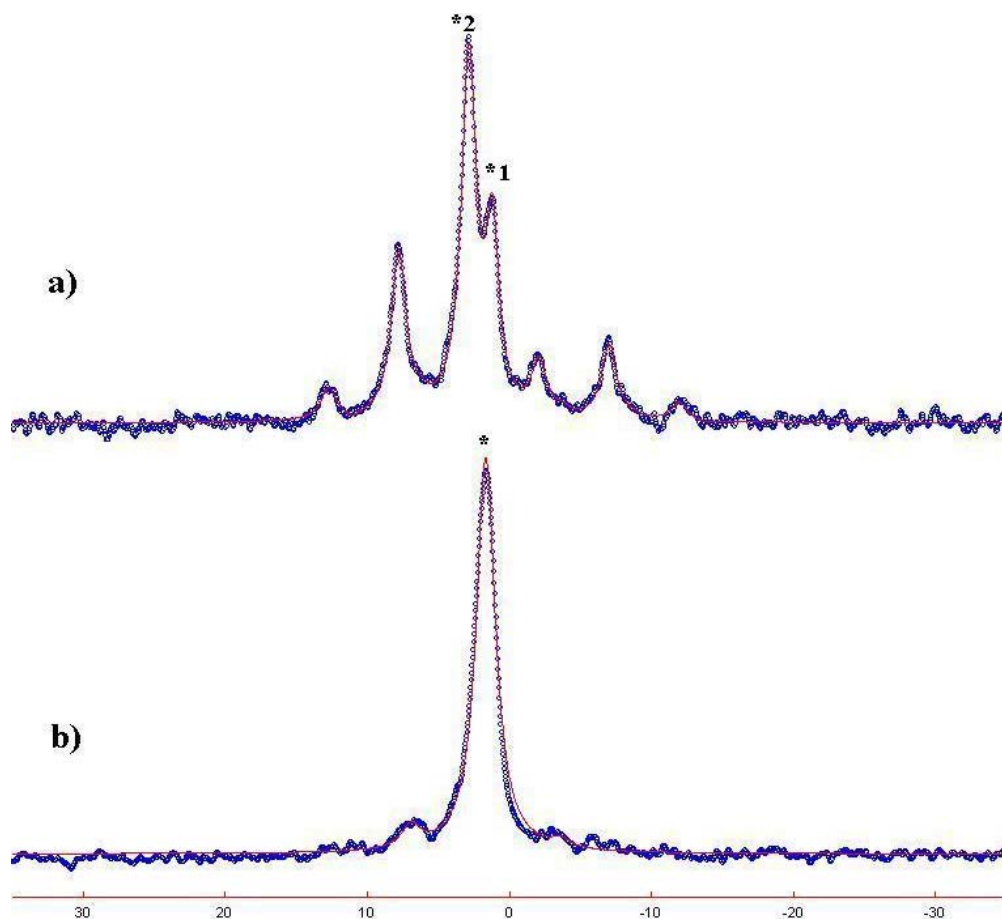


Figure 3.7: CP-MAS ^{31}P solid-state NMR spectra of 2mol% phosphorylated peptides reconstituted in DOTAP lipid bilayer at pH 7.5, 93% r.h. and at room temperature. a) (Pser-9)LS14 b) (Pser-6)LS14 at spinning frequency of 1KHz. Circled line is experimental spectra whereas smooth line is simulated spectra. Isotropic peaks are denoted by a star sign.

a sharp signal intensity at 14 ppm and a broad equi-intensive resonance from 14 ppm to 40 ppm is observed (Figure 3.5a). These data are suggestive of two different ^{31}P serine populations in the sample. Whereas the first one resembles in CSA of the Pserine 6 site and the second population exhibits under reduced motional averaging. In order to reduce the motional averaging, the phosphorylated peptides reconstituted in oriented DOTAP lipid bilayers were investigated at low temperature. Below -10°C , considerable line broadening was observed in proton-decoupled ^{31}P solid-state NMR experiments indicating that amino acid side chain motions of (Pser-6)LS14 and (Pser-9)LS14 are restricted (Figure 3.6).

The sideband analysis allows the size of the average tensors to be obtained and are summarized in the following table.

Table 3.2: ^{31}P values of the principal tensor elements δ_{ii} and corresponding anisotropic parameters of phosphorylated peptides

	σ_{iso} (ppm)	η	δ (ppm)
L-phosphoserine	0	0.9	56.2
(Pser-6)LS14 dry peptide	-1.6	0.3	65.6
(Pser-9)LS14 dry peptide	-1.0	0.0	57.1
(Pser-6)LS14 in DOTAP	1.7	0.0	4.2
(Pser-9)LS14 in DOTAP	2.9(*2)	0.4	3.5
	1.3(*1)	-	-

Potential errors in σ_{xx} , σ_{yy} and σ_{zz} are ± 4 ppm; principal values are sorted as $|\sigma_{zz} - \sigma_{iso}| > |\sigma_{yy} - \sigma_{iso}| > |\sigma_{xx} - \sigma_{iso}|$, Δ_{CS} is the axially of the CSA tensor ($\sigma_{zz} - \sigma_{iso}$), η_{CS} is the asymmetry parameter of the CSA tensor $= (\sigma_{yy} - \sigma_{xx}) / (\sigma_{zz} - \sigma_{iso})$

The observation of the (partial) collapse of the spectra when unoriented samples are measured at the magic angle, indicates that there is considerable motional averaging of the phosphoserine side chain, when the LS14 peptides are reconstituted in hydrated DOTAP lipid bilayers. Intriguingly, (Pser-6)LS14 exhibit a single peak, whereas (Pser-9)LS14 exhibit one of the peaks similar to (Pser-6)LS14 when reconstituted in DOTAP lipid bilayers. This indicates that another contribution undergoing less averaging. Nevertheless, to proceed further, it is necessary to understand the nature of orientation i.e. whether the orientation is due to the whole peptide around

bilayer normal or from the side chains. However, the residual anisotropy indicates that the motional averaging is not complete. Therefore, the obtained distribution function can be further used to derive orientational constraints from aligned samples to derive a model for the interactions.

The goal of the entire discussion is not to state the definitive model of orientation or motion, but rather to test the feasibility and to give an indication of how this data may be used further to understand the orientation of the phosphorylated peptides in membranes in future works. However, an in depth qualitative analysis of orientation and motional behaviour of the phosphate attached to serines is needed to reiterate the statements about the orientational behavior of phosphorylated peptides reconstituted in lipid bilayers.

Chapter 4

Membrane associated α -helical segments of Bcl- X_L and Bax-C terminus investigations by solid-state NMR spectroscopy

4.1 Introduction

Apoptotic cell death is thought to be mediated through two main pathways¹⁰⁸, one through death receptors and the other using mitochondrial pathways. However, there are different hypotheses for explaining the permeabilization of the mitochondrial outer membrane. While one theory says that mitochondrial outer membrane (MOM) is nonspecifically ruptured; the other theory proposes the formation of ion-channels that allow cytochrome c release^{109,110}.

The B cell lymphocyte-2 (Bcl-2) family of proteins is known to play a key role in controlling mitochondrial membrane permeation (MMP) and anomalous expression of these proteins has been implicated in several diseases, including cancer, autoimmunity, AIDS, stroke and myocardial infraction¹¹¹. Anti-apoptotic proteins such as Bcl-2, Bcl- X_L inhibit MMP, whereas pro-apoptotic Bcl-2 homologues such as Bax, Bak, and BH3-only proteins induce MMP^{112,113}. Confocal microscopy and immuno fluorescence analysis on Bcl- X_L proteins have revealed their different local-

izations within the cell e.g. MOM, endoplasmic reticulum(ER) and nuclear envelope (NE) membranes^{114,115}. However, the Bax protein is known to exist primarily as a monomer in the cytosol¹¹⁶ of healthy cells and oligomerizes during apoptosis. Upon undefined pro-apoptotic signaling, Bax is assumed to undergo conformational changes,^{117,118}, resulting in translocation and integration into the mitochondrial outer membrane^{119,120,121}. The solution structure of Bax reveals that its COOH-terminal tail (α -helix9) folds back into a hydrophobic pocket of the protein which is also the binding site for the BH3 domains of other Bcl-2 family members¹¹⁸. The conformational change that allows the carboxy terminus to enter mitochondrial membranes must disengage the C-terminus from the protein, thereby exposing the hydrophobic BH3 binding pocket to participate in dimer formation. This would indicate that structural changes are associated with Bax activation. The exact mechanism of the association of Bax with the mitochondrial outer membrane during apoptosis is not well understood. As the carboxyl terminus is essential for targeting to mitochondria¹¹⁷, it is desirable to investigate the membrane association of full length Bax and in particular its C terminus.

The anti-apoptotic Bcl-X_L three-dimensional structure showed structural similarities to the pore-forming domains of bacterial colicins E1, A and diphtheria toxin^{122,123,124}. The three-dimensional structures of Bcl-2 family members consist of two central, predominantly hydrophobic α -helices surrounded by six or seven amphipathic α -helices of varying lengths. A long, unstructured loop is present between the first two α -helices, whereas the soluble pore-forming domain of Colicin A consists of 10 α -helices with two outer layers (helices 1, 2, and 3-7, respectively) sandwiching a middle layer of three helices (8-10). Helices 8 and 9 form a hairpin. In their solution structures, Bcl-X_L proteins contain two central helices (alpha5 and alpha6 in Bcl-X_L) surrounded by amphipathic helices. The proteins also contain flexible loops connecting the helices¹²². However, solution NMR studies of Bcl-X_L indicate major unfolding and an open structure in micelles¹²⁵. The structural similarity of the Bcl-2 proteins to diphtheria toxin and colicins suggested that the proteins could possess a channel-forming activity¹²². This contention is also supported by observation of ionic channels using lipid bilayers and liposomes¹²⁴.

In order to understand the exact function of Bcl-X_L, it is desirable to understand their association with lipid bilayers. For studying membrane interactions, it is necessary to have full length of Bcl-X_L protein including its hydrophobic C-terminus available in considerable quantities. Site directed mutagenesis and dele-

tion constructs have clearly indicated the implication of the $\alpha 5$ and $\alpha 6$ helices of Bcl-X_L in ion-channel activity, cytotoxicity, and interaction with pro-apoptotic proteins^{126,127,128}. Unfortunately, the expression and purification of full length Bcl-2 family proteins remains difficult with yields unsuitable for a full fledged solid-state NMR structural investigations. Whereas work on optimizing the conditions for preparations of full length Bcl-2 proteins continues in our laboratory, we have studied individual domains of the proteins which can be obtained by solid-phase peptide synthesis. The structural details of membrane-associated Bcl-X_L and Bax proteins in their monomeric or channel forming conformations (a process associated with reorganization of their tertiary structure) certainly increase our knowledge about how these proteins fulfill their regulatory functions and hence how their malfunction lead to apoptotic cell death^{124,129,130}. Therefore we have investigated Bax-C terminus, $\alpha 5$ -loop- $\alpha 6$ and the hydrophobic C terminus of Bcl-X_L reconstituted in phospholipid bilayers. Using proton-decoupled ³¹P and ¹⁵N solid-state NMR spectroscopy, we try to understand how these peptides interact with the membrane bilayers for stable insertion.

For the analysis of the structure, dynamics, and orientational distribution of helical peptides reconstituted in membrane bilayers, solid-state NMR spectroscopy has been employed as a successful method^{31,32,33}. Site-specific isotope labeling of amino acids made it more reliable for solid-state NMR which yields a sensor for the orientation and dynamics at the site of particular residue(s). In static oriented samples, the chemical shift of ¹⁵N labelled peptide is dependent on the alignment of the polypeptide with respect to the magnetic field direction. As a consequence, the well-characterized ¹⁵N chemical shift provides information for the membrane alignment of helical peptides. ¹⁵N chemical shifts smaller than the isotropic value are correlated with helix orientations approximately parallel to the membrane surface, whereas larger chemical shifts are indicative of transmembrane alignments³¹.

4.2 Materials and methods

HLH, Bcl-X(C) and Bax-C peptides were prepared by solid-phase peptide synthesis on a Millipore 9050 or an Applied Biosystems 433A automatic peptide synthesizer using Fmoc (9-fluorenylmethyloxycarbonyl) chemistry^{72,73}.

The HLH peptide (RDGVN~~W~~GRIVAF~~FS~~FGGALCVESVDKEMQVLVSRIA~~AW~~-

MATYLNDHLE) has been synthesized by using a Tentagel R PHB-Glu(t-Bu) resin (RAPP Polymer, Tubingen, Germany). By applying double couplings at each step, by acetylating non-reacted fragments and in particular, and by using the 'pseudo proline' method⁷⁴ at the Phenylalanine-serine(13-14), Glutamic acid-serine(22-23), and Valine-serine(32-33) positions (Fmoc-Phe-Ser(Ψ -Me, Me Pro)-OH; Fmoc-Glu(OtBu)-Ser(Ψ -Me, Me Pro)-OH; Fmoc-Val-Ser(Ψ -Me, Me Pro)-OH purchased from Nova Biochem), we have got a good yield during the HLH synthesis. At the 11th and 36th positions of HLH, the ¹⁵N labeled derivative of alanine was inserted (Cambridge Isotopes Inc., USA).

The Bcl-X(C) peptide (ERFNRWFLTGMTVAGVLLGSLFSRK) was synthesized by using a Tentagel R PHB-Gly Fmoc resin (RAPP Polymer, Tubingen, Germany). The yield of Bcl-X(C) was improved by applying double couplings at each step. At the 14th position of Bcl-X(C), ¹⁵N labeled derivative of alanine was inserted (Cambridge Isotopes Inc. USA).

The synthetic products were purified by reversed phase high performance liquid chromatography using an acetonitrile/water gradient (218TP54 Column, C18, 300Å, 5 mm, 4.6 mm i.d. 250 mm; Vydac France).

The Bax C terminal peptide (GTPTWQTVTIFVAGVLTASLTIWKKMG) was synthesized by growing the chain on a Fmoc-Lys(Boc)-wang resin (Nova-biochem, Darmstadt, Germany). Peptide yield was improved by double coupling all the residues. At the 13th position of Bax C, the ¹⁵N labeled derivative of alanine was introduced (Cambridge Isotopes Inc., USA). The synthetic peptide was then purified by using reversed phase high performance liquid chromatography using an acetonitrile / water gradient (Prontosil 300-5-C4 5.0m column; Bischoff Chromatography, Leonberg, Germany). The identity and purity of the synthesized peptides were analyzed by using the matrix-assisted laser desorption ionization mass spectrometry (MALDI-MS) and analytical reverse phase HPLC.

The lipids 1-palmitoyl-2-oleoyl-*sn*-glycero-3-phosphocholine (POPC) as well as the 1-palmitoyl-2-oleoyl-*sn*-glycero-3-phospho-L-serine (POPS), and 1,2-dioleoyl-*sn*-glycero-3-phosphoethanolamine (DOPE) were purchased from Avanti Polar Lipids (Birmingham, AL). The phospholipid 1,2-dioleoyl-*sn*-glycero-3-[phospho-*rac*-(1-glycerol)] (DOPG) was purchased from Sigma Aldrich (Lyon, France)

In order to reconstitute Bcl-X_L in oriented membrane bilayers, 10 mg of the peptide was dissolved in 5 ml of hexafluoroisopropanol. In parallel about 150 mg of DOPC:DOPG (70:30%) lipid was dissolved in 4.5 ml of chloroform. The lipid

and peptide solutions were mixed to yield 1 mol% peptide-to-lipid molar ratio. As addition of water/ buffer results in phase separations during the sample preparations, the pH of the HLH was not modified by addition of aqueous NaOH and a final pH of 6.5 was obtained.

Bcl-X(C) samples were prepared by dissolving around 11 mg of the peptide (2 mol% of the lipid) in 2 ml of trifluoroethanol. At this stage, the pH of the sample was set to 7.5 pH by using about 65 μl of 1 mM Tris buffer and 45 μl 1 N NaOH. In parallel, about 250 mg POPC were dissolved in dichloromethane. Mixing the appropriate amounts of peptide and lipid solutions resulted in clear solutions.

In order to reconstitute the Bax-C peptide into oriented lipid bilayers, about 11 mg peptide was dissolved in hexafluoroisopropanol (3 ml) and mixed with 250 mg of POPC. During the preparation the pH of the sample was set to 7.5 pH using 65 μl of 1mM Tris buffer and 60 μl 1N NaOH and the peptide-to-lipid molar ratios were maintained at 2 mol%.

The lipid-peptide mixtures were then applied onto 30 ultra-thin cover glasses (9×22 mm; Paul Marienfeld GmbH & Co. KG, Lauda-Konigshofen, Germany), first dried in air and thereafter in high vacuum (1.8×10^{-2} mbar) over night. The samples were thereafter equilibrated in a closed chamber of 93% relative humidity. This condition of the gas phase is obtained due to contact with saturated salt solution of KNO_3 ,⁷⁵. After 3-5 days the glass plates were stacked on the top of each other and the stacks were stabilized and sealed with teflon tape and plastic wrappings.

For solid-state NMR spectroscopy the samples were introduced into the flattened coils⁷⁶ of a double-resonance probe and inserted into the magnetic field (9.4 Tesla) of a Bruker Avance 400 MHz wide-bore solid-state NMR spectrometer. The samples were oriented with the membrane normal parallel to the B_0 field of the spectrometer. Proton-decoupled ^{15}N solid-state NMR spectra were acquired using MOIST cross-polarization²⁸ and the following parameters: ^1H B_1 field of approximately 45KHz, 1ms contact time, 3s recycle delay, spectral width: 37 KHz, 512 data points, number of acquisitions: 46000. During acquisition the sample was cooled with a stream of air at room temperature. An exponential apodization function (corresponding to a line-broadening of 200 Hz) was applied before Fourier transformation. Chemical shift values are referenced with respect to NH_4Cl (41.5 ppm) corresponding to approximately 0 ppm for liquid NH_3 .

The static ^{31}P solid-state NMR spectra were acquired using a phase cycled Hahn echo pulse sequence^{131,132} and by using the following parameters: ^{31}P 90° pulse

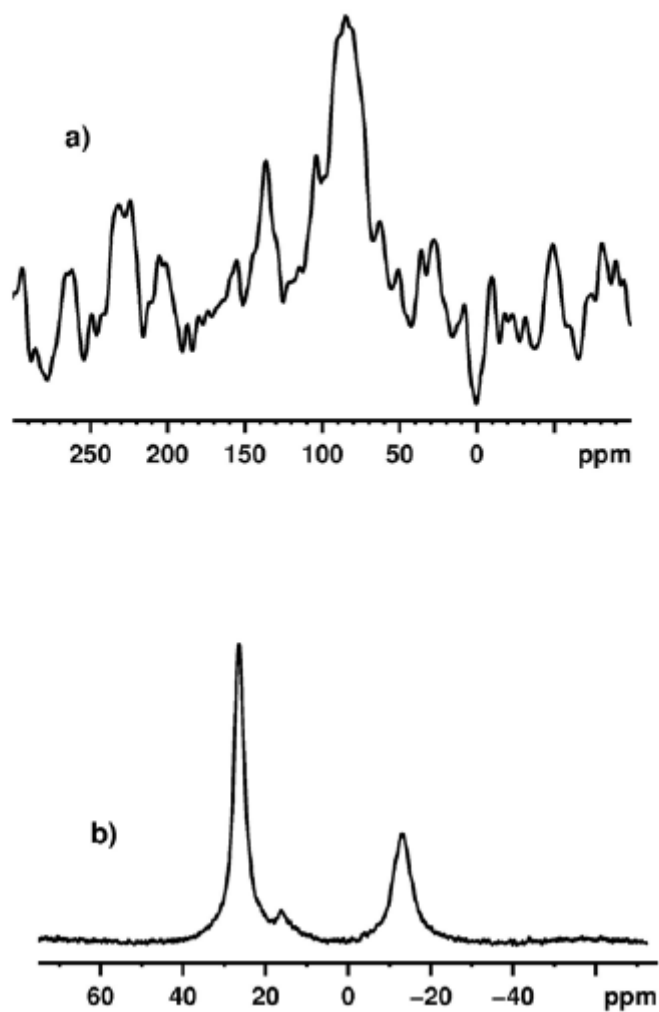


Figure 4.1: Oriented solid-state NMR spectra of 1mol% $\alpha 5$ -loop- $\alpha 6$ reconstituted in 70:30% DOPC:DOPG. a) Proton-decoupled ^{15}N solid-state NMR spectrum and b) ^{31}P solid-state NMR spectrum of $\alpha 5$ -loop- $\alpha 6$. Note that a small peak around 18 ppm may be due to the lipid degradation.

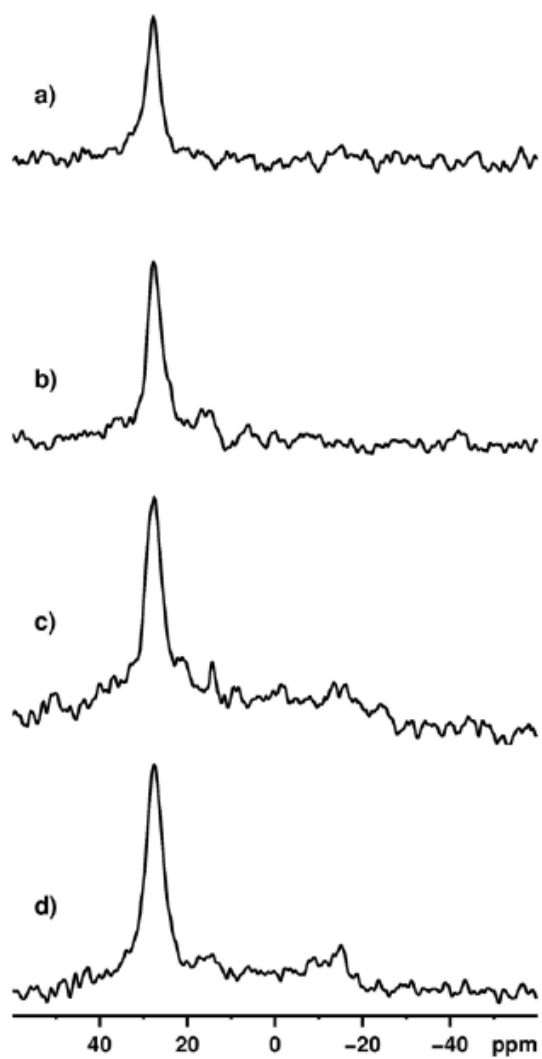


Figure 4.2: ^{31}P solid-state NMR spectra of control of $\alpha 5$ -loop- $\alpha 6$ reconstituted in lipid bilayer. a) 0.5 mol % b) 1.0 mol % c) 1.5 mol % and d) 2 mol % of $\alpha 5$ -loop- $\alpha 6$.

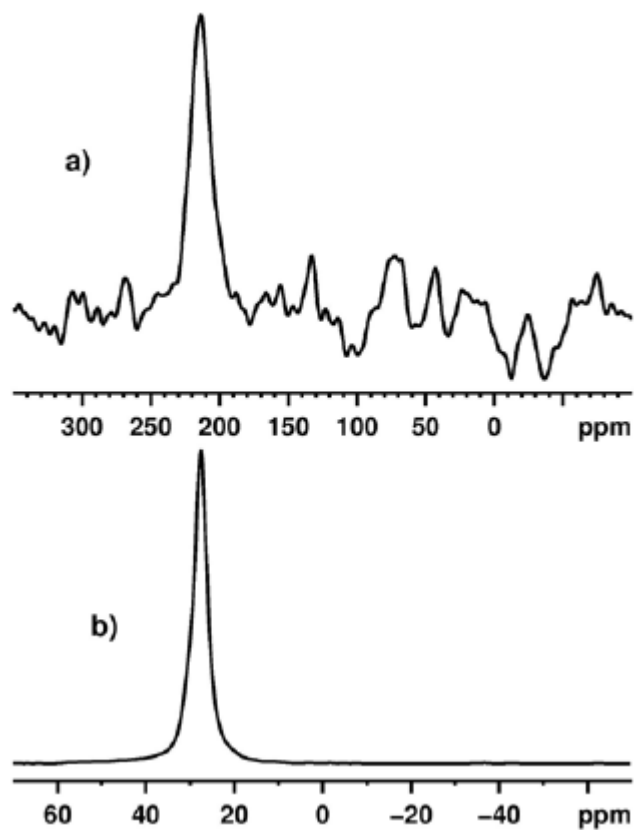


Figure 4.3: Proton-decoupled solid-state NMR spectra of 2 mol% Bcl-X(C) reconstituted in POPC. a) Proton-decoupled ^{15}N solid-state NMR spectrum and b) ^{31}P solid-state NMR spectrum of Bcl-X(C).

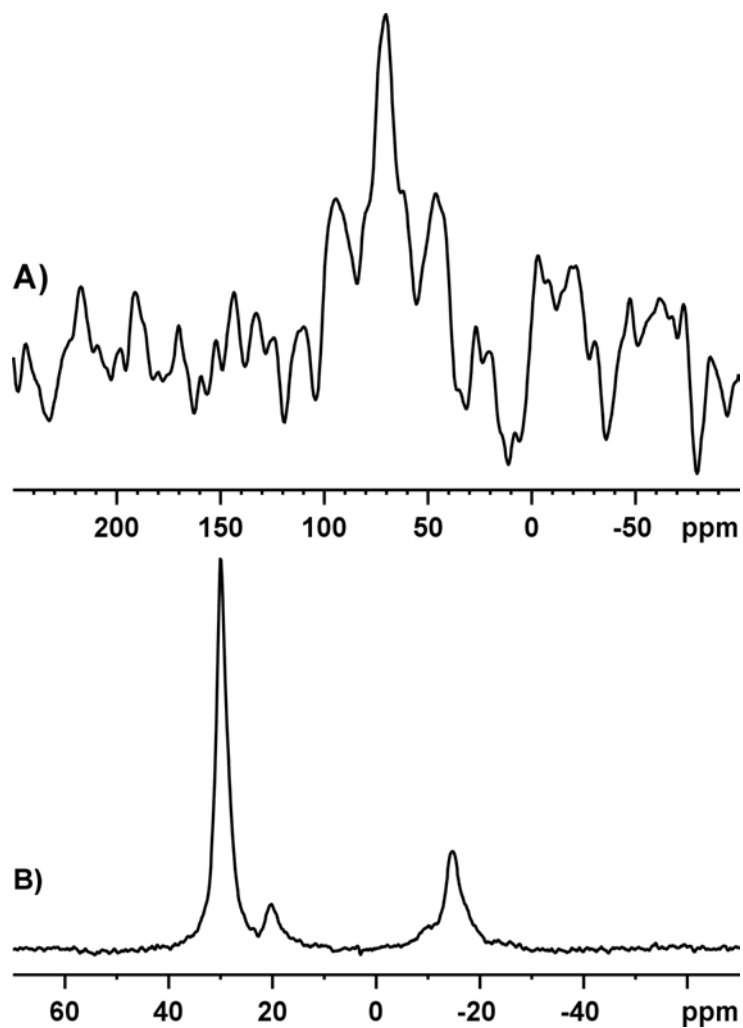


Figure 4.4: Proton-decoupled solid-state NMR spectra of 2mol% Bax-C reconstituted in POPC bilayers. a) Proton-decoupled ^{15}N solid-state NMR spectrum and b) ^{31}P solid-state NMR spectrum of Bax-C. Note that a small peak around 20 ppm may be due to the lipid degradation due to extended hydration.

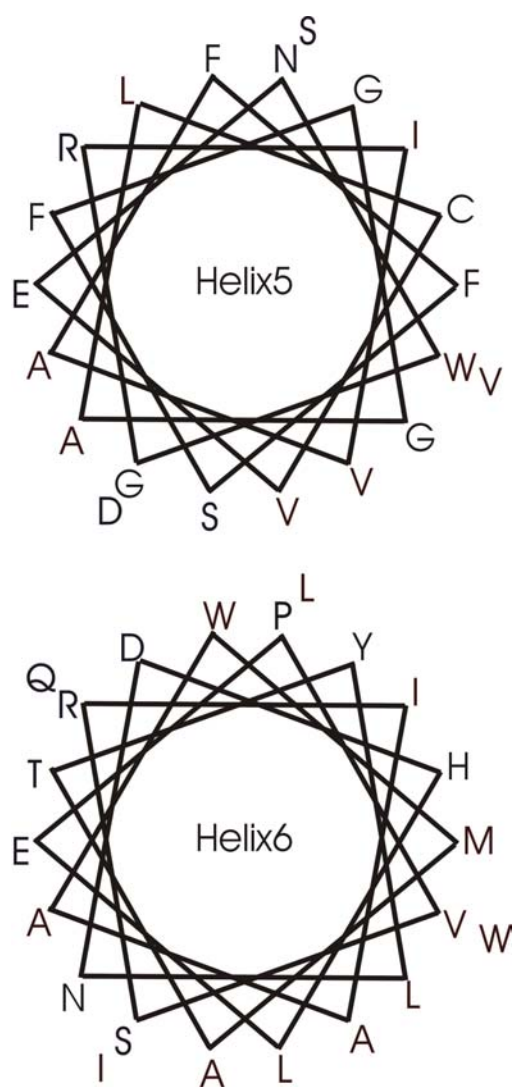


Figure 4.5: Helical wheel representation of $\alpha 5$ and $\alpha 6$ of Bcl-X_L

length 2.2 μ s, recycle delay 3 s, spectral width 26 KHz, 512 data points, number of acquisitions 500. During acquisition the sample was cooled with a stream of air at room temperature. An exponential apodization function (corresponding to a line-broadening of 30 Hz) was applied before Fourier transformation. Chemical shift values were referenced with respect to H_3PO_4 corresponding to approximately 0 ppm.

4.3 Results

In our solid-state NMR investigations, the peptides were reconstituted into mechanically oriented phospholipid membranes, that are spread along the glass surfaces with their normal parallel to the B_0 field. ^{31}P -NMR spectra of these peptides show one predominant ^{31}P resonance observed around 28 ppm (Figure 4.1b, 4.3b and 4.4b). This demonstrates that the phospholipid molecules are oriented with their long axes parallel to the magnetic field direction. However, peptide induced conformational changes or small misalignment of the membranes in the lipid headgroup region¹³³, result in minor contributions to the total ^{31}P signal intensity at chemical shift frequencies between 30 and -22 ppm.

Proton-decoupled ^{15}N solid-state NMR spectra of HLH, Bcl-X(C) and Bax-C polypeptides in oriented lipid bilayers are shown in figure 4.1a, 4.3a and 4.4a respectively. The ^{15}N label is positioned in the central portion of helical segments of $\alpha 5$ and $\alpha 6$ and these NMR spectra are indicative of the orientation of helical polypeptides with respect to the lipid bilayer. From the oriented sample, each spectrum consists of a relatively narrow single line with a resonance frequency within the span of the chemical shift anisotropy (ranging from ~ 230 to 60 ppm^{78,79}). This demonstrates that all the peptides and ^{15}N labeled residues are immobilized by strong interactions with lipid membranes.

In proton-decoupled ^{15}N solid-state NMR, a resonance with maximum intensity at 88 ppm was observed for the two ^{15}N labeled alanines at positions 11 and 36 of HLH. These sites are located almost in the central part of the $\alpha 5$ and $\alpha 6$ helices respectively (Figure 4.5). This value indicates an approximately in-plane orientation of this helix-loop-helix structure. In order to test whether the amount of peptide added to the lipid membranes disrupts the bilayer structure, proton-decoupled ^{31}P spectra at different HLH-to-lipid molar ratio were also recorded (Figure 4.2). The

data indicate that at 1 mol% of helix-loop-helix peptide does not disrupt the membrane bilayer structure.

Figure 4.3a shows proton-decoupled the ^{15}N solid-state NMR spectrum of Bcl-X(C) reconstituted in POPC lipid bilayer. A narrow resonance is observed for the peptide at 213 ppm which is indicative of a transmembrane orientation. The ^{31}P solid-state NMR spectrum of the same sample is clearly indication of an ordered and well oriented POPC bilayer.

Although the signal to noise ratio of the spectrum of Bax-C (Fig. 4.4a) is low, its one predominant resonance at 69ppm is clearly resolved. The ^{15}N chemical shift frequency of the labelled alanine residue in the middle of the helix is characteristic of helix orientations parallel to the membrane surface. Although, both Bcl-X(C) and Bax-C samples were prepared using the same molar ratio, distorted peaks from the ^{31}P solid-state NMR spectrum of the Bax-C sample indicate that contributions resulting from the peptide induced conformational changes in the lipid bilayer.

4.4 Discussion

Structural changes involved in the activation of Bcl-2 family members during apoptosis remain largely unknown. We have investigated segments of Bax and Bcl-X_L with the aim to better understand the mechanism of membrane insertion and the structural organization of these peptides. Earlier investigations indicate that Bcl-X_L and Bax form pores in lipid bilayers and vesicles¹³⁴. However, numerous studies have shown that the C-terminus of the anti-apoptotic proteins Bcl-X_L and Bcl-2 is essential for its membrane insertion and anti-apoptotic function.

Anti-apoptotic Bcl-X_L protein has been proposed to be anchored by its tail containing the C-terminal hydrophobic helix¹³⁵. Mutagenesis analysis on Bcl-X_L suggested a mitochondrial consensus sequence for the C-terminus of Bcl-X_L¹³⁶. Due to their two basic residues in their C-terminus, it was proposed that Bcl-X_L protein are targeted to the MOM¹³⁷. Interestingly, the Bcl-X_L C-terminus fullfils the criteria established for mitochondrial pre-sequences in being around 20 amino acids long, being able to form a basic helix^{138,139,140} and being followed by one or two basic amino acids^{141,142}.

To our knowledge for the first time, using proton-decoupled ^{15}N solid-state NMR spectroscopy (Figure 4.3), we were able to show that the C-terminus of Bcl-x_L is in-

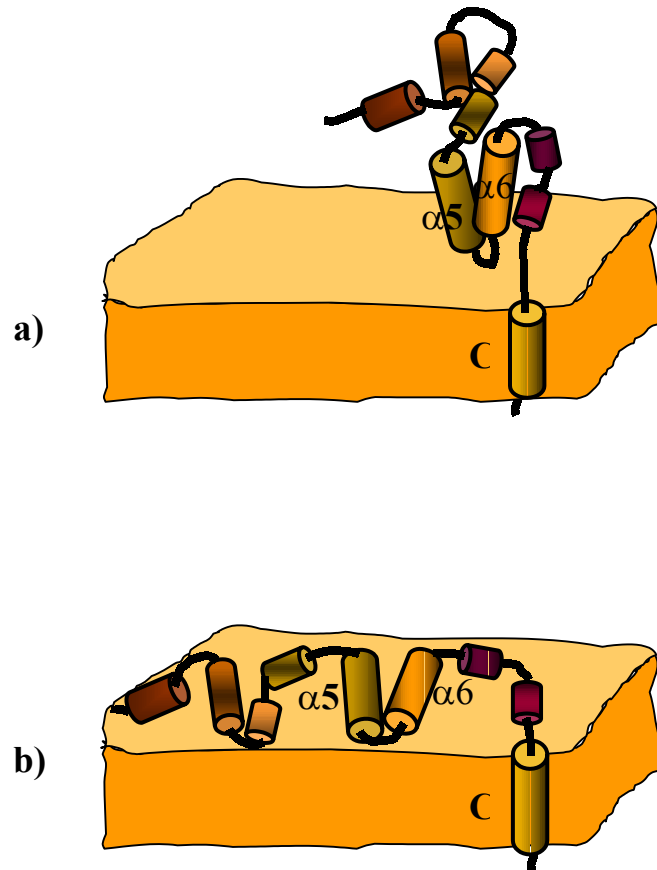


Figure 4.6: Stepwise insertion of helical fragments of Bcl-X_L. The series include first anchoring of the hydrophobic C-terminus (Fig.4.6a), position of channel forming helical hairpin approximately parallel on the membrane surface (Fig.4.6b) .

serted into the membrane in a transmembrane fashion. We studied the $\alpha 5$ -loop- $\alpha 6$ segment at pH 6.5 and in the presence of anionic lipid, because such an environment was also used during ion-channel measurements of the Bcl-X_L protein¹²⁴. This is thought to favor electrostatic interactions between the lipids and the charged peptide. From the proton-decoupled ¹⁵N solid-state NMR result (Figure 4.1), it is evident that $\alpha 5$ -loop- $\alpha 6$ of Bcl-X_L is oriented in-plane with the membrane under the conditions used in our investigations. The proton-decoupled ¹⁵N solid-state NMR data of uniformly ¹⁵N labeled Bcl-X_L protein (lacking the C-terminus) also indicates that the protein is associated with the phospholipid bilayer with its helices parallel to the membrane surface (unpublished data from Aisenbrey, C. Bechinger, B. and Lakey, J. H.). Nevertheless, we can not rule out the possibility that an equilibrium exists between an in-plane and a transmembrane oriented hairpin¹⁴³ under different conditions e.g. highly acidic pH, as proposed by the umbrella model. The channel hypothesis of Bcl-X_L proposes that under low pH condition, Bcl-X_L oligomerizes and inserts into the lipid bilayer to form ion-channels via their hydrophobic 5 and 6 helices^{124,144,145}.

Under the conditions tested here, only a small amount of transmembrane helices would be undetectable by solid-state NMR measurements due to the signal-to-noise ratio. Therefore, we propose the penknife model as an intermediate state of Bcl-X_L, which involves the flipping out of $\alpha 5$ and $\alpha 6$ helices into the membrane like a penknife opening with their hydrophobic surfaces.

Evidence for such a dynamic model also exists for the pore forming domains of colicin A. Liposome bound colicin A revealed that the channel was anchored into the membrane by the hydrophobic C-terminal like an 'umbrella' model¹⁴⁶. Subsequent studies on Colicin A by disulfide bond engineering proposed 'penknife' model, where the channel domain may be bound to the membrane surface with the helical axes approximately parallel to the plane of the membrane and to the other uninserted helices^{147,148}.

However, it might be interesting to investigate whether these $\alpha 5$ and $\alpha 6$ insert into the membrane either by increasing the fraction of negatively-charged lipids or by lowering the bulk pH. This will help in understanding the influence of electrostatic effects on the interaction assisted insertion of helical hairpin into the membrane. Also, it would be worthwhile to investigate the influence of interactions between membrane-bound helices during the insertion process as they might also play a piv-

otal role^{50,149} in the insertion of the pore-forming domain into the membrane.

At least two questions remain to be answered: (i) Is the previously observed channel activity of Bcl-X_L protein at non-physiological pH (pH 4) meaningful, in spite of the observation of changes in pH during apoptosis. (ii) What is the structural basis of the functional differences between Bcl-X_L and Bax proteins? In the proposed umbrella model of Bcl-X_L¹⁴³, the structural investigations were performed with proteins lacking the hydrophobic C-terminus. Therefore it is still intriguing to know whether the full length Bcl-X_L protein can simultaneously accommodate transmembrane insertion of the helix-loop-helix and the hydrophobic C-terminus.

The ensemble of data obtained from our experiments suggests that the hydrophobic C-terminus of Bcl-X_L may function as a signal anchor that also mediates targeting and insertion of the protein into the mitochondrial outer membrane. The bulk of anti-apoptotic Bcl-X_L resides in the membrane surface and only the C-terminal is inserted inside the mitochondrial outer membrane. It is possible that the domain of Bcl-X_L exposed to cytosol could segregate a pro-apoptotic protein e.g. Bax from entering the mitochondrial outer membrane. Therefore it is suggestive that the C-terminus Bcl-X_L is inserted into the mitochondrial outer membrane for protecting the mitochondria from the apoptotic cell death.

The questions remains whether receptors in the mitochondrial outer membrane can discriminate between amphipathic helices and hydrophobic tail-anchoring proteins? Detailed investigations on translocase in the outer membrane of mitochondria (TOM) complex indicate that components of the TOM complex, Tom20, Tom22 and Tom70, can independently act for binding the discrete parts of a mitochondrial precursor protein^{150,151}.

A common mechanism of insertion into membranes between Bcl-2 and Bax has also been suggested mainly on the basis of the structural similarity of their hydrophobic C-terminal and their co-localisation^{144,152}. However, the anchoring function of C-terminus of pro-apoptotic Bax is far less clear. In contrast to Bcl-X_L C-terminus, the proton-decoupled ¹⁵N solid-state NMR data (Figure 4.4a) show that the Bax-C terminus is associated with planar phospholipid membranes at orientations parallel to the surface. Previously it has been demonstrated that the complete deletion or the replacement of C-terminus of Bax by a random coiled sequence enhances membrane insertion of Bax¹⁵³. In spite of both N- and C- termini truncation, Bax mutant still exhibited a binding activity to mitochondria. From the mutagenesis data, it was also proposed that C-terminus of Bax in its native conformation prevents Bax

and mitochondria interaction¹⁵³. Even though Bax-C terminus is hydrophobic, in a cell-free system it has been shown that the hydrophobicity alone cannot impact its specific targeting¹³⁵. In support of this view, F. Vallette and co-workers¹⁵⁴ suggested that in a cell-free system, Bax interacts with the membrane not as a transmembrane fashion. Studies of Bax lacking its C-terminus exhibit that this protein still interacts with mitochondria and kills both mammalian¹⁵⁴ and yeast cells^{153,155}. This suggests that the C-terminus of Bax is not a key element for the mitochondrial targeting and insertion. Therefore, the C-terminal hydrophobic end of Bax may not contain a membrane anchoring signal.

However, it remains possible that the proton gradients that exist across mitochondrial membrane induce Bax conformational changes resulting in the integration of its C-terminus. Also, mutagenesis studies¹¹⁷ have shown that a single amino acid substitution of the C-terminal end of Bax allows its mitochondrial localization. It was suggested that the N- and C terminal ends cooperate in the insertion into the mitochondria. Thus, the in-plane orientation in membrane bilayers may be an intermediate step during activation and membrane insertion of Bax.

Previous studies on Bax also suggested the death of cells by two probable mechanisms: one was linked to Bax channel-formation in the membrane by its alpha5-alpha6 helices^{128,156}. Another mechanism was attributed to the ability of Bax to dimerize with pro-apoptotic Bcl-2 family proteins through its BH3 (alpha-helix2) domain, thereby negating their cell survival functions^{157,158}. Experimental results of Gerd Heimlich and coworkers¹⁵⁹ indicate that Bax without the C-terminal domain can also induce cytochrome c release similar to the full-length Bax proteins. In this study, the deletion of the putative pore forming alpha-helices-5 and -6, restrained the insertion of Bax protein into the mitochondrial membranes. This also reduces cytochrome c-releasing activity of Bax protein. Therefore, it is possible that the C-terminus of Bax is associated in the membrane surface free to interact with its own hydrophobic groove or with the groove of anti-apoptotic proteins thereby burying the hydrophobic residues¹⁶⁰. This might explain the increased solubility of Bax. However, under suitable apoptotic activation conditions, Bax may undergo a conformational change, thereby disengaging its C-terminus for insertion into the mitochondrial outer membrane. Therefore from all the experimental results^{117,153,154,155} we suggest that the Bax C-terminus may be involved for Bax conformation and its solubility in cytosol rather than membrane anchoring.

Chapter 5

^{15}N and ^{31}P solid-state NMR studies of antimicrobial peptides NK-2 and Citropin 1.1. in lipid bilayers

5.1 Introduction

Antimicrobial peptides (AMP) are found in host defence settings and exhibit antimicrobial activity at physiological concentrations. More than 840 antimicrobial peptide sequences have been reported so far *, which comprise 10-50 amino acids. They are known to act against both Gram-positive and Gram-negative bacteria, yeast and fungal strains, protozoa and viruses. In some cases, peptides can also have anti-cancer and haemolytic activities.

Structurally, AMPs belong to three distinct classes based on their 3D structures¹⁶¹: (i) Linear alpha-helical peptides free of cysteines and often of amphipathic structure (ii) peptides with three disulphide bonds with a flat dimeric beta-sheet structure and (iii) peptides with unusual bias in certain amino acids, such as proline, arginine, tryptophan or histidine. Commonly, a positive net charge (to facilitate

*<http://www.bbcm.univ.trieste.it/~tossi/pag2.htm>

binding to bacterial phospholipids) and an amphipathicity with a hinge helps the peptide to associate with the bacterial membrane.

In spite of considerable variation in primary and secondary structures of these antimicrobial peptides, common mechanistic features have been suggested. First, the peptides interact with anionic phospholipids of the microbial membrane. This will lead to membrane permeabilization and pore formation by either peptide-induced ion conduction or leakage through the lipid bilayers. Ultimately cell lysis causes cell death. At least four mechanisms for disruption of membrane integrity have been suggested: (i) the barrel-stave model which is accompanied by a highly cooperative self association of membrane-bound peptides, but is unlikely to be generally applicable to alpha-helical antimicrobial peptides, given the variability in their makeup (ii) The wormhole model, where the antibiotic peptides influence the mobility and structure of fatty acid chains of phospholipids causing the formation of a pore lined with phospholipids and amphipathic molecules. The membrane then loses its selective barrier function between intra- and extracellular medium (iii) The carpet-like model, in which peptide molecules accumulate with an alignment parallel to the surface. The adsorbed peptides disrupt the packing of the lipid molecules, thereafter, the membrane becomes leaky and the cell can no longer maintain an osmotic gradient, (iv) The detergent-like effect, which disintegrates the vesicular membranes by the strain imposed from a high local concentration of the peptide. In-plane inserted peptides and membrane thinning cause disturbance of the bilayer packing within a diameter of $\leq 100 \text{ \AA}$. By the density fluctuation of peptides and associated modulations of local concentrations can result in stochastic membrane openings resulting those observed in more well-defined channels. Notably such 'channels' have also been characterized in the presence of detergents.

The presence of a positive net charge, the hydrophobicity and the alpha-helicity of the peptides have been regarded as major factors effecting their antibacterial activity^{162,163,164,165,166,167,168}. Other studies have revealed that the increase in the net positive charge of membrane-active peptides results in an improvement of their antibacterial activity^{169,170}. It seems possible that the positive net charge and helicity have been adopted to increase the efficiency against bacterial targets, which are characterized by differences in cell wall and cell-membrane.

Amphibian skin is one of the sources of antimicrobial peptides. The discovery of many frog and toads skin peptides has been reported in recent years¹⁷¹. Citropin is an antibiotic and anticancer agent secreted from the glandular skins of Australian

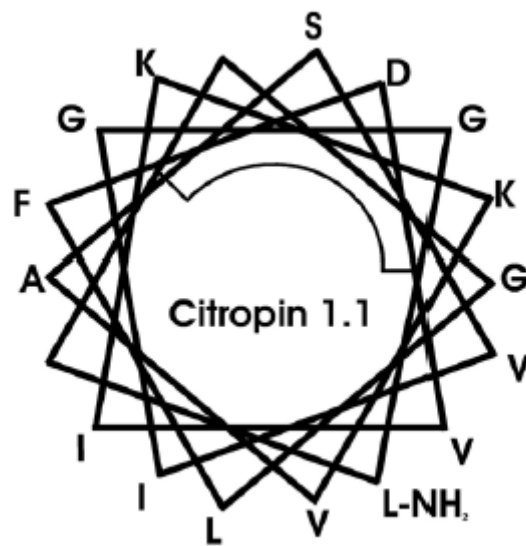


Figure 5.1: Helical wheel representation of citropin 1.1. Note the clear separation of hydrophilic and hydrophobic residues.



Figure 5.2: View of NK-2 region within NK-Lysin. The dark region represents the part of the structure that resembles the synthetic peptide antibiotic NK2 (39-65) deduced from the NK-lysine sequence⁸².

Blue Mountains tree frog *Litoria.citropa*^{172,173}. The peptide has been shown to inhibit neuronal nitric oxide synthase (nNOS) even at 10^{-6} M concentration range. This concentration is significantly less than that required to cause lysis of red blood cells¹⁷⁴. Citropin is known to be particularly effective against Gram-positive bacteria¹⁷². From the solution NMR studies, it is proposed that citropin 1.1 adopts an amphipathic α -helical structure in water/trifluoroethanol mixture¹⁷². The helical wheel diagram of citropin 1.1 shown in figure 5.1.

Another peptide of interest is 27-residues synthetic analog peptide NK-2 (KILRGVCKKIMRTFLRRISKDILTGKK) in which, leucine, serine and tryptophan residues from NK-lysin (figure 5.2) were replaced by valine6, threonine13 and lysine20 respectively. This peptide represents the cationic core region (39-65) of the potent effector molecule NK-lysin (Natural Killer)¹⁷⁵. Earlier studies about NK-2 show that, it exhibits potent activity against bacteria without being toxic against human cells^{175,176,177}. It has been shown that NK-2 adopts an amphipathic alpha-helical structure in hydrophilic environments, i.e, in water¹⁷⁵. We reconstituted NK-2 in POPE:POPG bilayer, at 4:1 ratio. POPG is only abundant in bacterial cell membranes and furthermore as a negatively charged lipid it should act electrostatic counterpart for the cationic peptide. On the other hand, POPE is a critical membrane component because it exhibits a non-planar bilayer structure which is assumed to support membrane fusion or membrane destruction in the case of peptide antibiotics NK-2. Interestingly, the helix-loop-helix structure of the region corresponding to NK-2 within the NK-lysin 3D-structure resembles to the structure of cecropin A¹⁷⁸. Figure 2 shows a view of the NK-2 region inside NK-Lysin.

To understand the function of these antibacterial peptides, the orientation of the peptides in phospholipid bilayer membranes was investigated in this study using proton-decoupled ^{15}N and ^{31}P solid-state NMR spectroscopy. In order to establish the orientation of a peptide or protein domain within the membrane^{37,179,180}, the wealth of information available from orientational dependent NMR frequencies has been used^{15,181}. Generally, in an alpha-helix the amide NH bonds align approximately parallel to the long helical axis. The ^{15}N chemical shifts < 100 ppm are therefore indicative of helix alignments approximately parallel to the membrane surface, whereas chemical shift values > 180 ppm are associated with transmembrane orientations¹⁶. In this chapter, we report the investigations of the structure-function relationship of citropin 1.1 and the NK-2 peptides.

5.2 Materials and methods

The Citropin 1.1 and NK-2 peptides were prepared by solid-phase peptide synthesis on a Millipore 9050 or an Applied Biosystems 433A automatic peptide synthesizer using Fmoc (9-fluorenylmethyloxycarbonyl) chemistry^{72,73}.

Citropin1.1 was synthesized by using a TentaGel S RAM-Leu-Fmoc resin (RAPP Polymer, Tubingen, Germany). This results in C-terminal carboxy amides after the cleavage reaction. At the 10th position of citropin1.1 (cf page iv), the ¹⁵N labeled derivative of alanine was inserted (Cambridge Isotopes Inc., USA). The synthetic products were purified using reversed phase high performance liquid chromatography using an acetonitrile / water gradient and a Vydac 218TP54 Column, C18, 300 Å, 5 mm, 4.6 mm i.d. × 250 mm (Nantes, France).

NK-2 peptides (GLFDVIKKVASVIGGL-NH₂) were synthesized by using the standard synthetic protocols of double coupling for all the residues and by using a Fmoc-Lys(Boc)-wang resin (Novabiochem, Darmstadt, Germany). Either position 6 or 18 of NK-2 (cf page iv), were labelled with the ¹⁵N derivative of valine and isoleucine, respectively (Cambridge Isotopes Inc., USA). The synthetic products were purified using reversed phase high performance liquid chromatography using an acetonitrile / water gradient and a Prontosil 300-5-C4 5.0 μm column (Bischoff Chromatography, Leonberg, Germany).

The identity and purity of the synthesized peptides were analyzed using matrix-assisted laser desorption ionization mass spectrometry (MALDI-MS) and analytical reverse phase HPLC. The lipids 1-palmitoyl-2-oleoyl-*sn*-glycero-3-phosphocholine (POPC), 1-palmitoyl-2-oleoyl-*sn*-glycero-3-[phospho-*rac*-(1-glycerol)] (POPG) and 1-palmitoyl-2-oleoyl-*sn*-glycero-3-phos-phoethanolamine (POPE) were purchased from Avanti Polar Lipids (Birmingham, AL).

In order to reconstitute citropin 1.1 peptide into oriented lipid bilayers, typically 10 mg peptide was dissolved in hexafluoroisopropanol (3 ml) and mixed with 250 mg of POPC lipid in hexafluoroisopropanol. The peptide-to-lipid molar ratio was maintained at 2 mol%. During the preparation the pH of the sample was set to 7.5 using about 65 μl of 2mM Tris buffer and 1N NaOH.

About 11 mg the NK-2 peptide was dissolved in hexafluoroisopropanol. After dissolving the peptide in hexafluoroisopropanol a pH of 6.5 was obtained and the peptide was then mixed with 130 mg (POPE: POPG 4:1) lipids in dichloromethane/methanol

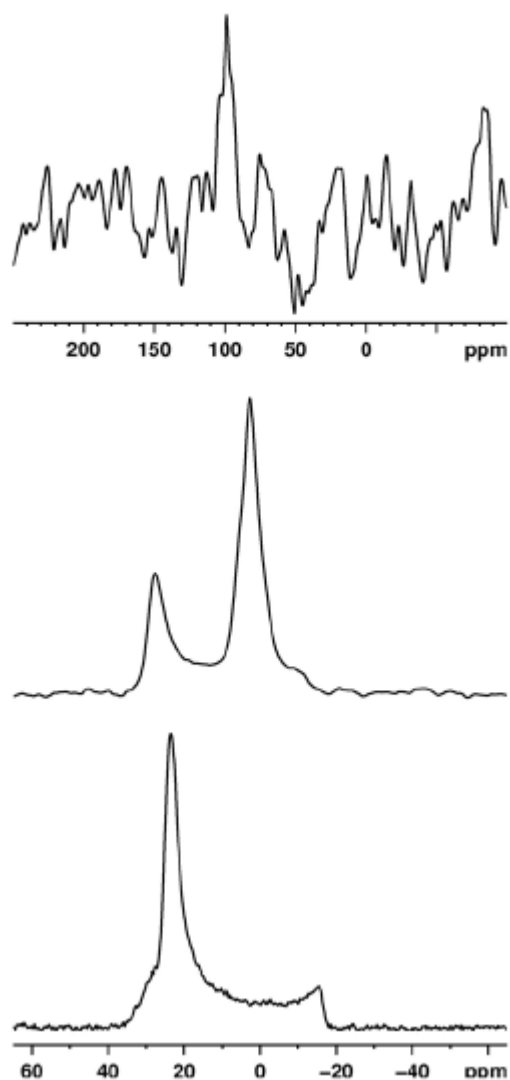


Figure 5.3: Proton-decoupled solid-state NMR spectra of 2mol% NK-2 ^{15}N Val6 in 4:1 POPE:POPG bilayer at room temperature. a) Proton-decoupled ^{15}N solid-state NMR spectrum and b) proton-decoupled ^{31}P solid-state NMR spectra before and c) after 6 hrs incubation at 30° C which is correspond to the above ^{15}N solid-state NMR spectrum a) .

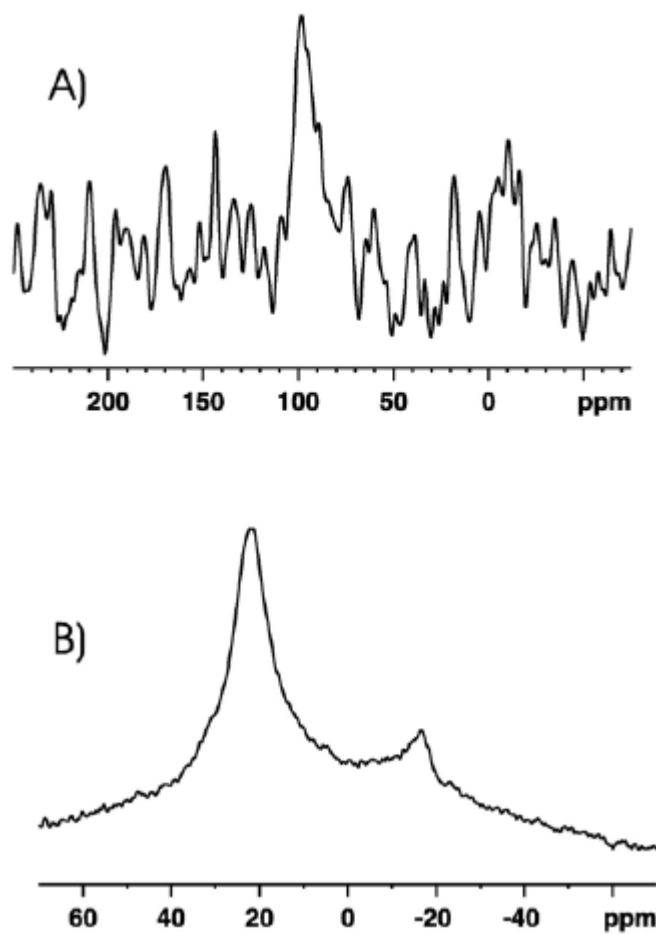


Figure 5.4: Proton decoupled solid-state NMR spectra of 2mol% NK-2 ^{15}N Ile18 in 4:1 POPG:POPE bilayer at room temperature. a) Proton-decoupled ^{15}N solid-state NMR spectrum and b) proton-decoupled ^{31}P solid-state NMR spectrum. Note that the sample was not incubated at 30° C.

(2ml/1ml). The peptide-to-lipid molar ratio therefore was 2 mol%. Since addition of water/buffer results in phase separations during the preparation, this sample was prepared without aqueous additions.

The lipid-peptide mixtures were applied onto 30 ultra-thin cover glasses (9×22 mm; Paul Marienfeld GmbH & Co. KG, Lauda-Konigshofen, Germany), first dried in air and thereafter in high vacuum (1.8×10^{-2} mbar) over night. Thereafter, the samples were equilibrated in a closed chamber where a defined relative humidity 93 % was obtained by contact with a saturated salt solution of KNO_3 ⁷⁵. After 3-5 days the glass plates were stacked on the top of each other. The stacks were stabilized and sealed with teflon tape and plastic wrappings.

For solid-state NMR spectroscopy the samples were introduced into the flattened coils⁷⁶ of a double-resonance probe and inserted into the magnetic field (9.4 Tesla) of a Bruker Avance 400 MHz wide-bore solid-state NMR spectrometer. The samples were oriented with the membrane normal parallel to the B_0 field of the spectrometer. Proton-decoupled ^{15}N solid-state NMR spectra were acquired using the MOIST cross-polarization pulse sequence²⁸. The static solid-state NMR spectra were acquired using the following parameters: ^1H B_1 field of approximately 45 KHz, 1ms contact time, 3s recycle delay, spectral width: 37KHz, 512 data points, approximate number of acquisitions 40000. During acquisition the sample was cooled with a stream of air at room temperature. An exponential apodisation corresponding to a line-broadening of 200 Hz was applied before Fourier transformation. NH_4Cl (41.5 ppm) was used as a reference corresponding to approximately 0 ppm for liquid NH_3 .

5.3 Results

We prepared citropin 1.1 and NK-2 peptides by using solid-phase peptide synthesis, labelled with ^{15}N at a single site within the central part of the polypeptide reconstituted into uniaxially oriented lipid bilayers and investigated by proton-decoupled ^{15}N and ^{31}P solid-state NMR spectroscopy. The orientational dependence of the ^{15}N chemical shift interaction serves as a source of structural information.

Proton decoupled solid-state NMR spectra of NK-2 peptides specifically labelled with ^{15}N at positions Val6 or Ile18 and reconstituted in phospholipid bilayers are shown in figure 5.3 and figure 5.4. Figures 5.3a and 5.4a represent proton-decoupled ^{15}N solid-state NMR spectra, while figures 5.3b, 5.3c and 5.4b show proton-decoupled

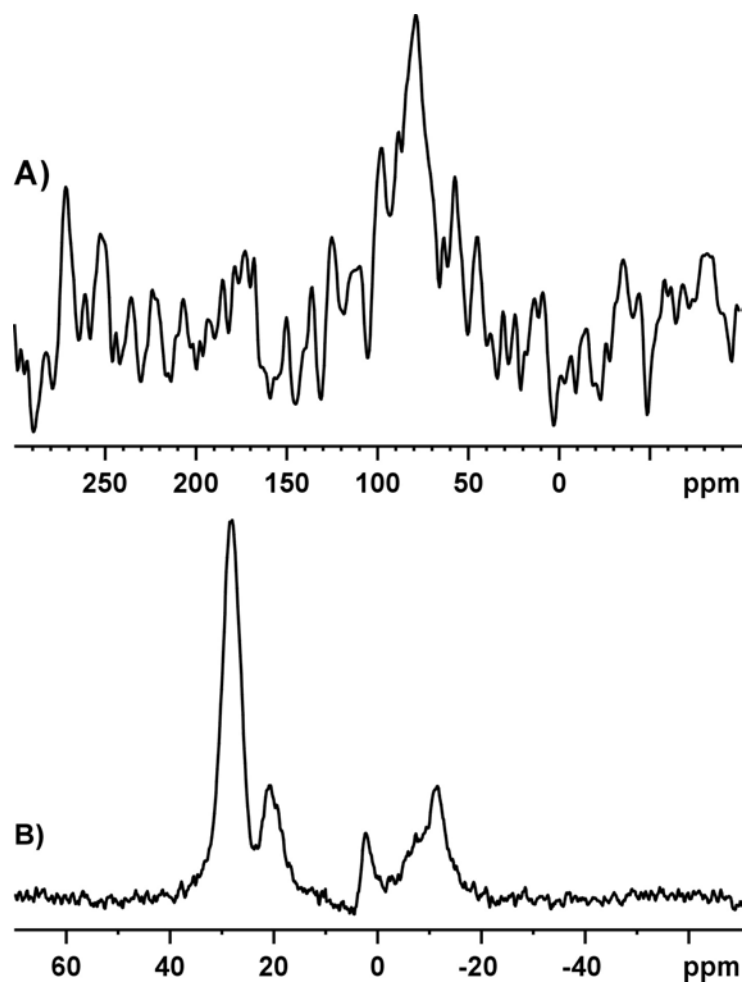


Figure 5.5: Proton-decoupled solid-state NMR spectra of 2mol% citropin 1.1 labelled with ^{15}N at Ala10, in POPC bilayer at room temperature. a) Proton-decoupled ^{15}N solid-state NMR spectrum and b) ^{31}P solid-state NMR spectrum.

^{31}P solid-state NMR spectra obtained from the same samples. Both ^{15}N spectra indicate that the ^{15}N -labeled residues are structured and immobilized on the time scale of the ^{15}N chemical shift interaction. A single ^{15}N resonance is observed at 98 ppm for ^{15}N -Val6 (Figure 5.3A) and at 94 ppm for ^{15}N -Ile18 (Figure 5.4A). The values less than 110 ppm indicate peptide alignments approximately parallel to the bilayer surface, albeit the 98 ppm value suggests a high degree of motion and a considerable tilt away from perfect in-plane¹⁸².

Interestingly, oriented ^{31}P NMR spectrum of NK-2 ^{15}N -Val6 in POPE:POPG lipid bilayers indicates a separation of POPE and POPG lipid phases (Figure 5.3B), and a homogeneous mixing after 6 hours at 30°C and storage at -20°C (Figure 5.3C). Note the improved alignment of the lipid phase after the incubation step. Thus, the lipid mixing was accomplished after heating well above the lipid phase transitions of POPE ($T_c=26.1^\circ$)¹⁸³ and POPG ($T_c=-4^\circ$)[†]. Figure 5.5A. shows the ^{15}N resonance of Ala-10 of citropin 1.1 oriented in POPC lipid bilayers. The resonance at 77 ppm demonstrates the alignment of the N-H bond of citropin 1.1 approximately perpendicular to the field and parallel to the surface of the lipid bilayer. Figure 5.5B shows the ^{31}P NMR spectrum of the same sample, where additional small peaks become apparent due to degradation after extended storage at high hydration.

5.4 Discussion

Previous studies of citropin 1.1 and NK-2 indicate that these antimicrobial peptides adopt alpha-helix conformations in the hydrophilic environments^{172,175}. The current investigation of proton-decoupled ^{15}N solid-state NMR spectra indicate that citropin 1.1 and NK-2 peptides interact with oriented lipid bilayers in such a manner that they adopt a unique set of alignments.

As the sample was inserted into the NMR magnet with orientations of the bilayer normal parallel to the B_0 field, the data indicate an alignment of the ^{15}N - ^1H vector approximately parallel to the bilayer surface. In an α -helical structure, the amide NH bonds orient approximately parallel to the long axis. Therefore, proton-decoupled ^{15}N solid-state results indicate that the helices accompanying Val6 and Ile18 of NK-2 and Ala10 of citropin1.1 are oriented approximately parallel to the

[†]<http://www.lipidat.chemistry.ohio-state.edu>

membrane surface (Figure 5.3-5.5).

Amphipathic antimicrobial peptides often (when solid-state NMR spectroscopy has been used) exhibit their activity by orienting in-plane to the lipid membrane interface with their polar part inserted between the lipid headgroups and the hydrophobic face buried inside the hydrocarbon core. Peptides in this situation modulate the physical properties of the host membrane e.g. decrease the membrane thickness, modify of the molecular order parameter along the lipid chains or alter the preferred bilayer curvature^{184,185,186}. Peptides adsorbed into the membrane surface have been shown to perforate the membrane bilayer. At higher concentrations, the interfacially adsorbed amphipathic peptides might self-assemble within the membrane plane into a 'carpet' and cause cooperative transitions of the macroscopic phase properties of the membranes^{187,188,189,190}.

A large diversity of phospholipids exist in biological membranes. It is thought that specific membrane activities are related to the physicochemical properties of the phospholipid membranes^{191,192}. Especially the chemical compositions of microorganisms and physical conditions of the membranes are of interest since it has been suggested that these characteristics play an important role in the regulations of antimicrobial activities^{68,193}. Cationic antimicrobial peptides preferentially bind to membranes containing acidic phospholipids such as PG or PS due to strong electrostatic interactions^{194,195}. This has been demonstrated with cecropins¹⁹⁶, and magainins¹⁹⁷. However, the outer leaflets of eukaryotic cell membranes predominantly contain zwitterionic phospholipids such as phosphatidylcholine¹⁹⁸. In many cases a direct correlation was found between the strength of membrane permeation and the potency to kill bacteria¹⁶⁷. For example, gramicidin S and human neutrophil peptide exhibit a high permeating activity on PE/PG membranes, matching the composition of the inner membrane of *Escherichia coli*, also highly active on this bacterium¹⁹⁹.

The antibiotic and anticancer activities of citropins and similar type peptides are believed to be due to the disruption of the cell membrane. In an alpha helical conformation, at least 16-18 amino acid residues are required to span the lipid bilayer of bacterial or cancer cells^{50,200,201}. Although citropin 1.1 adopts an alpha-helical structure¹⁷², the length is too short to span the lipid bilayer. Therefore, the antibacterial activity of citropin 1.1 cannot be easily explained by pore-formation through transmembrane helical aggregates. Our results suggest that the lytic activity of citropin peptides is due to peptides oriented parallel to the membrane surface

in a carpet-like manner⁵⁰. This eventually result in the transient destabilization of the membrane and bilayer openings.

However, our data do not exclude that, there might be peptide aggregation on the membrane surface as a precursory condition for pore formation.^{194,202,203,204}.

Interestingly, NK-2 peptides are known to act by direct physical destabilization of the target cell membrane. A probable explanation about the mode of action of NK-2 is that, it might be due to the curvature strain exerted by the peptide on the lipid bilayer upon NK-2 binding. The positive net charge of NK-2 peptide (+10) helps for binding and electrostatic interactions. When NK-2 is associated with the headgroups of the membrane, the helical axis is oriented parallel to the interface. Other antibiotic peptides have been shown to cause membrane thinning, with the amount of thinning being directly proportional to the peptide-to-lipid ratio^{205,206}. Interestingly, the neutron diffraction data (unpublished results Regine Willumeit, et al GKSS, Geesthacht) exhibit a significant difference in the position of the NK-2 peptide for both POPE and POPG membranes. While the peptide associated with the interface of POPE bilayers, the peptide inserts parallel to POPG membrane surface but penetrates much deeper into the bilayers. Biosensor experiments also revealed a binding capability of NK-2 for the PE surface¹⁷⁵. However, there was no binding of the NK-2 observed to PC monolayers. Being embedded in the PE headgroup region, the peptide increases the area of the membrane. At the same time, the volume of the hydrocarbon region of remains constant, therefore the hydrocarbon thickness decreases in proportion to the areal increase, and in turn this curvature strain causes the collapse of the bacterial membrane. It is suggestive that NK-2 binding would promote this curvature strain, which subsequently leads to the collapse of the bacterial cytoplasmic membrane. The effect of curvature stress on the membrane disruption has also been observed for other lytic peptides such as magainin 2 or gramicidin S^{195,207}.

Earlier several antimicrobial peptides have been widely studied by using different biophysical techniques. For example, solid state NMR measurement of ¹⁵N-labeled magainin oriented in membrane bilayer,^{76,179,208,209} Raman²¹⁰, fluorescence⁸⁷ and differential scanning calorimetry measurements²¹¹ all indicated that even at high and moderate lipid-to-peptide ratios, magainin is oriented parallel to the membrane surface. Apart from that oriented circular dichroism measurements have indicated that the peptide orientation depends on the amounts of the peptide bound to the membrane²⁰⁵. At relatively low peptide concentration the helices adopt an in-plane

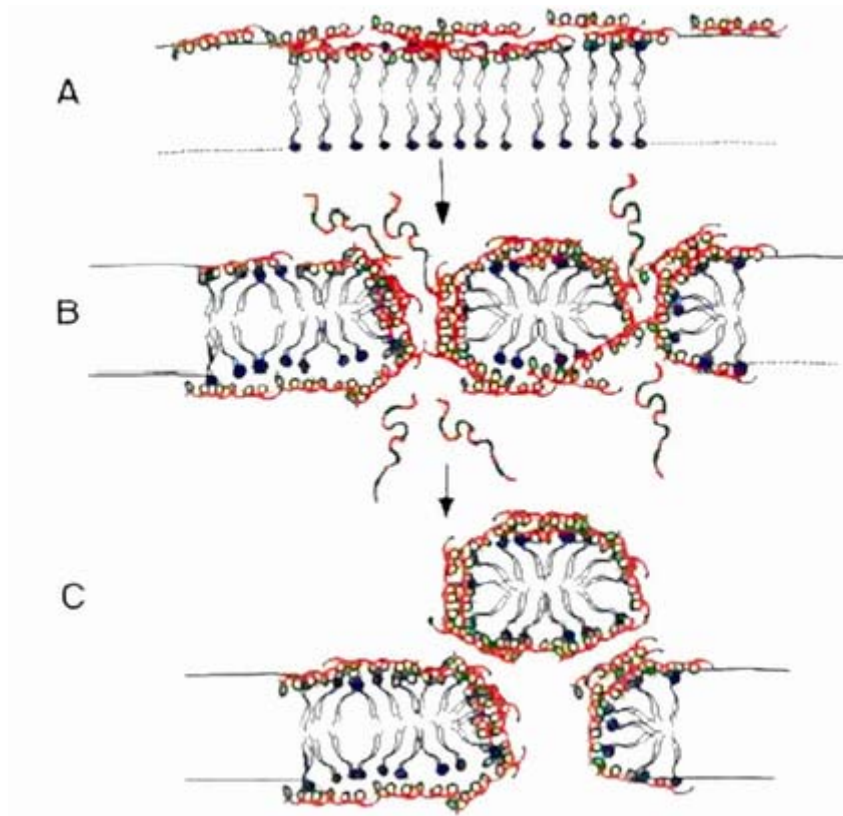


Figure 5.6: Schematic representation of carpet model at 2mol% of NK-2 and citropin 1.1 peptides. A) Peptides orient parallel to the membrane surface. B) & C) When a threshold concentration of peptide monomers is reached, the membrane goes into pieces.

orientation to the membrane surface. Whereas at higher peptide-to-lipid ratios (e.g. 1:30) a considerable fraction of the membrane bound peptide reorients perpendicular to the plane of the lipid bilayer. While attenuated total reflectance FTIR spectroscopy study on cecropin P1 indicates that this peptide initially orients parallel to the membrane, even without entering to the hydrophobic environment^{164,212}.

Our result suggest that the lytic activity of NK-2 and citropin peptides are due to peptides oriented parallel to the membrane surface where at higher peptide-to-lipid ratios, they aggregate in a carpet-like manner (Figure 5.6). At low concentrations, the continuous diffusion of peptides in the membrane is associated with the changing distances between them and orientation with respect to each other. Fluctuations of local concentration might thus result in stochastic openings in the membrane as observed in the case of magainins^{213,214}.

Chapter 6

Conclusions

In this section, the results from my research have been summarized with conclusions.

In chapter 2, the ^{15}N chemical shift observed for the LS peptides in all the samples that we tested indicates that an alignment parallel to the membrane surface is the preferred configuration of this series of amphipathic peptides when interacting with the lipid bilayer. The in-plane alignment ideally reflects the perfect amphipathic separation of polar and hydrophobic residues as it allows the serines to be exposed to the water phase when at the same time the leucines are immersed in the bilayer interior.

The close to 1:1 distribution of ^{15}N signals indicates that the IP \leftrightarrow TM equilibrium is governed by a free enthalpy close to zero under these conditions. This shows that relatively small energetic changes can indeed modify the distribution of signal intensities when the membrane hydration level or the sample pH are changed.

This experimental data can thus be concluded by a model where the peptide in the water phase is in dynamic equilibrium with the membrane-inserted configurations, adopting in-plane (IP) or transmembrane (TM) alignments.

In contrast to LS21 channels, the LS14 peptide remains surface-associated under all conditions tested. This data suggests that LS14 is associated with the lipid interface but is in conformational and / or topological exchange with the membrane-associated layer.

From chapter 3, data from the proton-decoupled ^{15}N solid-state NMR indicate that (Pser-6)LS14 and (Pser-9)LS14 peptides exhibit in-plane orientation when

reconstitute in DOTAP lipid. Proton-decoupled ^{31}P static and MAS solid-state NMR experimental data to characterize the phosphorylated peptide indicate the presence of motion. Low-temperature experiments indicate the possible restriction of amino acid side chain motions. More qualitative analysis of both orientation and motional behaviour of these phosphorylated peptide in lipid bilayer is needed for a complete characterization.

In chapter 4, data from the proton-decoupled ^{15}N and ^{31}P solid-state NMR experiments indicate that the helix5-loop-helix6 domain of Bcl- X_L is oriented in-plane whereas the hydrophobic C-terminus of Bcl- X_L adopts a transmembrane orientation in lipid bilayers. However, Bax-C terminus is orientated in-plane when reconstituted into lipid bilayers.

These experimental results suggest the possible association of monomeric Bax on the surface of planar phospholipid membranes. In contrast, isolated C-terminus of Bcl- X_L exhibits a transmembrane alignment. The α 5-loop- α 6 domain of Bcl- X_L is oriented parallel to the surface but a dynamic exchange between transmembrane and in-plane alignment might exist. We propose the penknife model as an intermediate state of Bcl- X_L , which involves the flipping out of α 5 and α 6 helices into the membrane like a penknife opening their hydrophobic surfaces while C-terminus remains anchored to the membrane.

In final chapter 5, experimental results by ^{15}N and ^{31}P solid-state NMR investigations show that NK-2 and citropin 1.1 peptides bind to the surface of phospholipid membranes in a parallel orientation. From the results, we suggest that the lytic activity of NK-2 and citropin peptides is because they are oriented parallel to the membrane surface. This results in the transient destabilization of the membrane and bilayer openings.

Bibliography

- [1] Nelson. David L and Cox. Michael M. Principles of biochemistry (fourth edition). *W.H. Freeman and Company*, 2004.
- [2] J.J.H.H.M. De Pont and A. Watts. Modulation of lipid polymorphism by lipid-protein interactions. *Progress in Protein-Lipid Interactions, Elsevier, New York.*, 2:89–142, 1986.
- [3] S. B. Hladky and D. A. Haydon. Discreteness of conductance change in bimolecular lipid membranes in the presence of certain antibiotics. *Nature*, 225 (5231):451–3, 1970.
- [4] S. W. Cowan, T. Schirmer, G. Rummel, M. Steiert, R. Ghosh, R. A. Paupit, J. N. Jansonius, and J. P. Rosenbusch. Crystal structures explain functional properties of two e. coli porins. *Nature*, 358(6389):727–33, 1992.
- [5] D. A. Doyle, J. Morais Cabral, R. A. Pfuetzner, A. Kuo, J. M. Gulbis, S. L. Cohen, B. T. Chait, and R. MacKinnon. The structure of the potassium channel: molecular basis of k⁺ conduction and selectivity. *Science*, 280(5360): 69–77, 1998.
- [6] K. Lundstrom. Structural genomics on membrane proteins: mini review. *Comb Chem High Throughput Screen*, 7(5):431–9, 2004.
- [7] C. Binda, P. Newton-Vinson, F. Hubalek, D. E. Edmondson, and A. Mattevi. Structure of human monoamine oxidase b, a drug target for the treatment of neurological disorders. *Nat Struct Biol*, 9(1):22–6, 2002.
- [8] R. Henderson and P. N. Unwin. Three-dimensional model of purple membrane obtained by electron microscopy. *Nature*, 257(5521):28–32, 1975.

-
- [9] Y. Kimura, D. G. Vassylyev, A. Miyazawa, A. Kidera, M. Matsushima, K. Mitsuoka, K. Murata, T. Hirai, and Y. Fujiyoshi. Surface of bacteriorhodopsin revealed by high-resolution electron crystallography. *Nature*, 389(6647):206–11, 1997.
- [10] K. Murata, K. Mitsuoka, T. Hirai, T. Walz, P. Agre, J. B. Heymann, A. Engel, and Y. Fujiyoshi. Structural determinants of water permeation through aquaporin-1. *Nature*, 407(6804):599–605, 2000.
- [11] C. Fernandez and K. Wuthrich. Nmr solution structure determination of membrane proteins reconstituted in detergent micelles. *FEBS Lett*, 555(1):144–50, 2003.
- [12] Roland Riek, Konstantin Pervushin, and Kurt Wuthrich. Trosy and crinept: Nmr with large molecular and supramolecular structures in solution. *Trends in Biochemical Sciences*, 25(10):462–468, 2000.
- [13] K. Pervushin, D. Braun, C. Fernandez, and K. Wuthrich. [15n,1h]/[13c,1h]-trosy for simultaneous detection of backbone 15n-1h, aromatic 13c-1h and side-chain 15n-1h2 correlations in large proteins. *J Biomol NMR*, 17(3):195–202, 2000.
- [14] K. Pervushin, R. Riek, G. Wider, and K. Wuthrich. Transverse relaxation-optimized spectroscopy (trosy) for nmr studies of aromatic spin systems in 13c-labeled proteins. *J. Am. Chem Soc.*, 120:6394–6400, 1998.
- [15] S.J. Opella. Nmr and membrane proteins. *Nat Struct Biol*, 4 Suppl:845–8, 1997.
- [16] B. Bechinger, C. Aisenbrey, and P. Bertani. The alignment, structure and dynamics of membrane-associated polypeptides by solid-state nmr spectroscopy. *Biochim Biophys Acta*, 1666(1-2):190–204, 2004.
- [17] C. Glaubitz and A. Watts. Magic angle-oriented sample spinning (maoss): a new approach toward biomembrane studies. *J. Magn. Reson.*, 130:305316, 1998.
- [18] C. Sizun and B. Bechinger. Bilayer sample for fast or slow magic angle oriented sample spinning solid-state nmr spectroscopy. *Journal of the American Chemical Society*, 124(7):1146–1147, 2002.
-

-
- [19] CH. Wu, A. Ramamoorthy, and SJ. Opella. High-resolution heteronuclear dipolar solid-state nmr spectroscopy. *Journal of Magnetic Resonance, Series A*, 109(2):270–272, 1994.
- [20] J. Wang, J. Denny, C. Tian, S. Kim, Y. Mo, F. Kovacs, Z. Song, K. Nishimura, Z. Gan, and R. Fu. Imaging membrane protein helical wheels. *Journal of Magnetic Resonance*, 144(1):162–167, 2000.
- [21] Francesca M. Marassi and Stanley J. Opella. A solid-state nmr index of helical membrane protein structure and topology. *Journal of Magnetic Resonance*, 144(1):150–155, 2000.
- [22] R. Xu, B. Ayers, D. Cowburn, and TW. Muir. Chemical ligation of folded recombinant proteins: segmental isotopic labeling of domains for nmr studies. *Proc Natl Acad Sci U S A*, 96(2):388–93, 1999.
- [23] Tom W. Muir, Dolan Sondhi, and Philip A. Cole. Expressed protein ligation: A general method for protein engineering. *PNAS*, 95(12):6705–6710, 1998.
- [24] K. Schmidt-Rohr and H. W. Spiess. Multidimensional solid-state nmr and polymers. *Academic press*, 1996.
- [25] M. Mehring. Principles of high resolution nmr in solids. *Springer-Verlag, New York*, 1983.
- [26] Smith. Scott A, Palke. William E, and J.T. Gerig. The hamiltonion of nmr part 1. *Concepts in Magnetic Resonance*, 4:107–144, 1992.
- [27] Smith. Scott A, Palke. William E, and J.T. Gerig. The hamiltonion of nmr part 2. *Concepts in Magnetic Resonance*, 4:181–204, 1992.
- [28] M. H. Levitt, D. Suter, and R. R. Ernst. Spin dynamics and thermodynamics in solid-state nmr cross polarization. *The Journal of Chemical Physics*, 84(8): 4243–4255, 1986.
- [29] S. R. Hartmann and E. L. Hahn. Nuclear double resonance in the rotating frame. *Phys. Rev.*, 128:2042–2053, 1962.
- [30] JJ. de Vries and HJC. Berendsen. Nuclear magnetic resonance measurements on a macroscopically ordered smectic liquid crystalline phase. *Nature*, 221: 1139–1140, 1969.
-

-
- [31] B. Bechinger, L. M. Gierasch, M. Montal, M. Zasloff, and S. J. Opella. Orientations of helical peptides in membrane bilayers by solid state nmr spectroscopy. *Solid State Nuclear Magnetic Resonance*, 7(3):185–191, 1996.
- [32] R. Smith, F. Separovic, T. J. Milne, A. Whittaker, F. M. Bennett, B. A. Cornell, and A. Makriyannis. Structure and orientation of the pore-forming peptide, melittin, in lipid bilayers. *J Mol Biol*, 241(3):456–66, 1994.
- [33] CL. North, M. Barranger-Mathys, and DS. Cafiso. Membrane orientation of the n-terminal segment of alamethicin determined by solid-state ^{15}N nmr. *Biophys. J.*, 69(6):2392–2397, 1995.
- [34] TA. Cross. Solid-state nuclear magnetic resonance characterization of gramicidin channel structure. *Methods Enzymol*, 289:672–96, 1997.
- [35] Mads Bak, Robert P. Bywater, Morten Hohwy, Jens K. Thomsen, Kim Adelhorst, Hans J. Jakobsen, Ole W. Sorensen, and Niels C. Nielsen. Conformation of alamethicin in oriented phospholipid bilayers determined by ^{15}N solid-state nuclear magnetic resonance. *Biophys. J.*, 81(3):1684–1698, 2001.
- [36] S. Yamaguchi, T. Hong, A. Waring, R. I. Lehrer, and M. Hong. Solid-state nmr investigations of peptide-lipid interaction and orientation of a beta-sheet antimicrobial peptide, protegrin. *Biochemistry*, 41(31):9852–62, 2002.
- [37] S. Lambotte, P. Jasperse, and B. Bechinger. Orientational distribution of alpha-helices in the colicin b and el channel domains: A one and two dimensional n- ^{15}N solid-state nmr investigation in uniaxially aligned phospholipid bilayers. *Biochemistry*, 37(51):18128–18128, 1998.
- [38] A. J. Oakley, B. Martinac, and M. C. Wilce. Structure and function of the bacterial mechanosensitive channel of large conductance. *Protein Sci*, 8(10):1915–21, 1999.
- [39] J. F. Leite and M. Cascio. Structure of ligand-gated ion channels: critical assessment of biochemical data supports novel topology. *Mol Cell Neurosci*, 17(5):777–92, 2001.
- [40] D. C. Rees, G. Chang, and R. H. Spencer. Crystallographic analyses of ion channels: lessons and challenges. *J Biol Chem*, 275(2):713–6, 2000.
-

-
- [41] R. B. Bass, K. P. Locher, E. Borths, Y. Poon, P. Strop, A. Lee, and D. C. Rees. The structures of btudc and mscc and their implications for transporter and channel function. *FEBS Lett*, 555(1):111–5, 2003.
- [42] R. Dutzler. Structural basis for ion conduction and gating in clc chloride channels. *FEBS Lett*, 564(3):229–33, 2004.
- [43] CE. Dempsey. The actions of melittin on membranes. *Biochim Biophys Acta*, 1031(2):143–61, 1990.
- [44] MS. Sansom. The biophysics of peptide models of ion channels. *Prog Biophys Mol Biol*, 55(3):139–235, 1991.
- [45] G. A. Woolley, A. Dunn, and B. A. Wallace. Gramicidin-lipid interactions induce specific tryptophan side-chain conformations. *Biochem Soc Trans*, 20(4):864–7, 1992.
- [46] B. Bechinger. Structure and functions of channel-forming peptides: Magainins, cecropins, melittin and alamethicin. *Journal of Membrane Biology*, 156(3):197–211, 1997.
- [47] H. Duclohier. Helical kink and channel behaviour: a comparative study with the peptaibols alamethicin, trichotoxin and antimioebin. *Eur Biophys J*, 33(3):169–74, 2004.
- [48] G. Spach, H. Duclohier, G. Molle, and J. M. Valleton. Structure and supramolecular architecture of membrane channel-forming peptides. *Biochimie*, 71(1):11–21, 1989.
- [49] M. Montal. Design of molecular function: channels of communication. *Annu Rev Biophys Biomol Struct*, 24:31–57, 1995.
- [50] Y. Shai. Molecular recognition between membrane-spanning polypeptides. *Trends Biochem Sci*, 20(11):460–4, 1995.
- [51] PI. Haris. Synthetic peptide fragments as probes for structure determination of potassium ion-channel proteins. *Biosci Rep*, 18(6):299–312, 1998.
- [52] B. Bechinger. Understanding peptide interactions with the lipid bilayer: a guide to membrane protein engineering. *Current Opinion in Chemical Biology*, 4(6):639–644, 2000.
-

- [53] I. T. Arkin. Structural aspects of oligomerization taking place between the transmembrane alpha-helices of bitopic membrane proteins. *Biochim Biophys Acta*, 1565(2):347–63, 2002.
- [54] C. Tian, P. F. Gao, L. H. Pinto, R. A. Lamb, and T. A. Cross. Initial structural and dynamic characterization of the m2 protein transmembrane and amphipathic helices in lipid bilayers. *Protein Sci*, 12(11):2597–605, 2003. Journal Article.
- [55] W. F. DeGrado, H. Gratkowski, and J. D. Lear. How do helix-helix interactions help determine the folds of membrane proteins? perspectives from the study of homo-oligomeric helical bundles. *Protein Sci*, 12(4):647–65, 2003.
- [56] F. Heitz and G. Spach. Ionic channels of some glycine-rich synthetic polypeptides. *Biochem Biophys Res Commun*, 105(1):179–85, 1982.
- [57] P. De Santis, A. Palleschi, M. Savino, A. Scipioni, B. Sesta, and A. Verdini. Poly(dl-proline), a synthetic polypeptide behaving as an ion channel across bilayer membranes. *Biophys Chem*, 21(3-4):211–5, 1985.
- [58] George W. Gokel, Paul H. Schlesinger, Natasha K. Djedovic, Riccardo Ferdani, Egan C. Harder, Jiabin Hu, W. Matthew Leevy, Jolanta Pajewska, Robert Pajewski, and Michelle E. Weber. Functional, synthetic organic chemical models of cellular ion channels. *Bioorganic and Medicinal Chemistry*, 12(6):1291–1304, 2004.
- [59] J. D. Lear, Z. R. Wasserman, and W. F. DeGrado. Synthetic amphiphilic peptide models for protein ion channels. *Science*, 240:1177–1181, 1988.
- [60] T. Iwata, S. Lee, O. Oishi, H. Aoyagi, M. Ohno, K. Anzai, Y. Kirino, and G. Sugihara. Design and synthesis of amphipathic 3(10)-helical peptides and their interactions with phospholipid bilayers and ion channel formation. *J Biol Chem*, 269(7):4928–33, 1994.
- [61] Gokel. George W and Mukhopadhyay. Anindita. Synthetic models of cation-conducting channels. *Chem. Soc. Rev*, 30(5):274 – 286, 2001.
- [62] Eric Biron, Francois Otis, Jean-Christophe Meillon, Martin Robitaille, Julie Lamothe, Patrick Van Hove, Marie-Eve Cormier, and Normand Voyer. Design,
-

- synthesis, and characterization of peptide nanostructures having ion channel activity. *Bioorganic and Medicinal Chemistry*, 12(6):1279–1290, 2004.
- [63] LA. Chung, J. Lear, and WF. DeGrado. Fluorescence studies of the secondary structure and orientation of a model ion channel peptide in phospholipid vesicles. *Biochemistry*, 31:6608–6616, 1992.
- [64] KS. kerfeldt, JD. Lear, ZR. Wasserman, LA. Chung, and WF. DeGrado. Synthetic peptides as models for ion channel proteins. *Accounts of Chemical Research*, 26:191–197, 1993.
- [65] P. K. Keinker, W. F. DeGrado, and JD. Lear. A helical-dipole model describes the single-channel current rectification of un-charged peptide ion channel. *Proceedings of National Acedamy of Science USA*, 91:4859–4863, 1994.
- [66] D. Chen, J. Lear, and B. Eisenberg. Permeation through an open channel: Poisson-nernst-planck theory of a synthetic ionic channel. *Biophys J*, 72(1):97–116, 1997.
- [67] G. R. Diekmann, J D. Lear, Q. Zhong, M. P. Klein, W. F. DeGrado, and KA. Sharp. Exploration of structural features defining the conduction properties of a synthetic ion channel. *Biophysics Journal*, 76:2517–2533, 1999.
- [68] B. Bechinger. The structure, dynamics and orientation of antimicrobial peptides in membranes by multidimensional solid-state nmr spectroscopy. *Biochimica Et Biophysica Acta-Biomembranes*, 1462(1-2):157–183, 1999.
- [69] B. Bechinger. Structure and function of membrane-lytic peptides. *Critical Reviews in Plant Sciences*, 23(3):271–292, 2004.
- [70] C. Aisenbrey and B. Bechinger. Tilt and rotational pitch angle of membrane-inserted polypeptides from combined 15n and 2h solid-state nmr spectroscopy. *Biochemistry*, 43(32):10502–10512, 2004.
- [71] C Walker, M Selby, A Erickson, D Cataldo, J Valensi, and GV Next. Cationic lipids direct a viral glycoprotein into the class i major histocompatibility complex antigen-presentation pathway. *PNAS*, 89(17):7915–7918, 1992.
-

- [72] E. Atherton, W. Hubscher, R. C. Sheppard, and V. Woolley. Synthesis of a 21-residue fragment of human proinsulin by the polyamide solid phase method. *Hoppe Seylers Z Physiol Chem*, 362(7):833–9, 1981.
- [73] GY Han and LA Carpino. The 9-fluorenylmethoxycarbonyl amino-protecting group. *J. Org. Chem*, 37:3404–3409, 1972.
- [74] Thomas Haack and Manfred Mutter. Serine derived oxazolidines as secondary structure disrupting, solubilizing building blocks in peptide synthesis. *Tetrahedron Letters*, 33(12):1589–1592, 1992.
- [75] F. E. M. O'Brien. The control of humidity by saturated salt solutions. *J. Sci. Instrum.*, 25:73–76, 1948.
- [76] B. Bechinger, Y. Kim, L. E. Chirlian, J. Gesell, J. M. Neumann, M. Montal, J. Tomich, M. Zasloff, and S. J. Opella. Orientations of amphipathic helical peptides in membrane bilayers determined by solid-state nmr spectroscopy. *J Biomol NMR*, 1(2):167–173, 1991.
- [77] T. G. Oas, C.J. Hartzell, FW. Dahlquist, and G.P. Drobny. Determination of the ^{15}N and ^{13}C chemical shift tensors of l- ^{13}C alanyl-l- ^{15}N alanine from the dipole-coupled patterns. *J. Am. Chem. Soc. Rev*, 109:5962–5966, 1987.
- [78] CJ. Hartzell, M. Whitfield, T. G. Oas, and GP. Drobny. Determination of the ^{15}N and ^{13}C chemical shift tensors of l- ^{13}C alanyl-l- ^{15}N alanine from the dipole-coupled powder patterns. *J. Am. Chem. Soc.*, 109:5966–5969, 1987.
- [79] A. T. Shoji, T. Ozaki, K. Fujito, Deguchi, S. Ando, and I. Ando. ^{15}N -nmr chemical shift tensors and conformation of some ^{15}N -labeled polypeptides in the solid state. *Macromolecules*, 22:2860–2863, 1989.
- [80] T.A. Cross and Q. Teng. The in situ determination of the ^{15}N chemical shift tensor orientation in a polypeptide. *Journal of Magnetic Resonance*, 85:439–447, 1989.
- [81] D. K. Lee and A. Ramamoorthy. A simple one-dimensional solid-state nmr method to characterize the nuclear spin interaction tensors associated with the peptide bond. *J Magn Reson*, 133(1):204–6, 1998.
-

- [82] H. Le and E. Oldfield. Correlation between ^{15}N nmr chemical shifts in proteins and secondary structure. *J Biomol NMR*, 4(3):341–348, 1994.
- [83] A. Shoji, T. Ozaki, T. Fujito, K. Deguchi, S. Ando, and I. Ando. ^{15}N chemical shift tensors and conformation of solid polypeptides containing ^{15}N -labeled l-alanine residue by ^{15}N nmr. 2. secondary structure reflected in $[\sigma]_{22}$. *J. AM. CHEM. SOC.*, 112(12):4693–4697, 1990.
- [84] PK Kienker and JD. Lear. Charge selectivity of the designed uncharged ac-(lssllsl) $_3$ -conh $_2$. *Biophysical Journal*, 68:1347–1358, 1995.
- [85] B. Bechinger, R. Kinder, M. Helmle, T. C. B. Vogt, U. Harzer, and S. Schinzel. Peptide structural analysis by solid-state nmr spectroscopy. *Biopolymers*, 51(3):174–190, 1999.
- [86] Y. Shai. Mode of action of membrane active antimicrobial peptides. *Biopolymers*, 66(4):236–48, 2002.
- [87] K. Matsuzaki, O. Murase, H. Tokuda, S. Funakoshi, N. Fujii, and K. Miyajima. Orientational and aggregational states of magainin 2 in phospholipid bilayers. *Biochemistry*, 33(11):3342–3349, 1994.
- [88] Y. Shai. Mechanism of the binding, insertion and destabilization of phospholipid bilayer membranes by alpha-helical antimicrobial and cell non-selective membrane-lytic peptides. *Biochim Biophys Acta*, 1462(1-2):55–70, 1999.
- [89] B. Bechinger. Solid-state nmr investigations of interaction contributions that determine the alignment of helical polypeptides in biological membranes. *Febs Letters*, 504(3):161–165, 2001.
- [90] P. H. Axelsen, B. K. Kaufman, R. N. McElhaney, and R. N. Lewis. The infrared dichroism of transmembrane helical polypeptides. *Biophys J*, 69(6):2770–81, 1995.
- [91] Ruthven N. A. H. Lewis, Yuan-Peng Zhang, Feng Liu, and Ronald N. McElhaney. Mechanisms of the interaction of alpha-helical transmembrane peptides with phospholipid bilayers. *Bioelectrochemistry*, 56(1-2):135–140, 2002.
-

- [92] U. Harzer and B. Bechinger. Alignment of lysine-anchored membrane peptides under conditions of hydrophobic mismatch: A cd, n-15 and p-31 solid-state nmr spectroscopy investigation. *Biochemistry*, 39(43):13106–13114, 2000.
- [93] WC. Wimley and SH. White. Designing transmembrane alpha-helices that insert spontaneously. *Biochemistry*, 39(15):4432–42, 2000.
- [94] HW. Huang. Action of antimicrobial peptides: two-state model. *Biochemistry*, 39(29):8347–52, 2000.
- [95] F. Y. Chen, M. T. Lee, and H. W. Huang. Sigmoidal concentration dependence of antimicrobial peptide activities: a case study on alamethicin. *Biophys J*, 82(2):908–14, 2002.
- [96] H. Vogel. Comparison of the conformation and orientation of alamethicin and melittin in lipid membranes. *Biochemistry*, 26(14):4562–72, 1987.
- [97] Lin Yang, Thad A. Harroun, Thomas M. Weiss, Lai Ding, and Huey W. Huang. Barrel-stave model or toroidal model? a case study on melittin pores. *Biophys. J.*, 81(3):1475–1485, 2001.
- [98] C. M. Moraes and B. Bechinger. Peptide-related alterations of membrane-associated water: deuterium solid-state nmr investigations of phosphatidylcholine membranes at different hydration levels. *Magnetic Resonance in Chemistry*, 42(2):155–161, 2004.
- [99] S. Stankowski, U. D. Schwarz, and G. Schwarz. Voltage-dependent pore activity of the peptide alamethicin correlated with incorporation in the membrane: salt and cholesterol effects. *Biochim Biophys Acta*, 941(1):11–8, 1988.
- [100] A. J. Ramsey and P. F. Fitzpatrick. Effects of phosphorylation of serine 40 of tyrosine hydroxylase on binding of catecholamines: evidence for a novel regulatory mechanism. *Biochemistry*, 37(25):8980–6, 1998.
- [101] Andreas Tholey, Almut Lindemann, Volker Kinzel, and Jennifer Reed. Direct effects of phosphorylation on the preferred backbone conformation of peptides: A nuclear magnetic resonance study. *Biophys. J.*, 76(1):76–87, 1999.
- [102] Rammohan V. Rao, Eileen L. Holicky, Susan M. Kuntz, and Laurence J. Miller. Cck receptor phosphorylation exposes regulatory domains affecting
-

- phosphorylation and receptor trafficking. *Am J Physiol Cell Physiol*, 279(6): C1986–1992, 2000.
- [103] P. Henklein, R. Kinder, U. Schubert, and B. Bechinger. Membrane interactions and alignment of structures within the hiv-1 vpu cytoplasmic domain: effect of phosphorylation of serines 52 and 56. *Febs Letters*, 482(3):220–224, 2000.
- [104] R. G. Griffin. Solid state nuclear magnetic resonance of lipid bilayers. *Methods Enzymol*, 72:108–74, 1981.
- [105] TA. Cross. *Bull. Mag. Res.*, 14(1-4), 1992.
- [106] D. Massiot, F. Fayon, M. Capron, I. King, S. Le Calve, B. Alonso, J. O. Durand, B. Bujoli, Z. H. Gan, and G. Hoatson. Modelling one- and two-dimensional solid-state nmr spectra. *Magnetic Resonance in Chemistry*, 40(1):70–76, 2002.
- [107] SJ. Kohler and MP. Klein. Phosphorus-31 nuclear magnetic resonance chemical shielding tensors of l-o-serine phosphate and 3'-cytidine monophosphate. *J Am Chem Soc*, 99(25):8290–3, 1977.
- [108] C. Adcock, GR. Smith, and M.S.P. Sansom. Electrostatics and the selectivity of ligand-gated ion channels. *Biophysical Journal*, 75:1211–1222, 1998.
- [109] Ehya. Cheng, M. C. Wei, S. Weiler, R. A. Flavell, T. W. Mak, T. Lindsten, and S. J. Korsmeyer. Bcl-2, bcl-x-l sequester bh3 domain-only molecules preventing bax- and bak-mediated mitochondrial apoptosis. *Molecular Cell*, 8(3):705–711, 2001.
- [110] C. Michael Knudson, Kenneth S. K. Tung, Warren G. Tourtellotte, Gary A. J. Brown, and Stanley J. Korsmeyer. Bax-deficient mice with lymphoid hyperplasia and male germ cell death. *Science*, 270(5233):96–99, 1995.
- [111] JM. Adams and S. Cory. Life-or-death decisions by the bcl-2 protein family. *Trends Biochem Sci.*, 26:61–66, 2001.
- [112] MG. Vander Heiden and CB. Thompson. Bcl-2 proteins: regulators of apoptosis or of mitochondrial homeostasis? *Nature Cell Biology*, 1(8):E209–E216, 1999.
-

- [113] Anthony Letai, Michael C. Bassik, Loren D. Walensky, Mia D. Sorcinelli, Solly Weiler, and Stanley J. Korsmeyer. Distinct bh3 domains either sensitize or activate mitochondrial apoptosis, serving as prototype cancer therapeutics. *Cancer Cell*, 2(3):183–192, 2002.
- [114] Lisa Oliver, Muriel Priault, Karine Tremblais, Marie-Therese LeCabellec, Khaled Meflah, Stephen Manon, and Francois M. Vallette. The substitution of the c-terminus of bax by that of bcl-xl does not affect its subcellular localization but abrogates its pro-apoptotic properties. *FEBS Letters*, 487(2):161–165, 2000.
- [115] Oliver von Ahsen, Christian Renken, Guy Perkins, Ruth M. Kluck, Ella Bossy-Wetzell, and Donald D. Newmeyer. Preservation of mitochondrial structure and function after bid- or bax-mediated cytochrome c release. *J. Cell Biol.*, 150(5):1027–1036, 2000.
- [116] YT. Hsu, , and R.J. Youle. Bax in murine thymus is a soluble monomeric protein that displays differential detergent-induced conformations. *Journal of Biological Chemistry*, 273(17):10777–10783, 1998.
- [117] A. Nechushtan, C. L. Smith, Y. T. Hsu, and R. J. Youle. Conformation of the bax c-terminus regulates subcellular location and cell death. *Embo Journal*, 18(9):2330–2341, 1999.
- [118] Motoshi Suzuki, Richard J. Youle, and Nico Tjandra. Structure of bax: Coregulation of dimer formation and intracellular localization. *Cell*, 103(4):645–654, 2000.
- [119] A. Letai. Bh3 domains as bcl-2 inhibitors: prototype cancer therapeutics. *Expert Opin Biol Ther*, 3(2):293–304, 2003.
- [120] B. Antonsson, S. Montessuit, B. Sanchez, and J. C. Martinou. Bax is present as a high molecular weight oligomer/complex in the mitochondrial membrane of apoptotic cells. *Journal of Biological Chemistry*, 276(15):11615–11623, 2001.
- [121] Atan Gross, James M. McDonnell, and Stanley J. Korsmeyer. Bcl-2 family members and the mitochondria in apoptosis. *Genes Dev.*, 13(15):1899–1911, 1999.
-

- [122] SW. Muchmore, M. Sattler, H. Liang, RP. Meadows, JE. Harlan, HS. Yoon, D. Nettlesheim, B.S. Chang, C.B Thompson, S.L. Wong, S.C. Ng, and S.W. Fesik. X-ray and nmr structure of human bcl-x(1), an inhibitor of programmed cell death. *Nature*, 381:335–341, 1996.
- [123] S. L. Schendel, E. M. Click, R. E. Webster, and W. A. Cramer. The tola protein interacts with colicin e1 differently than with other group a colicins. *J Bacteriol*, 179(11):3683–90, 1997.
- [124] A. J. Minn, P. Velez, SL. Schendel, H. Liang, SW. Muchmore, S. W. Fesik, M. Fill, and CB. Thompson. Bcl-xl forms an ion channel in synthetic lipid membranes. *Nature*, 285:353 – 357, 1997.
- [125] J. A. Losonczi, E. T. Olejniczak, S. F. Betz, J. E. Harlan, J. Mack, and S. W. Fesik. Nmr studies of the anti-apoptotic protein bcl-xl in micelles. *Biochemistry*, 39(36):11024–33, 2000.
- [126] A. J. Minn, C. S. Kettlun, H. Liang, A. Kelekar, M. G. Vander Heiden, B. S. Chang, S. W. Fesik, M. Fill, and CB. Thompson. Bcl-xl regulates apoptosis by heterodimerization-dependent and -independent mechanisms. *EMBO J.*, 18:632–643, 1999.
- [127] Shigemi Matsuyama, Sharon L. Schendel, Zhihua Xie, and John C. Reed. Cytoprotection by bcl-2 requires the pore-forming alpha 5 and alpha 6 helices. *J. Biol. Chem.*, 273(47):30995–31001, 1998.
- [128] Shahrzad. Nouraini, Emmanuelle. Six, Shigemi. Matsuyama, Stainslaw. Krajewski, and John C. Reed. The putative pore-forming domain of bax regulates mitochondrial localization and interaction with bcl-xl. *Mol. Cell. Biol.*, 20(5): 1604–1615, 2000.
- [129] M. Sawada, P. Hayes, and S. Matsuyama. Cytoprotective membrane-permeable peptides designed from the bax-binding domain of ku70. *Nat Cell Biol*, 5(4):352–7, 2003.
- [130] H. L. Vieira, P. Boya, I. Cohen, C. El Hamel, D. Haouzi, S. Druillenec, A. S. Belzacq, C. Brenner, B. Roques, and G. Kroemer. Cell permeable bh3-peptides overcome the cytoprotective effect of bcl-2 and bcl-x(1). *Oncogene*, 21(13): 1963–77, 2002.
-

-
- [131] A. Pines, M. G. Gibby, and J. S. Waugh. Proton-enhanced nmr of dilute spins in solids. *The Journal of Chemical Physics*, 59(2):569–590, 1973.
- [132] M. Rance and R.A. Byrd. Obtaining high-fidelity spin-1/2 powder spectra in anisotropic media: phase-cycled hahn echo spectroscopy. *J. Magn. Reson.*, 52: 221–240, 1983.
- [133] P. G. Scherer and J. Seelig. Electric charge effects on phospholipid headgroups. phosphatidylcholine in mixtures with cationic and anionic amphiphiles. *Biochemistry*, 28(19):7720–8, 1989.
- [134] Paul H. Schlesinger, Atan Gross, Xiao-Ming Yin, Kazuhito Yamamoto, Mitsuyoshi Saito, Gabriel Waksman, and Stanley J. Korsmeyer. Comparison of the ion channel characteristics of proapoptotic bax and antiapoptotic bcl-2. *PNAS*, 94(21):11357–11362, 1997.
- [135] PK. Kim, F. Janiak-Spens, WS. Trimble, B. Leber, and DW. Andrews. Evidence for multiple mechanisms for membrane binding and integration via carboxyl-terminal insertion sequences. *Biochemistry*, 36(29):8873–8882, 1997.
- [136] Thomas Kaufmann, Sarah Schlipf, Javier Sanz, Karin Neubert, Reuven Stein, and Christoph Borner. Characterization of the signal that directs bcl-xl, but not bcl-2, to the mitochondrial outer membrane. *J. Cell Biol.*, 160(1):53–64, 2003.
- [137] Helen Everett, Michele Barry, Siow Fong Lee, Xuejun Sun, Kathryn Graham, James Stone, R. Chris Bleackley, and Grant McFadden. M111: A novel mitochondria-localized protein of myxoma virus that blocks apoptosis of infected leukocytes. *J. Exp. Med.*, 191(9):1487–1498, 2000.
- [138] HM. McBride, DG. Millar, JM. Li, and GC. Shore. A signal-anchor sequence selective for the mitochondrial outer membrane. *J. Cell Biol.*, 119(6):1451–1457, 1992.
- [139] Billie Egan, Traude Beilharz, Rebecca George, Sandra Isenmann, Sabine Gratzer, Binks Wattenberg, and Trevor Lithgow. Targeting of tail-anchored proteins to yeast mitochondria in vivo. *FEBS Letters*, 451(3):243–248, 1999.
-

-
- [140] Chika Horie, Hiroyuki Suzuki, Masao Sakaguchi, and Katsuyoshi Mihara. Characterization of signal that directs c-tail-anchored proteins to mammalian mitochondrial outer membrane. *Mol. Biol. Cell*, 13(5):1615–1625, 2002.
- [141] B. Wattenberg and T. Lithgow. Targeting of c-terminal (tail)-anchored proteins: understanding how cytoplasmic activities are anchored to intracellular membranes. *Traffic*, 2(1):66–71, 2001.
- [142] K Mihira. Targeting and insertion of nuclear-encoded preproteins into the mitochondrial outer membrane. *Bioessays.*, 22:364–371, 2000.
- [143] C. M. Franzin, J. Choi, D. Zhai, J. C. Reed, and F. M. Marassi. Structural studies of apoptosis and ion transport regulatory proteins in membranes. *Magn Reson Chem*, 42(2):172–179, 2004.
- [144] J. C. Reed. Double identity for proteins of the bcl-2 family. *Nature*, 387:773–776, 1997.
- [145] Sharon L. Schendel, Zhihua Xie, Myrta Oblatt Montal, Shigemi Matsuyama, Mauricio Montal, and John C. Reed. Channel formation by antiapoptotic protein bcl-2. *PNAS*, 94(10):5113–5118, 1997.
- [146] M. W. Parker, J. P. Postma, F. Pattus, A. D. Tucker, and D. Tsernoglou. Refined structure of the pore-forming domain of colicin a at 2.4 a resolution. *J Mol Biol*, 224(3):639–57, 1992.
- [147] D Duche, MW Parker, JM Gonzalez-Manas, F Pattus, and D Baty. Uncoupled steps of the colicin a pore formation demonstrated by disulfide bond engineering. *J. Biol. Chem.*, 269(9):6332–6339, 1994.
- [148] J. H. Lakey, D. Baty, and F. Pattus. Fluorescence energy transfer distance measurements using site-directed single cysteine mutants. the membrane insertion of colicin a. *J Mol Biol*, 218(3):639–653, 1991.
- [149] M. A. Lemmon and D. M. Engelman. Specificity and promiscuity in membrane helix interactions. *Q Rev Biophys*, 27(2):157–218, 1994.
- [150] T. Komiya, S. Rospert, C. Koehler, R. Looser, G. Schatz, and K. Mihara. Interaction of mitochondrial targeting signals with acidic receptor domains
-

- along the protein import pathway: evidence for the 'acid chain' hypothesis. *Embo J*, 17(14):3886–98, 1998.
- [151] C. Meisinger, J. Brix, K. Model, N. Pfanner, and M. T. Ryan. The preprotein translocase of the outer mitochondrial membrane: receptors and a general import pore. *Cell Mol Life Sci*, 56(9-10):817–24, 1999.
- [152] G. Kroemer. The proto-oncogene bcl-2 and its role in regulating apoptosis. *Nat Med*, 3:614–620, 1997.
- [153] M. Priault, P. F. Cartron, N. Camougrand, B. Antonsson, F. M. Vallette, and S. Manon. Investigation of the role of the c-terminus of bax and of tc-bid on bax interaction with yeast mitochondria. *Cell Death Differ*, 10(9):1068–1077, 2003.
- [154] Karine Tremblais, Lisa Oliver, Philippe Juin, Marie Therese Le Cabellec, Khaled Meflah, and Francois M. Vallette. The c-terminus of bax is not a membrane addressing/anchoring signal. *Biochemical and Biophysical Research Communications*, 260(3):582–591, 1999.
- [155] Angela Clow, William Greenhalf, and Bhabatosh Chaudhuri. Under respiratory growth conditions, bcl-x(1) and bcl-2 are unable to overcome yeast cell death triggered by a mutant bax protein lacking the membrane anchor. *Eur J Biochem*, 258(1):19–28, 1998.
- [156] SL. Schendel, M. Montal, and JC. Reed. Bcl-2 family proteins as ion-channels. *Cell Death Differ*, 5:372–380, 1998.
- [157] Kun Wang, Atan Gross, Gabriel Waksman, and Stanley J. Korsmeyer. Mutagenesis of the bh3 domain of bax identifies residues critical for dimerization and killing. *Mol. Cell. Biol.*, 18(10):6083–6089, 1998.
- [158] Hongbin Zha, Christine Aim-Semp, Takaaki Sato, and John C. Reed. Proapoptotic protein bax heterodimerizes with bcl-2 and homodimerizes with bax via a novel domain (bh3) distinct from bh1 and bh2. *J. Biol. Chem.*, 271(13):7440–7444, 1996.
- [159] G. Heimlich, A. D. McKinnon, K. Bernardo, D. Brdiczka, J. C. Reed, R. Kain, M. Kronke, and J. M. Jurgensmeier. Bax-induced cytochrome c release from
-

- mitochondria depends on alpha-helices-5 and -6. *Biochem J*, 378(Pt 1):247–55, 2004.
- [160] Andrew M. Petros, Edward T. Olejniczak, and Stephen W. Fesik. Structural biology of the bcl-2 family of proteins. *Biochimica et Biophysica Acta (BBA) - Molecular Cell Research*, 1644(2-3):83–94, 2004.
- [161] H. G. Boman. Peptide antibiotics and their role in innate immunity. *Annu Rev Immunol*, 13:61–92, 1995.
- [162] S. E. Blondelle and R. A. Houghten. Hemolytic and antimicrobial activities of the twenty-four individual omission analogues of melittin. *Biochemistry*, 30(19):4671–8, 1991.
- [163] S. E. Blondelle and R. A. Houghten. Design of model amphipathic peptides having potent antimicrobial activities. *Biochemistry*, 31(50):12688–94, 1992.
- [164] N. Sitaram and R. Nagaraj. Interaction of antimicrobial peptides with biological and model membranes: structural and charge requirements for activity. *Biochim Biophys Acta*, 1462(1-2):29–54, 1999.
- [165] J. E. Oh and K. H. Lee. Characterization of the unique function of a reduced amide bond in a cytolytic peptide that acts on phospholipid membranes. *Biochem J*, 352 Pt 3:659–66, 2000.
- [166] M. Dathe, T. Wieprecht, H. Nikolenko, L. Handel, W. L. Maloy, D. L. MacDonald, M. Beyermann, and M. Bienert. Hydrophobicity, hydrophobic moment and angle subtended by charged residues modulate antibacterial and haemolytic activity of amphipathic helical peptides. *FEBS Lett*, 403(2):208–12, 1997.
- [167] Z. Oren, J. Hong, and Y. Shai. A repertoire of novel antibacterial diastereomeric peptides with selective cytolytic activity. *J Biol Chem*, 272(23):14643–9, 1997.
- [168] M. Y. Kwon, S. Y. Hong, and K. H. Lee. Structure-activity analysis of brevinin 1e amide, an antimicrobial peptide from *Rana esculenta*. *Biochim Biophys Acta*, 1387(1-2):239–48, 1998.
-

- [169] K. Matsuzaki, K. Sugishita, M. Harada, N. Fujii, and K. Miyajima. Interactions of an antimicrobial peptide, magainin 2, with outer and inner membranes of gram-negative bacteria. *Biochim Biophys Acta*, 1327(1):119–30, 1997.
- [170] R. Bessalle, H. Haas, A. Gorla, I. Shalit, and M. Fridkin. Augmentation of the antibacterial activity of magainin by positive-charge chain extension. *Antimicrob Agents Chemother*, 36(2):313–7, 1992.
- [171] Andrea C. Rinaldi. Antimicrobial peptides from amphibian skin: an expanding scenario: Commentary. *Current Opinion in Chemical Biology*, 6(6):799–804, 2002.
- [172] K. L. Wegener, P. A. Wabnitz, J. A. Carver, J. H. Bowie, B. C. Chia, J. C. Wallace, and M. J. Tyler. Host defence peptides from the skin glands of the australian blue mountains tree-frog *Litoria citropa*. solution structure of the antibacterial peptide citropin 1.1. *Eur J Biochem*, 265(2):627–37, 1999.
- [173] P. A. Wabnitz, J. H. Bowie, J. C. Wallace, and M. J. Tyler. The citropin peptides from the skin glands of the australian blue mountains tree frog *Litoria citropa*. part 2: sequence determination using electrospray mass spectrometry. *Rapid Commun Mass Spectrom*, 13(17):1724–32, 1999.
- [174] Jason Doyle, Lyndon E. Llewellyn, Craig S. Brinkworth, John H. Bowie, Kate L. Wegener, Tomas Rozek, Paul A. Wabnitz, John C. Wallace, and Michael J. Tyler. Amphibian peptides that inhibit neuronal nitric oxide synthase. the isolation of lesueurin from the skin secretion of the australian stony creek frog *Litoria lesueuri*. *Eur J Biochem*, 269(1):100–109, 2002.
- [175] J. Andra and M. Leippe. Candidacidal activity of shortened synthetic analogs of amoebapores and nk-lysin. *Medical Microbiology and Immunology*, 188(3):117–124, 1999.
- [176] T. Jacobs, H. Bruhn, I. Gaworski, B. Fleischer, and M. Leippe. Nk-lysin and its shortened analog nk-2 exhibit potent activities against *Trypanosoma cruzi*. *Antimicrobial Agents and Chemotherapy*, 47(2):607–613, 2003.
- [177] M. Andersson, H. Gunne, B. Agerberth, A. Boman, T. Bergman, R. Sillard, H. Jornvall, V. Mutt, B. Olsson, and H. Wigzell. Nk-lysin, a novel effector
-

- peptide of cytotoxic t and nk cells. structure and cdna cloning of the porcine form, induction by interleukin 2, antibacterial and antitumour activity. *Embo J*, 14(8):1615–25, 1995.
- [178] T.A. Holak, A. Engstrom, P.J. Kraulis, G. Lindeberg, H. Bennich, T.A. Jones, A.M. Gronenborn, and G.M. Clore. The solution conformation of the antibacterial peptide cecropin a: A nuclear magnetic resonance and dynamical simulated annealing study. *BIOCHEMISTRY*, 27(20):7620–7629, 1988.
- [179] B. Bechinger, M. Zasloff, and S. J. Opella. Structure and orientation of the antibiotic peptide magainin in membranes by solid-state nuclear magnetic resonance spectroscopy. *Protein Sci*, 2(12):2077–2084, 1993.
- [180] FA. Kovacs and TA. Cross. Transmembrane four-helix bundle of influenza a m2 protein channel: structural implications from helix tilt and orientation. *Biophys. J.*, 73(5):2511–2517, 1997.
- [181] TA Cross and SJ. Opella. Solid-state nmr structural studies of peptides and proteins in membranes. *Curr. Opin. Struct. Biol.*, 4:574–581, 1994.
- [182] S. J. Opella, P. L. Stewart, and K. G. Valentine. Protein structure by solid-state nmr spectroscopy. *Q Rev Biophys*, 19(1-2):7–49, 1987.
- [183] Huang, Ching-hsien, and Shusen Li. Calorimetric and molecular mechanics studies of the thermotropic phase behavior of membrane phospholipids. *Biochimica et Biophysica Acta (BBA) - Reviews on Biomembranes*, 1422(3):273–307, 1999.
- [184] S. Ludtke, K. He, and H. Huang. Membrane thinning caused by magainin 2. *Biochemistry*, 34(51):16764–16769, 1995.
- [185] B. W. Koenig, J. A. Ferretti, and K. Gawrisch. Site-specific deuterium order parameters and membrane-bound behavior of a peptide fragment from the intracellular domain of hiv-1 gp41. *Biochemistry*, 38(19):6327–34, 1999.
- [186] R. M. Epanand and R. F. Epanand. Modulation of membrane curvature by peptides. *Biopolymers*, 55(5):358–63, 2000.
- [187] Z. Oren and Y. Shai. Mode of action of linear amphipathic alpha-helical antimicrobial peptides. *Biopolymers*, 47(6):451–463, 1998.
-

- [188] K. He, S. J. Ludtke, W. T. Heller, and H. W. Huang. Mechanism of alamethicin insertion into lipid bilayers. *Biophys J*, 71(5):2669–79, 1996.
- [189] Assaf Zemel, Deborah R. Fattal, and Avinoam Ben-Shaul. Energetics and self-assembly of amphipathic peptide pores in lipid membranes. *Biophys. J.*, 84(4):2242–2255, 2003.
- [190] Martin J. Zuckermann and Thomas Heimburg. Insertion and pore formation driven by adsorption of proteins onto lipid bilayer membrane-water interfaces. *Biophys. J.*, 81(5):2458–2472, 2001.
- [191] B. de Kruijff. Biomembranes. lipids beyond the bilayer. *Nature*, 386(6621):129–30, 1997.
- [192] W. Dowhan. Molecular basis for membrane phospholipid diversity: why are there so many lipids? *Annu Rev Biochem*, 66:199–232, 1997.
- [193] K. Lohner, A. Latal, G. Degovics, and P. Garidel. Packing characteristics of a model system mimicking cytoplasmic bacterial membranes. *Chem Phys Lipids*, 111(2):177–92, 2001.
- [194] K. Matsuzaki, O. Murase, N. Fujii, and K. Miyajima. An antimicrobial peptide, magainin 2, induced rapid flip-flop of phospholipids coupled with pore formation and peptide translocation. *Biochemistry*, 35(35):11361–8, 1996.
- [195] K. Matsuzaki, K.-I. Sugishita, N. Ishibe, M. Ueha, S. Nakata, K. Miyajima, and R.M. Epand. Relationship of membrane curvature to the formation of pores by magainin 2. *Biochemistry*, 37(34):11856–11863, 1998.
- [196] Ehud. Gazit and Yechiel. Shai. The assembly and organization of the alpha5 and alpha7 helices from the pore-forming domain of bacillusthuringiensis [image]-endotoxin. *J. Biol. Chem.*, 270(6):2571–2578, 1995.
- [197] Katsumi Matsuzaki, Ken-ichi Sugishita, and Koichiro Miyajima. Interactions of an antimicrobial peptide, magainin 2, with lipopolysaccharide-containing liposomes as a model for outer membranes of gram-negative bacteria. *FEBS Letters*, 449(2-3):221–224, 1999.
- [198] R. B. Gennis. Biomembranes. *Springer-Verlag, New York*, pages 151–158, 1989.
-

- [199] Karl Lohner and Elmar J. Prenner. Differential scanning calorimetry and x-ray diffraction studies of the specificity of the interaction of antimicrobial peptides with membrane-mimetic systems. *Biochimica et Biophysica Acta (BBA) - Biomembranes*, 1462(1-2):141–156, 1999.
- [200] D. Barra and M. Simmaco. Amphibian skin: a promising resource for antimicrobial peptides. *Trends Biotechnol*, 13(6):205–9, 1995.
- [201] R. M. Epanand, F. Naider, and J. M. Becker. Lipid-mediated a-factor interactions with artificial membranes. *Methods Enzymol*, 250:169–86, 1995.
- [202] E. Gazit, W. J. Lee, P. T. Brey, and Y. Shai. Mode of action of the antibacterial cecropin b2: a spectrofluorometric study. *Biochemistry*, 33(35):10681–92, 1994.
- [203] E. Gazit, A. Boman, H. G. Boman, and Y. Shai. Interaction of the mammalian antibacterial peptide cecropin p1 with phospholipid vesicles. *Biochemistry*, 34(36):11479–88, 1995.
- [204] M. Schumann, M. Dathe, T. Wieprecht, M. Beyermann, and M. Bienert. The tendency of magainin to associate upon binding to phospholipid bilayers. *Biochemistry*, 36(14):4345–51, 1997.
- [205] S. J. Ludtke, K. He, Y. Wu, and H. W. Huang. Cooperative membrane insertion of magainin correlated with its cytolytic activity. *Biochim Biophys Acta*, 1190(1):181–184, 1994.
- [206] W. T. Heller, A. J. Waring, R. I. Lehrer, T. A. Harroun, T. M. Weiss, L. Yang, and H. W. Huang. Membrane thinning effect of the beta-sheet antimicrobial protegrin. *Biochemistry*, 39(1):139–45, 2000.
- [207] E J Prenner, R N Lewis, K C Neuman, S M Gruner, L H Kondejewski, R S Hodges, and R N McElhaney. Nonlamellar phases induced by the interaction of gramicidin s with lipid bilayers. a possible relationship to membrane-disrupting activity. *Biochemistry*, 36(25):7906–7916, 1997.
- [208] B. Bechinger, M. Zasloff, and S. J. Opella. Structure and interactions of magainin antibiotic peptides in lipid bilayers: a solid-state nuclear magnetic resonance investigation. *Biophys J*, 62(1):12–14, 1992.
-

-
- [209] D. J. Hirsh, J. Hammer, W. L. Maloy, J. Blazyk, and J. Schaefer. Secondary structure and location of a magainin analogue in synthetic phospholipid bilayers. *Biochemistry*, 35(39):12733–12741, 1996.
- [210] R. W. Williams, R. Starman, K. M. Taylor, K. Gable, T. Beeler, M. Zasloff, and D. Covell. Raman spectroscopy of synthetic antimicrobial frog peptides magainin 2a and pgl. *Biochemistry*, 29(18):4490–6, 1990.
- [211] K. Matsuzaki, M. Harada, S. Funakoshi, N. Fujii, and K. Miyajima. Physicochemical determinants for the interactions of magainins 1 and 2 with acidic lipid bilayers. *Biochim Biophys Acta*, 1063(1):162–170, 1991.
- [212] Ehud Gazit, Israel R. Miller, Phil C. Biggin, Mark S. P. Sansom, and Yechiel Shai. Structure and orientation of the mammalian antibacterial peptide cecropin p1 within phospholipid membranes. *Journal of Molecular Biology*, 258(5):860–870, 1996.
- [213] D. Juretic, R. W. Hendler, F. Kamp, W. S. Caughey, M. Zasloff, and H. V. Westerhoff. Magainin oligomers reversibly dissipate delta microh+ in cytochrome oxidase liposomes. *Biochemistry*, 33(15):4562–70, 1994.
- [214] A. Vaz Gomes, A. de Waal, J. A. Berden, and H. V. Westerhoff. Electric potentiation, cooperativity, and synergism of magainin peptides in protein-free liposomes. *Biochemistry*, 32(20):5365–5372, 1993.
-

Publications

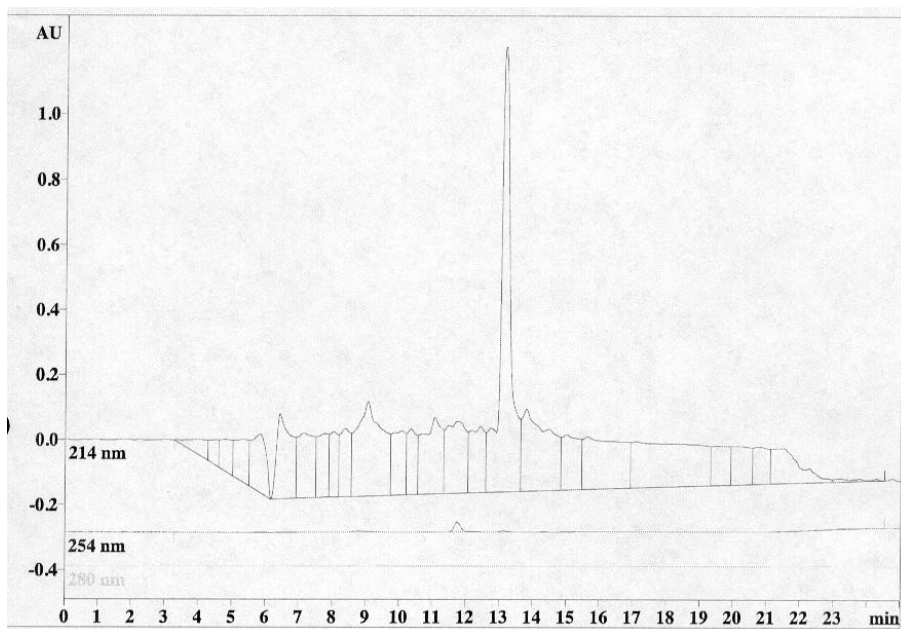
1. ^{15}N solid-state NMR spectroscopy investigations of the topological equilibria of a synthetic ion-channel peptide in oriented lipid bilayers. *Sudheendra U.S* and Burkhard Bechinger (to be submitted for publication)

2. Helical orientation of membrane associated model phosphorylated peptide-A comprehensive study of dynamics and orientational analysis of model membrane system. *Sudheendra U.S* , Philippe Bertani and Burkhard Bechinger (manuscript under preparation for publication)

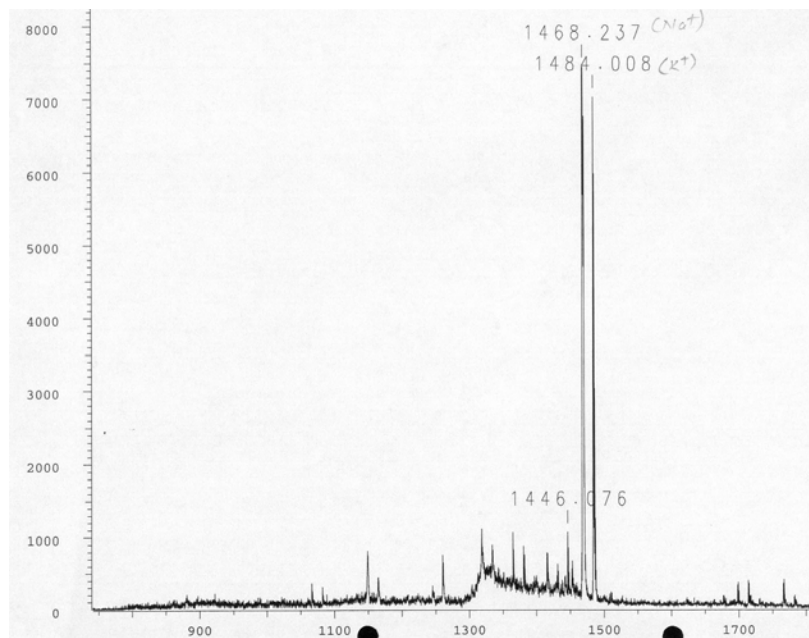
3. Membrane associated α -helical segments of Bcl- X_L and Bax-C terminus investigations by solid-state NMR spectroscopy. *Sudheendra U.S* and Burkhard Bechinger. (to be submitted for publication)

4. The position of the antibacterial peptide NK-2 in model membrane. Regine Willumeit , Jorg Andra, *Sudheendra U.S* and Burkhard Bechinger, Sebastian Linser, Mart Kumpudde, Thomas Hauss (to be submitted to Journal of Neutron Research)

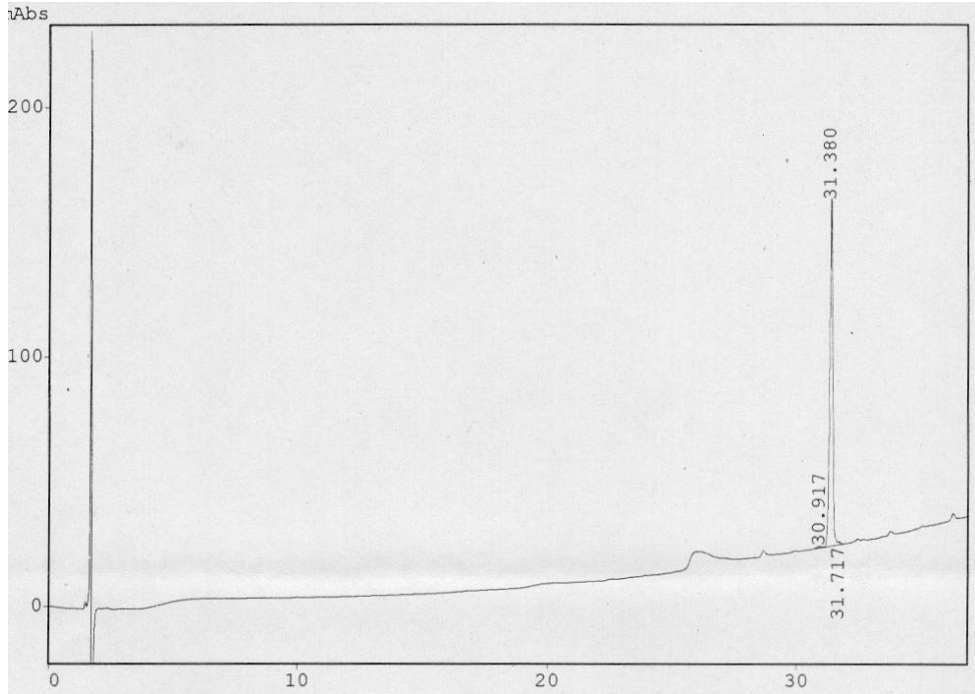
Purification and identification profiles of synthesized peptides



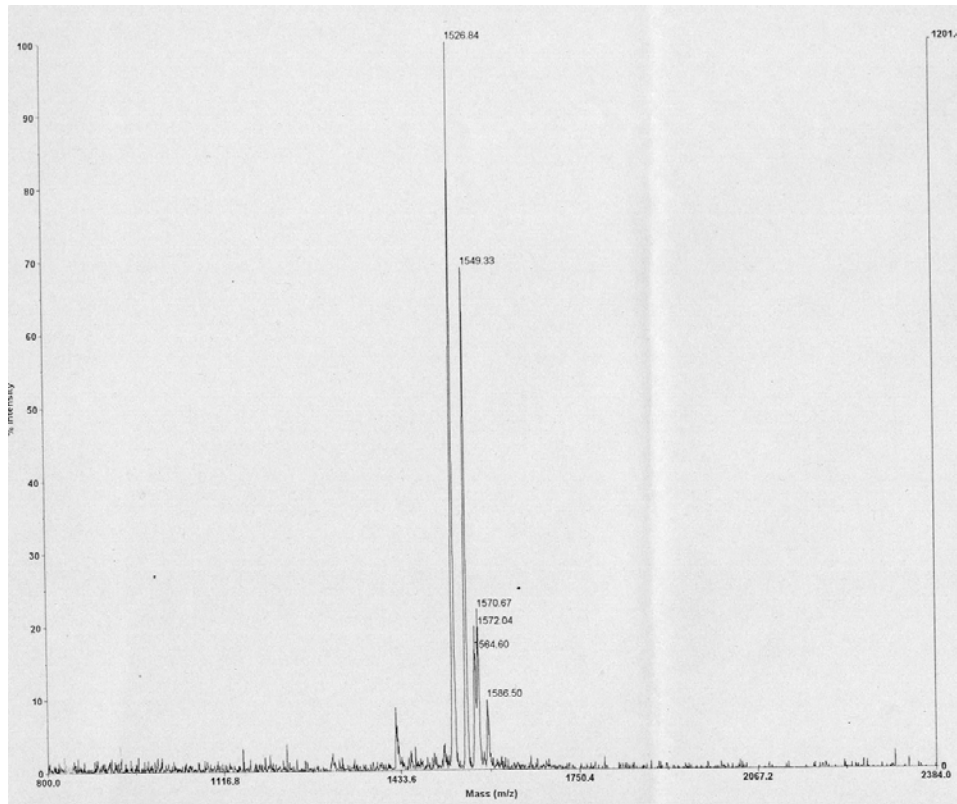
HPLC profile of LS14



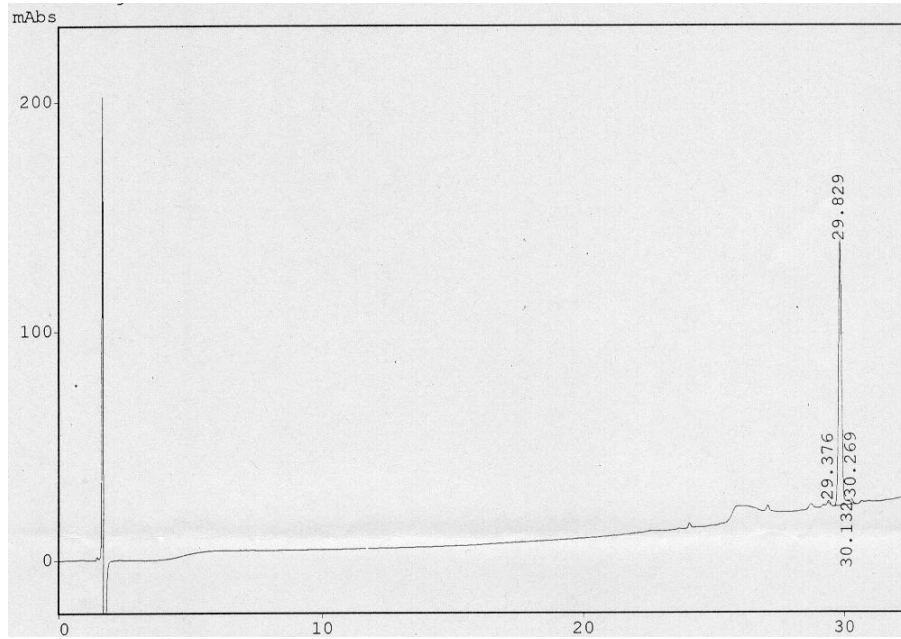
Mass spectrum of LS14



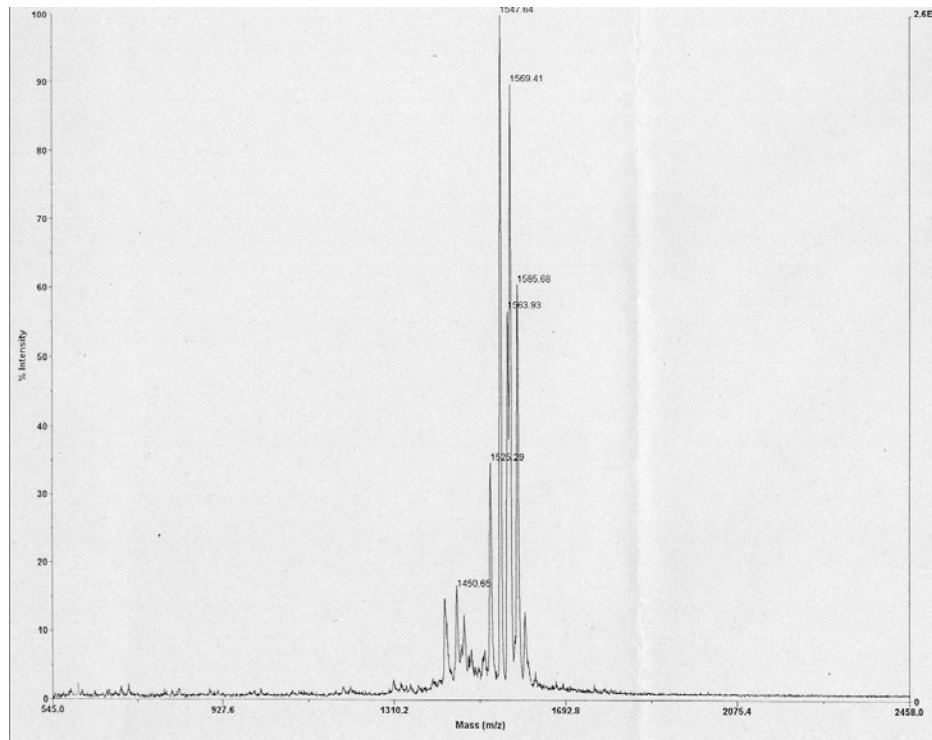
HPLC profile of (Pser-6)LS14



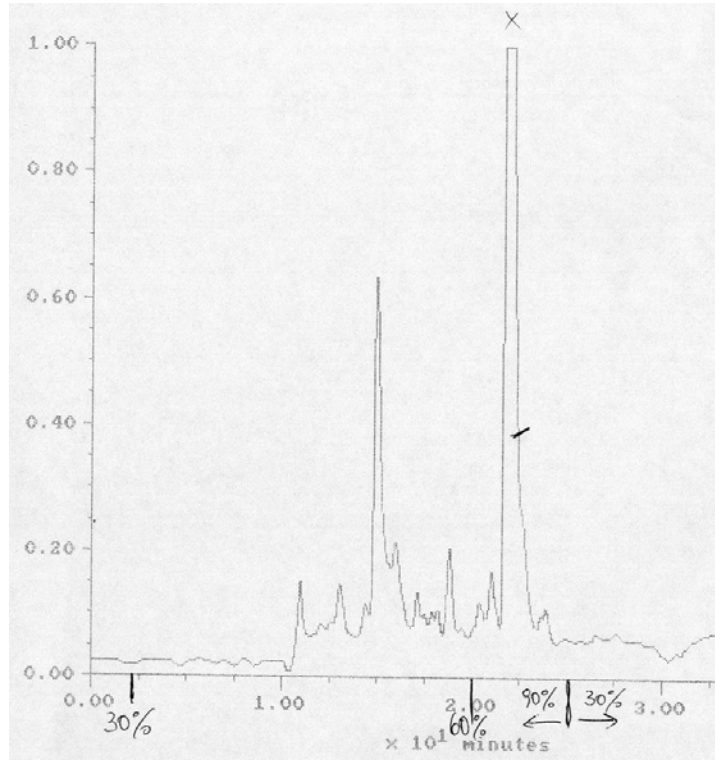
Mass spectrum of (Pser-6)LS14



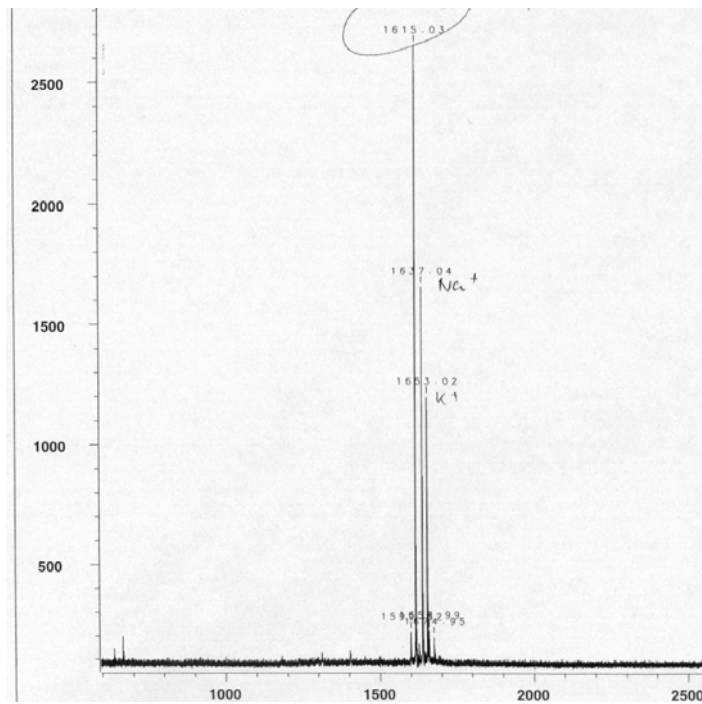
HPLC profile of (Pser-9)LS14



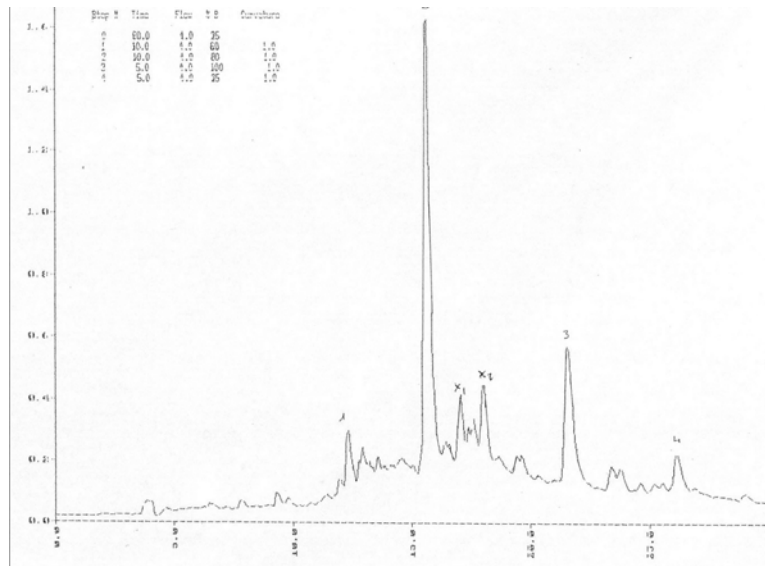
Mass spectrum of (Pser-9)LS14



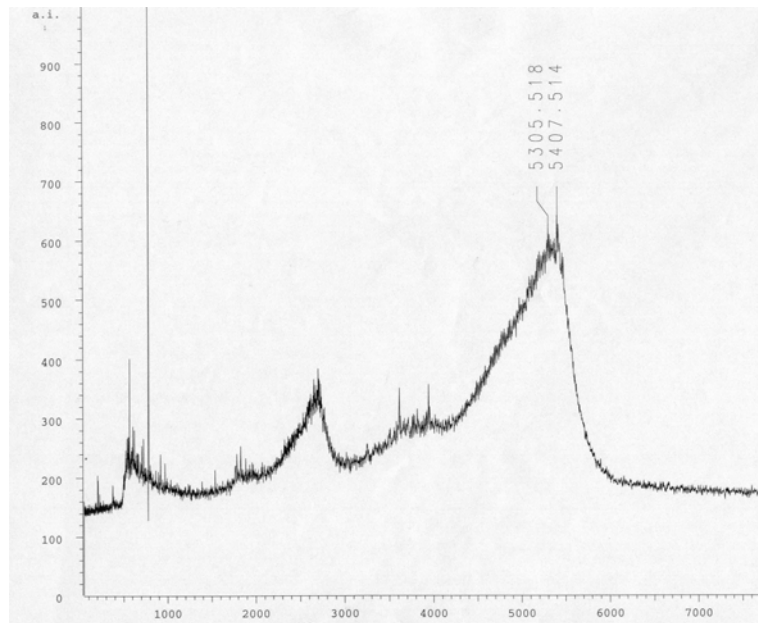
HPLC profile of Citropin1.1



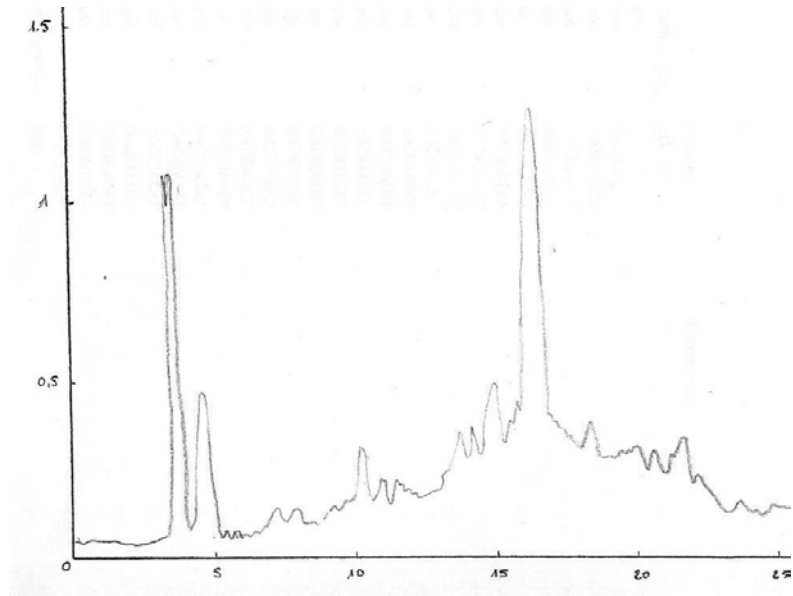
Mass spectrum of Citropin1.1



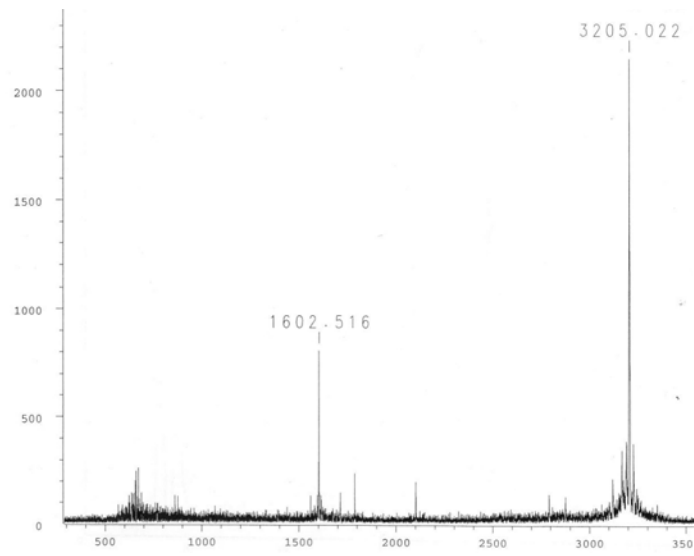
HPLC profile of HLH of Bcl-X_L



Mass spectrum of HLH of Bcl-X_L



HPLC profile of NK2



Mass spectrum of NK2